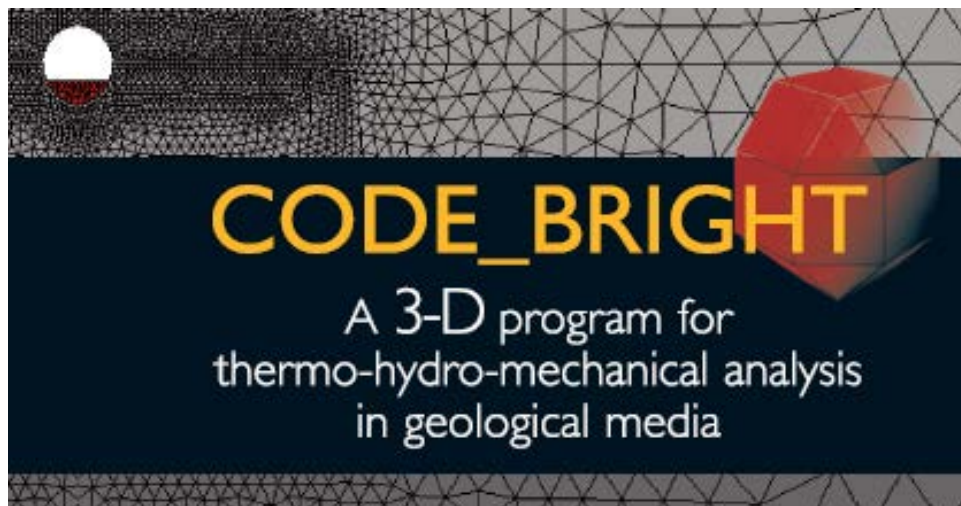# Workshop of
CODE_BRIGHT USERS

16th May 2019
Barcelona, Spain

Department of Civil and Environmental Engineering
UPC-BarcelonaTech
Barcelona, Spain

CIMNE
International Center for Numerical Methods in Engineering
Barcelona, Spain

CODE_BRIGHT

A 3-D program for thermo-hydro-mechanical analysis in geological media

WORKSHOP OF CODE_BRIGHT USERS

Barcelona, 16th May 2019

Department of Civil and Environmental Engineering

(UPC-BarcelonaTech, Barcelona, Spain)

CIMNE

(International Center for Numerical Methods in Engineering, Barcelona, Spain)

SWELLING PRESSURE TEST FOR BLOCK AND PELLET MIXTURE

He Lu, Antonio Gens

Department of Civil and Environmental Engineering
Technical University of Catalonia (UPC)
Campus Nord UPC, 08034 Barcelona, Spain
E-mail: lu.he@upc.edu,

Key words: Code_Bright, bentonite, swelling pressure, MX-80,block and pellet mixture

Abstract. *A simulation of the swelling pressure is modeled in Code_Bright using double structure model. The test includes a mixture sample of bentonite block and pellet to study the buffer swelling and homogenization evolution. The test has been performed for 672 days until reaching stability. As important outputs, the swelling pressure and the dry density are collected and studied from both pellet and block zone. From the simulation, the results can be well reproduced compared with the test. Both the final state and evolution are well studied in order to conclude the mechanical properties of the mixture.*

1 INTRODUCTION

This test has been developed by POSIVA(Finland) to study buffer swelling and homogenization evolution. A mixture of block and pellet is placed in a constant volume cell for a swelling pressure test. The mixture is initially unsaturated and the water flow into the test cell during the test. Test is terminated after 672 days which reached the stability.

The model is produced with the corresponding condition and test procedure in Code_Bright. Two double structure model are set for the two material. The calculation is performed until 700 days even though that the stability has been already reached before. The swelling stress, degree of saturation, suction change and water content and dry density are collected to compare with the laboratory results.

2 TEST DESCRIPTION

3.1 Equipment

Test is performed in a constant-volume cell with 100mm diameter and a height of 100mm, equipped with two axial piston at the top and bottom. Two radial piston are set at the midpoints of block and pellet zones in order to get the stress. Besides, the water content are detected in the center and four direction of the sample.The water supply on the top of the sample via a porous disc at the interface with the pellets zone.

3.2 Specimens

The bentonite block is compacted directly into the cell under a compaction to dry density of 1808kg/m3 with a height of 48.5mm.

The MX-80 pellets with pillow shape are placed on the top of block directly until a total height of 100 mm.

The parameters of block and pellet are listed in the table-1

	Initial w(%)	Initial ρ_d(kg/m^3)	Constant radius(mm)	Initial height(mm)
Block	16.3	1808	100	48.5
Pellets	15.3	904	100	51.5

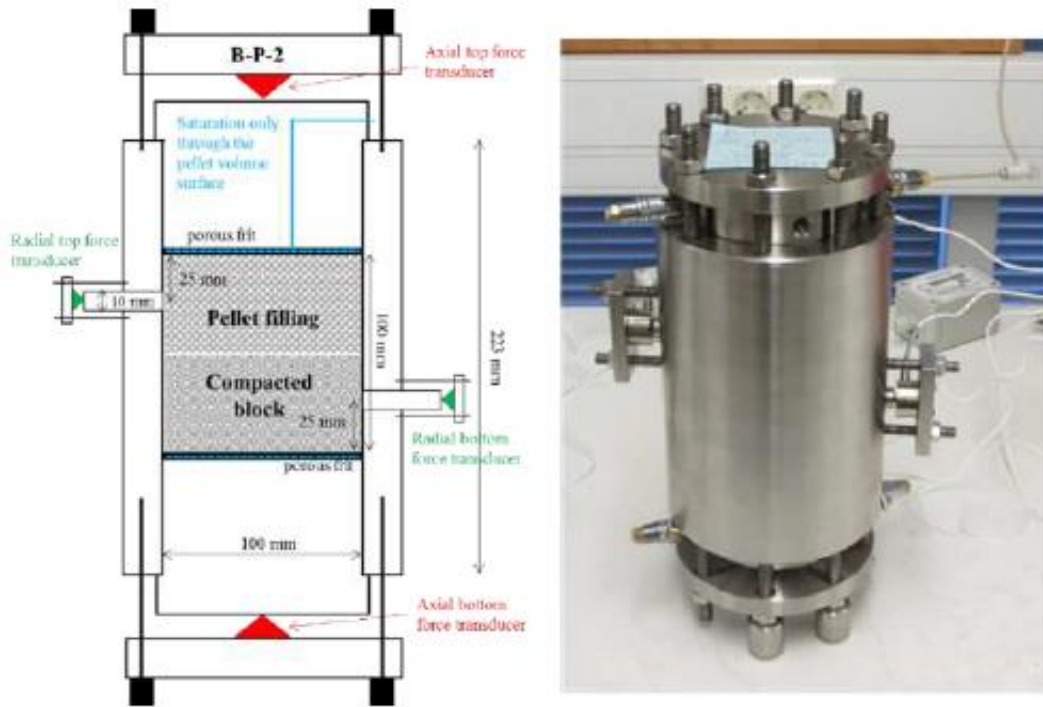Table 1 Initial properties for block and pellets zone

Figure 1 Schematic illustration and pictures of the block-pellet test system

3.3 Test procedure

The saturating solution are allow to flow into the test cell only from the top wetting circuit of the cell. The bottom circuit is open to atmosphere over the saturation period. The saturation and swelling is proceeding in the cell.

The test is terminated after 672 days when both axial and radial directions are reaching stability of stress. The final state is evolved to table 2 with contrast with the initial state.

Initial block/pellet height(mm)	Initial dry density(kg/m^3)	Axial P $_{block}$ (kPa)	Axial P $_{pellet}$ (kPa)	Final block/pellet height	Determined dry density(kg/m^3)
48.5/51.5	1342	1428	869	63.7/37.4	1332

Table 2 Initial and final dimensions, dry density and swelling stress of pellet and block

3 MODEL DESCRIPTION

The model used in this test is based on BExM using double structure mechanism. Mechanical and hydraulic parameters are defined separately for the pellet and block. The modified water retention curve are used.Coupled hydro-mechanical analysis has been performed in this test using the balance equations of stress and water.

4 RESULT AND DISCUSSION

4.1 Degree of saturation

The test has been performed for 672 days and the water has been input from the upper circuit. The initial degree of saturation are 85% and 21% respectively in the block and pellet region. The numerical model labeled by material is shown in the Figure 2.

Five group of results are collected from the depth of 12,30,50,67,95 mm from the bottom in Figure 3 which three of them are in the pellet region and the other two are in the block region.
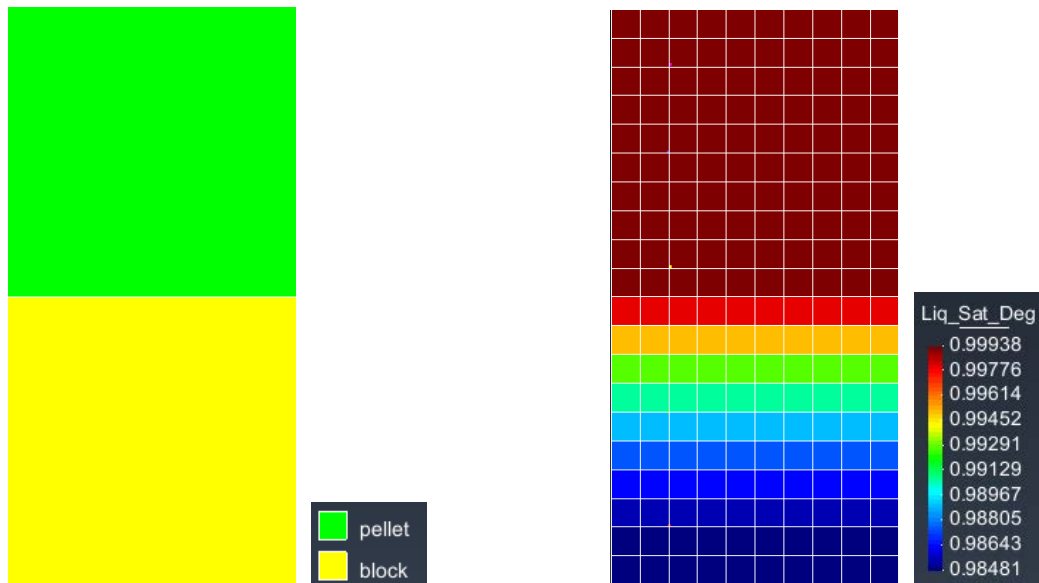

Figure 2 The geometry of the test and mesh with the contour fill of degree of saturation
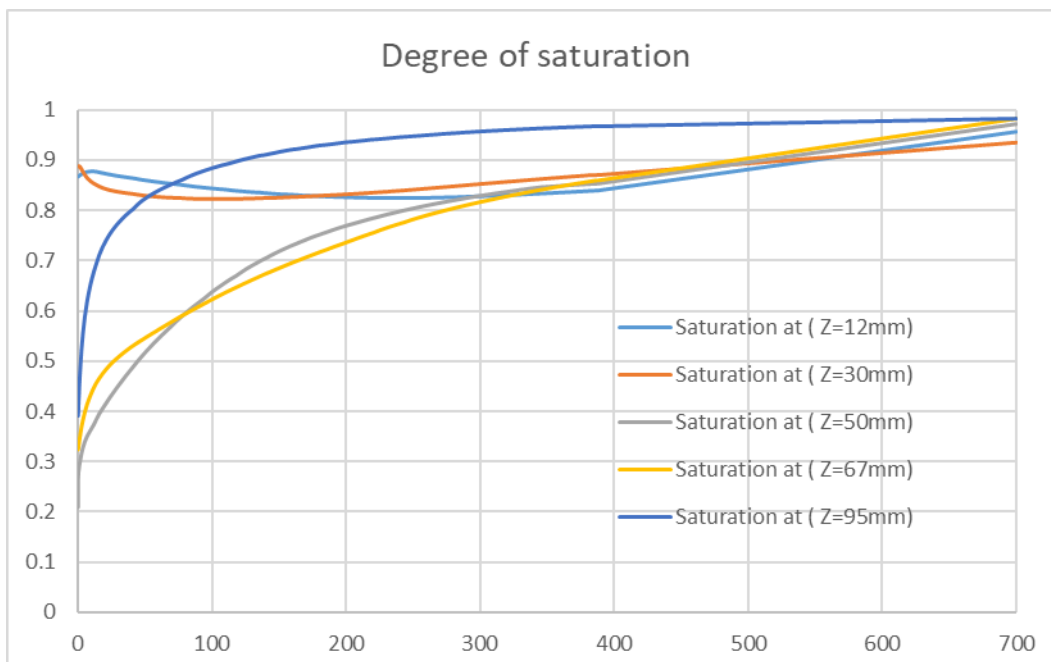

Figure 3 Degree of saturation function with time at different depth

The degree of saturation developed more rapidly to 1 at the depth more closed to the upper boundary in the pellet region which inputs the water. In the block region there is a decrease in the beginning deals to the supplement to the pellet which results to a delay of saturating. It is interesting to see the result of 50 mm, which theoretically should be lower as farer away from the access of the water, however the water supplement from the block contribute to this initial saturation.

4.2 Suction development

The suction develop at different depth are also collected in Figure 4, including both macro and micro suction evolved with time. Because the interchange from double structure mechanism, the micro-suction changes later than the macro suction. In general, the suction in the pellet zone decrease first because the closed to the access of water and also the higher porosity.
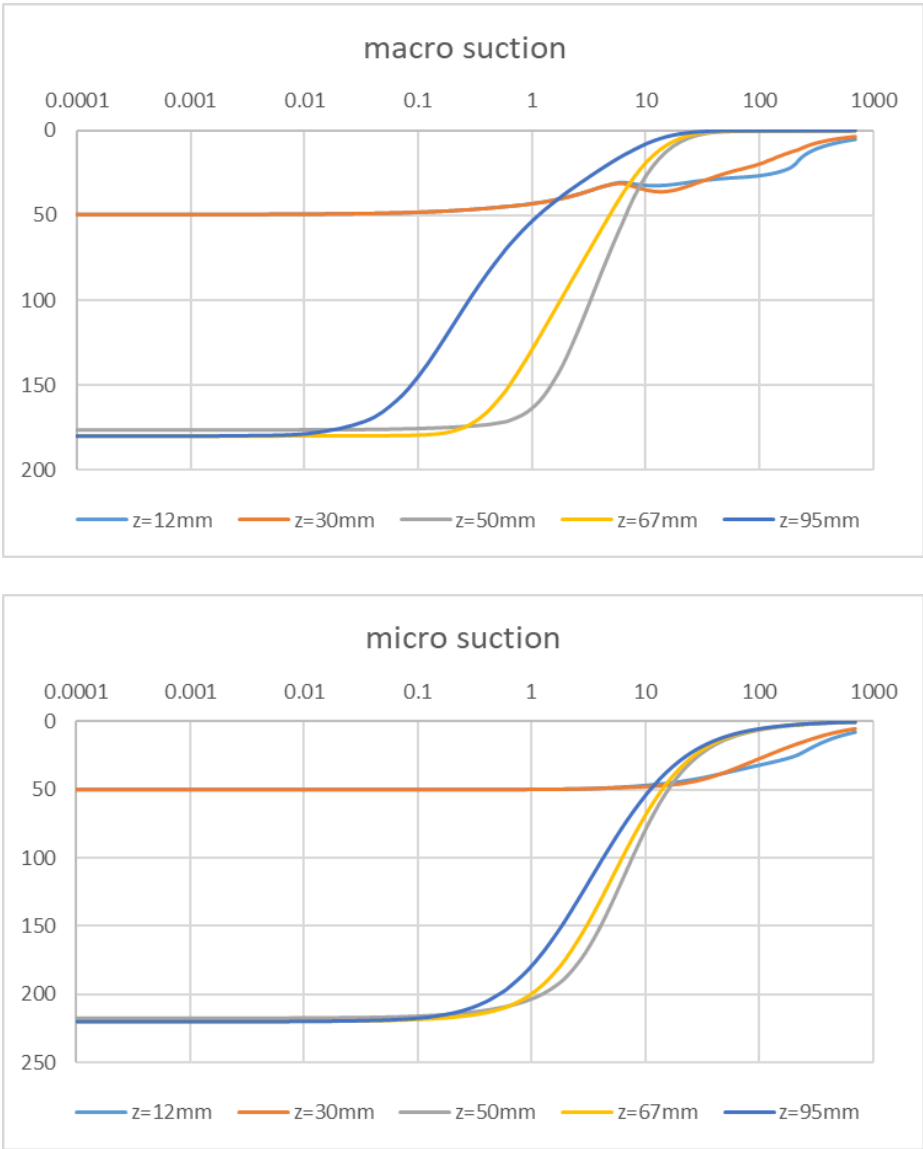

Figure 4 Macro and micro-suction function with time at different depth

4.3 Swelling stress

The swelling pressure is one of the main output of this test and can be detected directly during the test which is presented in solid line and the simulation results are in dot line in Figure 5. The measured stress is systematically higher in the block zone than the pellet zone. The stress difference between the block and pellets can be modeled with the different mechanical parameters. There is an obvious peak in the block zone referring to the saturation and suction decrease. However, the simulation result is not as abrupt as the beginning of the test result because the suction develop more stabilized. Meanwhile, the swelling stress in the pellet zone is more linearly since the high porosity in this zone. An earlier balance is reached in the pellets zone which corresponded to the suction development.
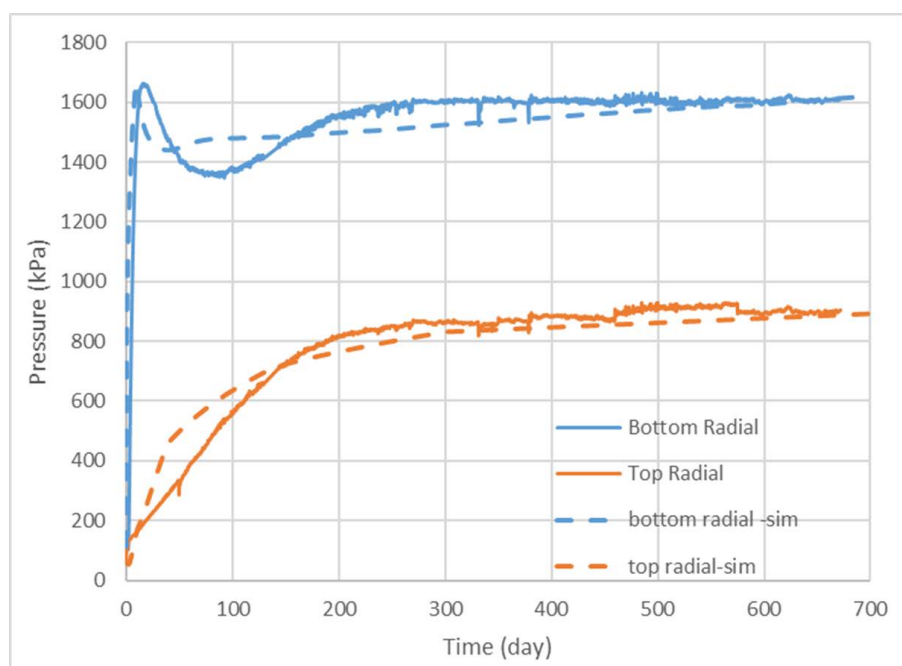

Figure 5 Swelling pressure in radial direction function of time

4.4 Water content and dry density

The water content refers to the final state of the mixture. From the experiment results, five group of the results are collected of different position. However, in Code Bright the results converge to only one group. The block zone stay lower because of the low porosity even though it is reaching totally saturated. From the dry density plot, the final homogeneous can be reached in for the two material from both experiment and simulation results which indicated that the test can be well reproduced.
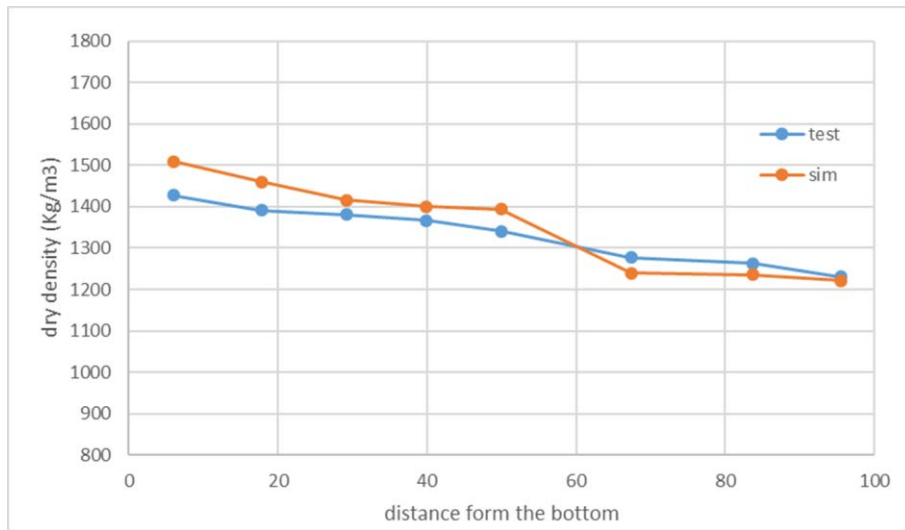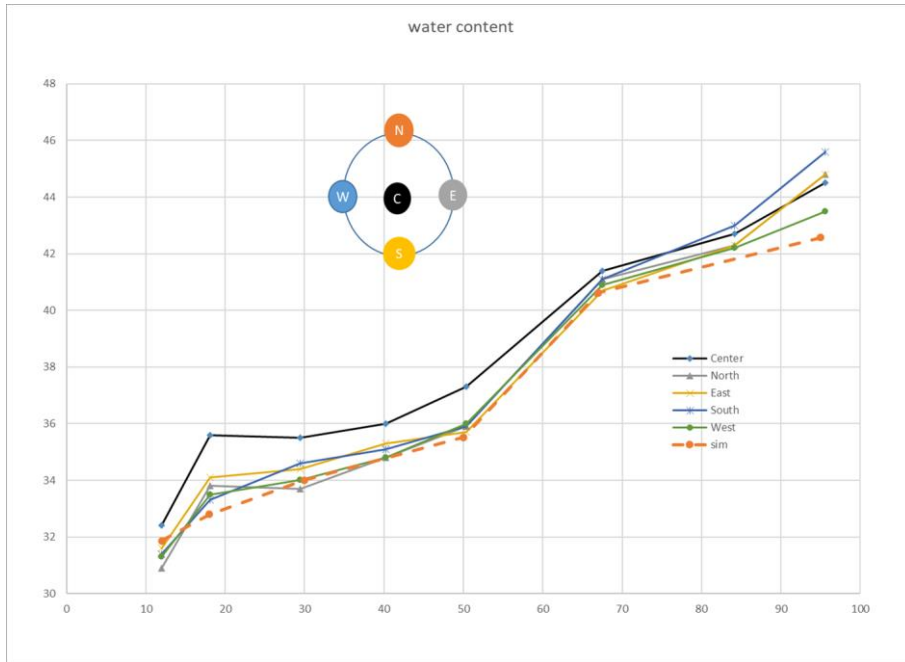
Figure 6 water content and dry density in the final state

4   CONCLUSIONS

In this paper, a simulation of the swelling test of a mixture of pellet and block.is carried out. The evolve of swelling stress, water content, degree of saturation has been collected and compared with the laboratory results.

As the water is input from the top circuit which directly connected to the pellet zone, the pellet is reaching to saturation more rapidly. Correspondingly, the macro suction decrease to zero directly in the pellets zone, while, in the block zone the suction more stable at the beginning. The swelling stress for the block is higher with a initial peak. As the high porosity in the pellet zone, even though the suction developed more rapidly, the swelling stress stay linearly. For the final state the mixture sample is reaching homogeneous with the linearly water content and dry density. With the comparison of both the evolution and the final state of the test, the model in Code Bright proved to be appropriate to reproduce the behavior of the MX-80 bentonite.

Reference

1. Gens, A., Sánchez, M., Guimaraes, L. D. N., Alonso, E. E., Lloret, A., Olivella, S., ... & Huertas, F. (2009). A full-scale in situ heating test for high-level nuclear waste disposal: observations, analysis and interpretation. Géotechnique, 59(4), 377.

2. Schatz, T., & Martikainen, J. (2012). Laboratory tests and analyses on potential Olkiluoto backfill materials. Posiva Oy.

3. Posiva, O. (2012). Safety case for the disposal of spent nuclear fuel at Olkiluoto. Features, events and processes 2012 (No. POSIVA--12-7). Posiva Oy.

4. Toprak, E. (2018). Long term response of multi-barrier schemes for underground radioactive waste disposal..

5. Guerra, A. M., Mokni, N., Delage, P., Cui, Y. J., Tang, A. M., Aimedieu, P., ... & Bornert, M. (2017). In-depth characterisation of a mixture composed of powder/pellets MX80 bentonite. Applied Clay Science, 135, 538-546

ASSESSMENT OF CODE_BRIGHT PROCESSING TIME USING PARALLEL VERSIONS

X. Pintado[*]

[*] AINS Group; Bertel Jungin aukio 9, 02600 Espoo, Finland
Email: xavier.pintado@ains.fi

Key words: H analysis, TH analysis, HM analysis, THM analysis, speed-up, parallel.

Abstract. *The constant development of the computers is a challenge for the developers of software, who should be able to take advantage of the new machines. The parallelization is one of the challenges, which means to use some threads simultaneously for carrying out the calculations. Version 8.4 of CODE_BRIGHT has some versions prepared for running in parallel with two, four and six threads in shared memory. Four cases have been run carrying out the calculations with different number of threads and assessing the improvement in computer time.*

1   INTRODUCTION

The development of the computers allows to improve the calculation time using some threads working in parallel. There are two different types of parallelization: parallelization with shared memory and with distributed memory. The parallelization with shared memory means that the threads are using the same memory when they are performing the calculations, so the data can be used efficiently by the threads involved in the calculation. In the parallelization with distributed memory, each thread or group of threads have their own memory when they carry out the calculations and share the results with some form of interconnection.
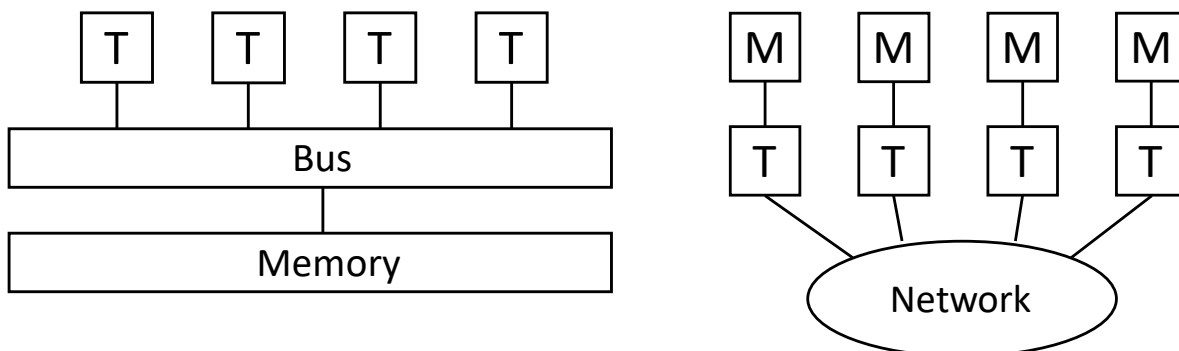

Figure 1. Shared memory with four threads (left) and distributed memory with four computers.

Shared memory is relatively easy to implement and requires, in some cases, a few lines of code but it is limited to a few units of threads because the efficiency drops as it will be seen later. Distributed memory can work efficiently with many threads but in this case, the implementation is much more difficult. In TH and THM modelling, distributed memory requires the division of the geometry and to solve the equations in each division. Obviously, there are interactions in each border.

2   SIMULATIONS DESCRIPTION

Four cases have been analysed. The first one is the hydraulic analysis of the Bátaapáti site (Figure 1), the place in Hungary where PURAM, the Hungarian nuclear waste agency, stores the low and

intermediate level nuclear wastes derived from the nuclear power plant in Paks, such as protective equipments and devices that get irradiated in the operational area of the plant[1]. The mesh is 3-D with tetrahedrons of 4 nodes that has 482 054 nodes and 2 746 310 elements (2 745 990 linear tetrahedrons with analytical integration and 320 linear triangles also with analytical integration) with one degree of freedom per node (liquid pressure).

The second case is a TH analysis of an "in situ" test carried out in Onkalo®[2] called FISST (Figure 2). FISST is a full-scale final spent nuclear fuel disposal test. The mesh is also 3-D with tetrahedrons of 4 nodes that has 186 718 nodes and 1 061 734 elements (1 052 615 linear tetrahedrons with analytical integration and 9 119 linear triangles also with analytical integration) with two degrees of freedom per node (liquid pressure and temperature).

The third case is a HM simulation of a shear test[3]. Although the test is clearly 3-D (a cylinder which is sheared at the middle plane), the analysis has been performed in 2-D plane strain. The mesh is 2-D with linear quadrilaterals (Figure 3) that has 4 125 nodes and 3 968 elements with three degrees of freedom in each node (vertical and horizontal displacements and liquid pressure).

The forth case is a THM simulation of the KBS-3V design for the storage of the spent nuclear fuel in Finland and Sweden[4,5]. The mesh is 3-D with linear tetrahedrons (Figure 4) that has 15 869 nodes and 77 797 elements with five degrees of freedom (the three displacements, liquid pressure and temperature).

The simulations have been performed with two different computers (Table 1). The Desktop computer is an HP 2240 Tower Workstation with an Intel® Core™ i7-6700 CPU @ 3.40 GHz 3.40 GHz (2 processors) and 64 GB RAM and the Power computer is an HP Z6 G4 Workstation with an Intel® Xeon® Gold 6134 CPU 3.20 GHz 3.19 GHz (2 processors) and 64.0 GB RAM.
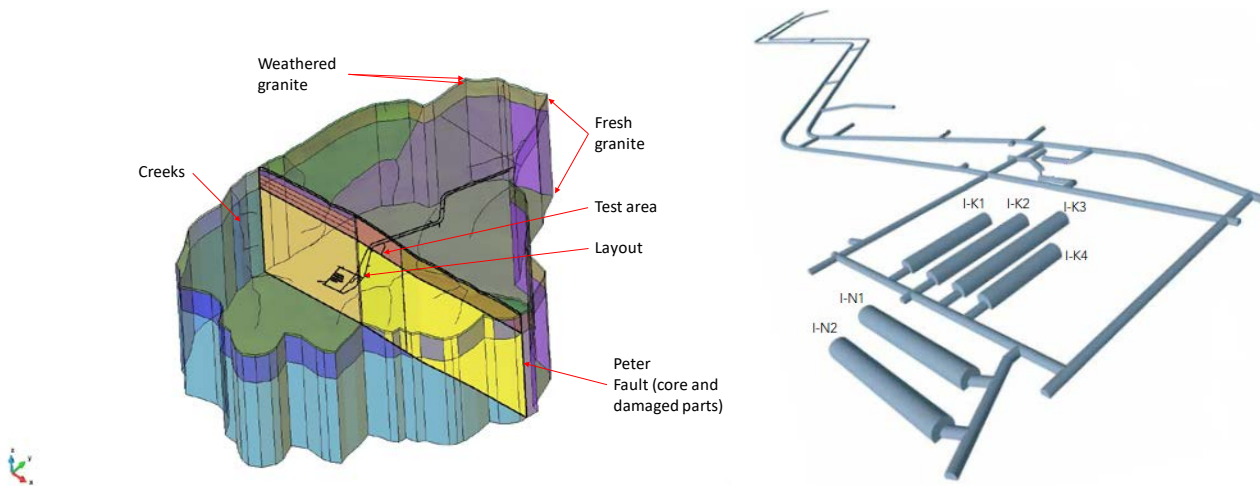

Figure 1. Bátaapáti site. Entire geometry (left) and tunnels network (right).
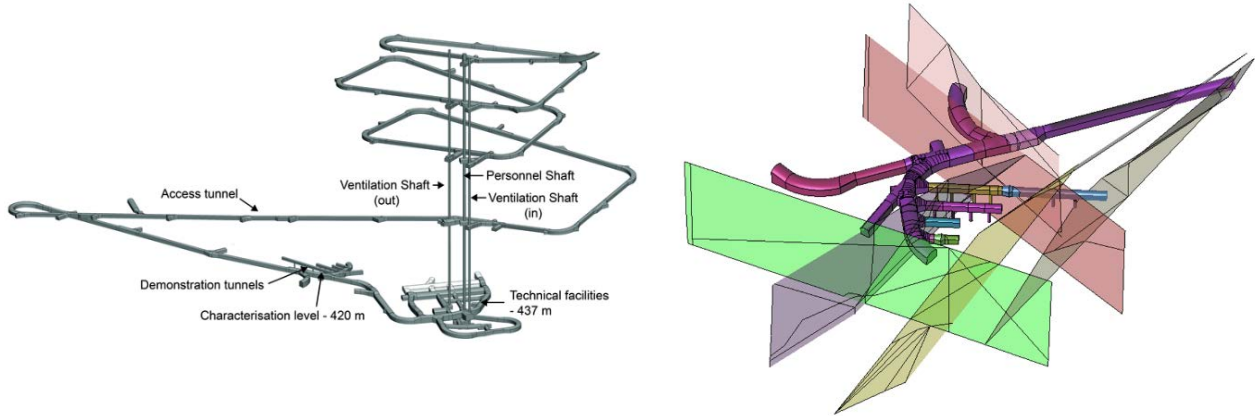
Figure 2. FISST test. Test location (demonstration tunnels, left) and tunnels network with fractures (right).
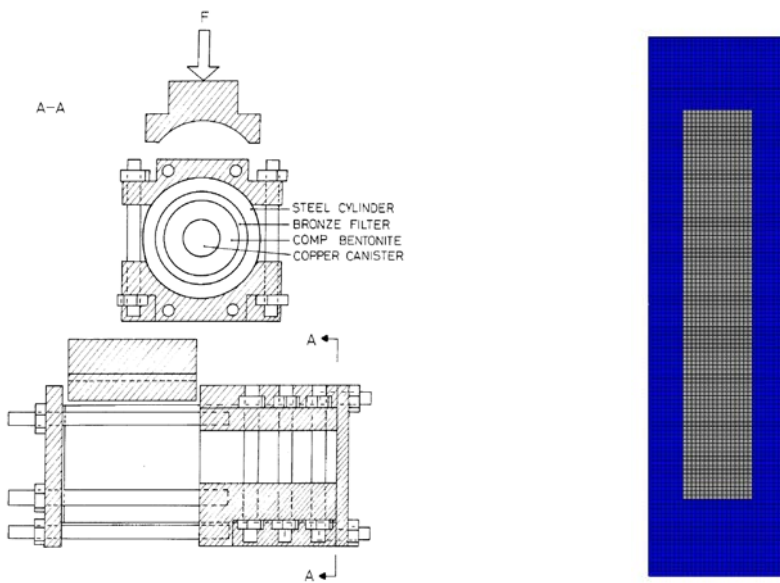

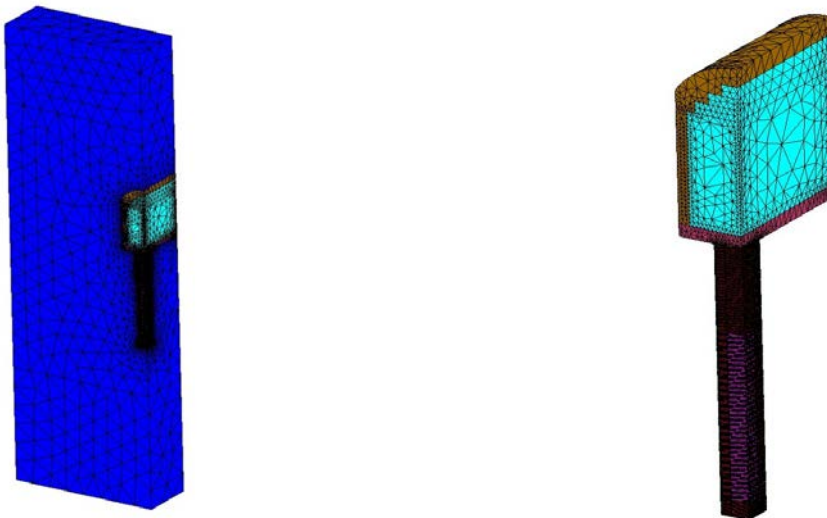**Figure 3.** Shear test. Test set-up (left) and mesh (right).

Figure 4. KBS-3V. Entire mesh (right) and detail of the EBS components (right).

3   RESULTS

The results are presented in Table 1. The Walk clock time has been calculated as it is indicated in https://deca.upc.edu/en/projects/code_bright/downloads (last accessed in May 2019). The real time is also presented although it is not an important parameter, especially when some processes are working at the same time, but it can help to know how efficient the computer is when it is carrying out calculations but the user is also doing normal activities related with preparation of documents (using Word) or data analysis (using e.g. Excel). The ratio Solver/Total is an important data because it gives what is the percentage of the CPU time that can be reduced with the parallel versions. Only this percentage of time can be reduced because the parallelization performed in CODE_BRIGHT only reduces the time used with the solver. The rest of the time cannot be reduced yet.

Table 1. Results. Time in seconds.

Case	Computer	Number of threads	Real time	CPU time	Walk clock time	Ratio (%) Solver/Total	Speed-up
Bátaapáti	Desktop	1	621900	94420	-	54.94	-
	Power	1	561120	118287	-	50.11	-
	Power	2	275820	143965	71982	56.96	1.64
	Power	4	236880	160000	40000	76.59	2.96
	Power	6	234420	206357	34393	80.84	3.44
FISST	Desktop	1	100800	100456	-	79.42	-
	Power	1	126780	126644	-	83.90	-
	Power	2	86820	151775	75887	85.95	1.67
	Power	4	69900	224132	56033	89.79	2.26
	Power	6	63840	286641	47773	91.68	2.65
Shearing	Desktop	1	437820	437497	-	43.31	-
	Power	1	464280	464258	-	44.27	-
	Power	2	543600	543568	271784	56.45	1.71
	Power	4	540117	540180	135029	56.34	3.44
	Power	6	547280	547224	91204	56.14	5.09
KBS_3V	Desktop	1	44700	44644	-	91.03	-
	Power	1	46320	46341	-	91.95	-
	Power	2	32400	61933	30966	91.87	1.50
	Power	4	24000	87164	21791	91.60	2.13
	Power	6	20820	110536	18423	91.43	2.51

It should be said that sometimes, the program runs well for certain versions and not for others, e.g. the program may run well with the version for one thread but not for versions with more than one thread. The executable programs are not the same.

In Table 1 it is possible to see that the Shearing case runs the best with the lowest ratio Solver/Total, this is quite strange and that the CPU time and the Real time seems to be the same as well.

Figure 5 compares the different speed-ups as function of the number of threads and Figure 6 compares the ratio Solver/Total as function of the number of threads.
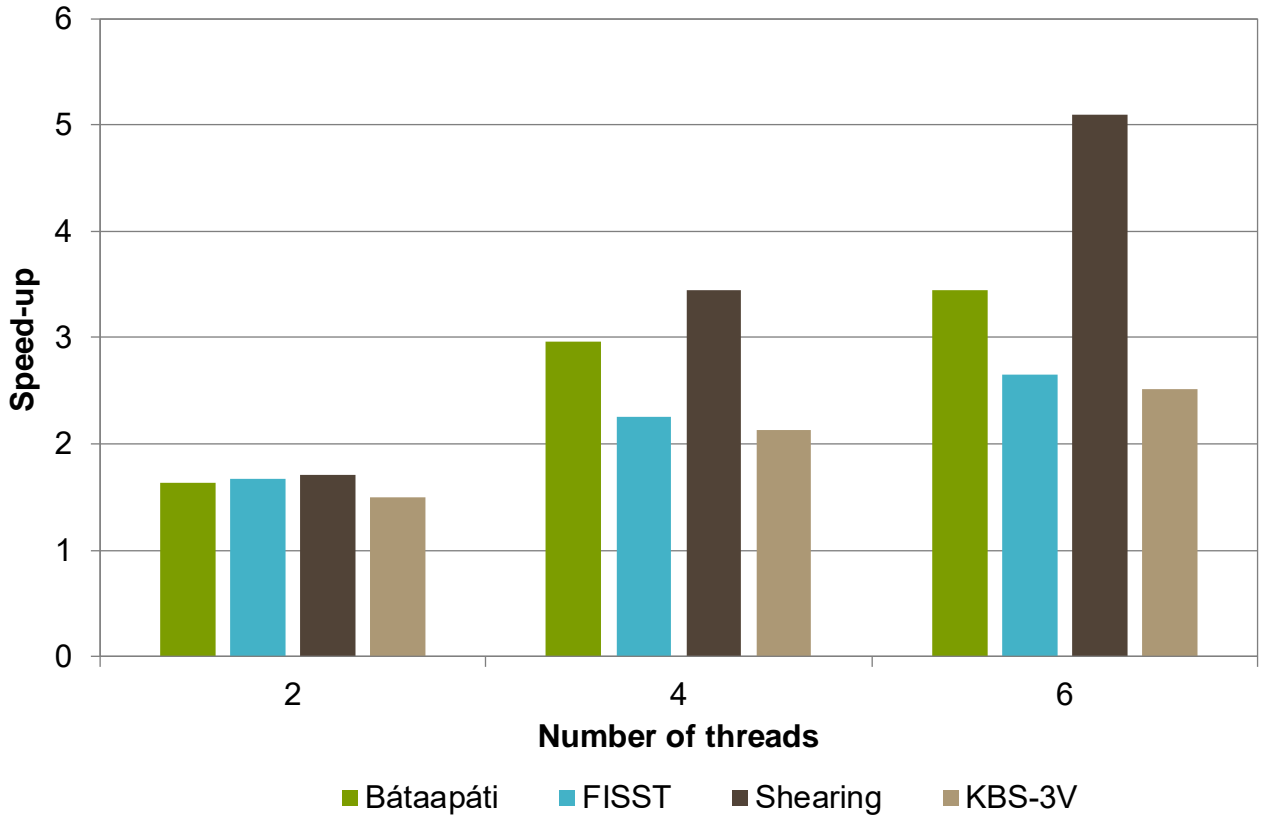
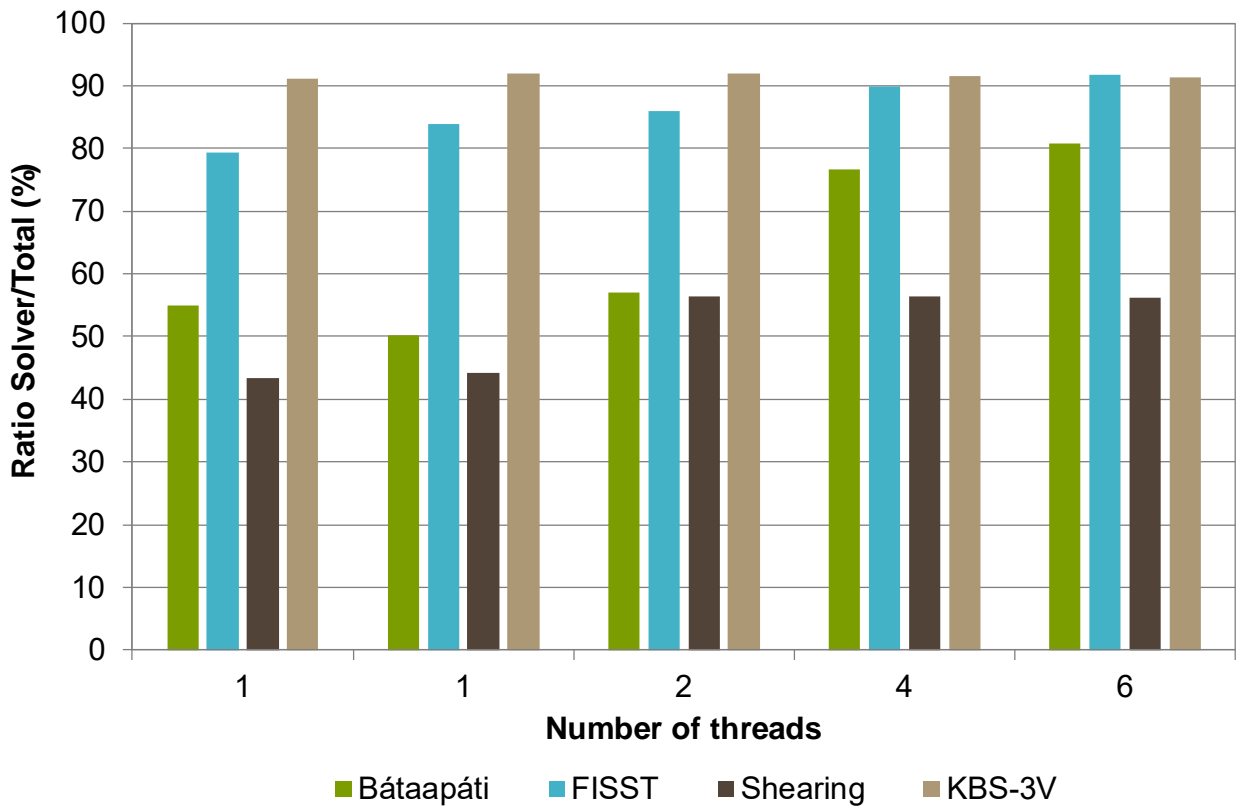**Figure 5.** Speed-up as function of the number of threads.

Figure 6. Ratio Solver/Total (%) as function of the number of threads. The first 1 corresponds to the Desktop computer and the second to the Power computer.

4 CONCLUSIONS

- Using parallel versions of CODE_BRIGHT reduces the Walk clock time, so the real time reduces which is a clear advantage.

- Except the Shearing case, which provides quite strange results, the reduction of Walk clock time does not depend on the size of the mesh, geometry (2-D or 3-D) or complexity of the equations solved (H, TH or THM).

- It is not possible to see a correlation between the ratio Solver/Total and the Speed-up although it is expected that the higher Solver/Total ratio the higher Speed-up.

REFERENCES

[1] PURAM (2015). PURAM annual report 2015. Szeksárd, Hungary.

[2] Posiva (2018). Anual report 2018. Eurajoki, Finland.

[3] Börgesson, L. (1986). Model shear tests of canisters with smectite clay envelopes in deposition holes. SKB TR 86-26. Stockholm, Sweden.

[4] SKB, 2010a. Design, production and initial state of the closure. SKB Technical Report TR-10-17, Stockholm, Sweden.

[5] SKB, 2010b. Buffer, backfill and closure process report for the safety assessment SR-site. SKB Technical Report TR-10-47, Stockholm, Sweden.

A VISCOPLASTIC DAMAGE MODEL COMBINED WITH STRAIN-SOFTENING FAILURE CRITERIONS FOR ROCK MASS

Fei Song[*], Alfonso Rodriguez-Dono[*†] and Sebastia Olivella[*]

[*] Department of Civil and Environmental Engineering
Technical University of Catalonia (UPC)
Campus Nord UPC, 08034 Barcelona, Spain

[†] Institute of Environmental Assessment and Water Research (IDAEA)
Spanish National Research Council (CSIC)
C/ Jordi Girona 18-26, 08034 Barcelona, Spain

Abstract. *Rock mass behaviour model selection, in particular, post-failure behaviour and time-dependent properties of rock masses are critical issues in the design of tunnels. Perzyna viscoplastic model combined strain-softening failure criterions are adopted in this paper, to simulate both the time-dependent and post-failure behaviour of rock masses. Mohr-Coulomb, as well as Hoek-Brown failure criterions are considered in this study. The numerical model is implemented into Finite Element Method software CODE_BRIGHT. As a validation step, the current results agree well with analytical solutions and FLAC 3D numerical results. Parametric analyses are then carried out to investigate the influences of viscosity of rock masses. This study provides a general numerical approach to obtain longitudinal deformation profiles for the excavation of tunnels in Strain-Softening time-dependent rock masses.*

1. INTRODUCTION

The convergence-confinement method is a useful tool for designing tunnels for underground excavations in rock masses. The method consists of three basic graphs: longitudinal deformation profiles (LDPs), support characteristic curves (SCCs), and ground reaction curves (GRCs).

Regarding the LDPs, some methods have been developed for tunnels constructed in elastic [1, 2], Elastic-Perfectly-Plastic [3, 4, 5] and Elastic-Brittle [6] rock masses. All these models, however, do not seem to properly model the behaviour of average quality rock masses [7, 8]. The plastic zone around excavations tends to be larger for strain-softening rock masses compared to Elastic-Perfectly-Plastic rock masses [9]. The response of rocks will differ depending on the selected behaviour model [9]. However, all these papers focus on the post-failure behaviours, but no time-dependent properties is considered.

Most types of rocks exhibit time-dependent behaviour [3], and the time dependency of tunnel convergence and supporting force is mainly due to the rock creep and tunnel face advancement [10, 11, 12]. In some engineering projects, the time effect can contribute up to 70% of the total deformation [13]. Time-dependency resulting in delayed deformation, and failure to account for the added displacements can result in false selecting the time of support installation, causing safety issues for the working [11, 12, 14].

In this study, we attempt to propose a general numerical approach to obtaining LDPs for tunnels excavated in Strain-Softening viscoplastic rock masses, with consideration of: (1) Strain-Softening failure criterions; and (2) time-dependent behaviour of rock masses. The Strain-Softening Mohr-Coulomb and Hoek-Brown failure criterions have been implemented into Finite Element Method (FEM) software CODE_BRIGHT.
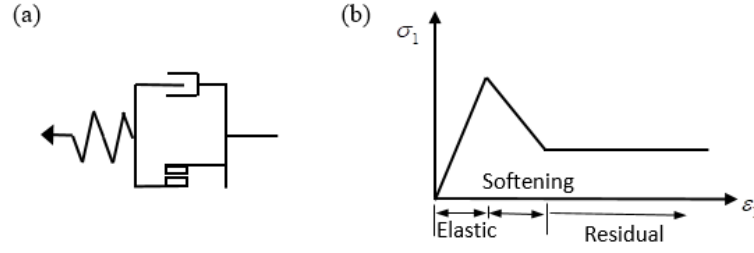
2. METHOLOGY

Figure 1. (a) Perzyna model; (b) strain-softening behaviour or rock.

In elastic-viscoplastic materials, the strain rate can be assumed as the summation of elastic and inelastic part [15, 16], as follows,

$$\dot{\varepsilon}_{ij} = \dot{\varepsilon}_{ij}^{e} + \dot{\varepsilon}_{ij}^{p} \tag{1}$$

where $\dot{\varepsilon}_{ij}^{e}$ is the elastic part of strain rate; $\dot{\varepsilon}_{ij}^{p}$ is the inelastic part, including viscous and plastic effects. The elastic component is assumed to obey the generalized Hooke's law. Perzyna model, as shown in Fig. 1(a), is adopted to simulate viscoplastic behaviour of rock mass. The plastic strain rate of Perzyna model can be expressed [15, 17], as follows,

$$\dot{\varepsilon}_{ij}^{p} = \frac{1}{\eta_{visco}} \langle \Phi(F) \rangle \frac{\partial G}{\partial \boldsymbol{\sigma}} \tag{2}$$

where $\boldsymbol{\sigma}$ is the stress matrix, η_{visco} is viscosity, F is the failure criterion, and G is the viscoplastic potential. The symbol $\langle \Phi(F) \rangle$ is defined as follows:

$$\langle \Phi(F) \rangle = \begin{cases} 0, & if\ F \leq 0 \\ \Phi(F), & if\ F > 0 \end{cases} \tag{3}$$

For simplicity, $\Phi(F) = F^{m} (m \geq 1)$ are adopted in this paper. The viscoplastic model can be simplified to Elastic-Perfectly-Plastic model, when η_{visco} tends to infinite.

Inelastic strain occurs when the stresses achieve a critical state, which can be defined by a yield surface $F = 0$. Only elastic deformation occurs when $F < 0$, and both elastic and plastic strains occurs when $F \geq 0$. In strain-softening damage model, the failure criterions depend not only on the stress tensor σ_{ij}, but also on softening parameter η [9, 18]. The failure criterion is defined as follows:

$$F(\sigma_{ij}, \eta) = 0 \tag{4}$$

Strain-Softening behaviour is characterized by a gradual transition from the peak failure criterion to a residual one, which is governed by the softening parameter η, as shown in Fig. 1(b). In strain-softening model, only elastic regime exists when $\eta = 0$, a softening regime occurs whenever $0 < \eta \leq \eta^{*}$, and the residual regime takes place when $\eta \geq \eta^{*}$ [9, 18]. η^{*} is the softening parameter that controlling the transformation between softening and residual regime. Softening parameter η is defined as follows,

$$\eta = \sqrt{\frac{3}{2} \cdot \left[\left(\varepsilon_x - \varepsilon_m\right)^2 + \left(\varepsilon_y - \varepsilon_m\right)^2 + \left(\varepsilon_z - \varepsilon_m\right)^2 + \left(\frac{1}{2}\gamma_{xy}\right)^2 + \left(\frac{1}{2}\gamma_{yz}\right)^2 + \left(\frac{1}{2}\gamma_{zx}\right)^2 \right]} \quad (5)$$

The expressions of Strain-Softening Mohr-Coulomb failure criterion [19, 20] can be expressed as follows,

$$F = \sqrt{J_2 \cdot (\cos\theta - \frac{1}{\sqrt{3}} \cdot \sin\varphi \cdot \sin\theta)^2 + a^2 \cdot \sin^2\varphi(\eta)} + p \cdot \sin\varphi(\eta) - c(\eta) \cdot \cos\varphi(\eta) \quad (6)$$

where $a = m_{mc} \cdot c \cdot \cot\varphi$. The value of hyperbolic parameter m_{mc} more closer to zero, the yield surface are more closer to hyperbolic shape.

The Strain-Softening Hoek-Brown failure criterion is shown as follows,

$$F = \left[\frac{4}{\sigma_{ci}} \cos^2\theta \cdot \sqrt{J_2} + \frac{2}{\sqrt{3}} \cdot m_{hb}(\eta) \cdot \cos\left(\theta + \frac{\pi}{6}\right)\right] \cdot \sqrt{J_2} - m_{hb}(\eta) \cdot \left(-p + \frac{s_{hb}(\eta) \cdot \sigma_{ci}}{m_{hb}(\eta)}\right) \quad (7)$$

where $m_{hb}(\eta)$, $s_{hb}(\eta)$ are strain-dependent plastic parameters in Hoek-Brown yield surface, respectively; σ_{ci} is of uniaxial compressive strength of intact rock.

Non-associate flow rule is adopted in the model, and the plastic potential in the form of:

$$G = p \cdot \sin\psi + \sqrt{J_2} \cdot \left(\cos\theta - \frac{1}{\sqrt{3}} \cdot \sin\psi \cdot \sin\theta\right) \quad (8)$$

where ψ is dilatancy angle.

3. NUMERICAL MODEL

The tunnels were 5m in diameter and the depth of 1500m implied a field stress of 37.5 MPa. Rock specific weight was 25 KN/m^3 and the Poisson's ratio v was 0.25. The rock masses were formed of a weak intact rock, with m_i=7 and σ_{ci} =35MPa. In CODE_BRIGHT models, the discretised area was 100m*100m. A symmetry axis was set for y=0. The normal displacements were fixed at zero at all boundaries, *i.e.* Dirichelet boundary conditions applied in these models, as shown in Fig. 2(a). Fig. 2(b) presents the mesh quality of GID model. Quadrilateral element type is adopted to mesh the models. Parameters of mechanical properties for the rock mass, are listed in Table 1.

		B2		D2	
		peak	residual	peak	residual
Mohr-Coulomb	Cohesion (MPa)	2.67	1.71	1.88	1.43
	Friction angle	25.7	19.4	20.6	17.5
Hoek-Brown	m_{hb}	1.68	0.637	0.821	0.516
	s_{hb}	0.011	0.0007	0.0013	0.0003
Elastic parameters	E (MPa)	15400		8660	
	v	0.25		0.25	

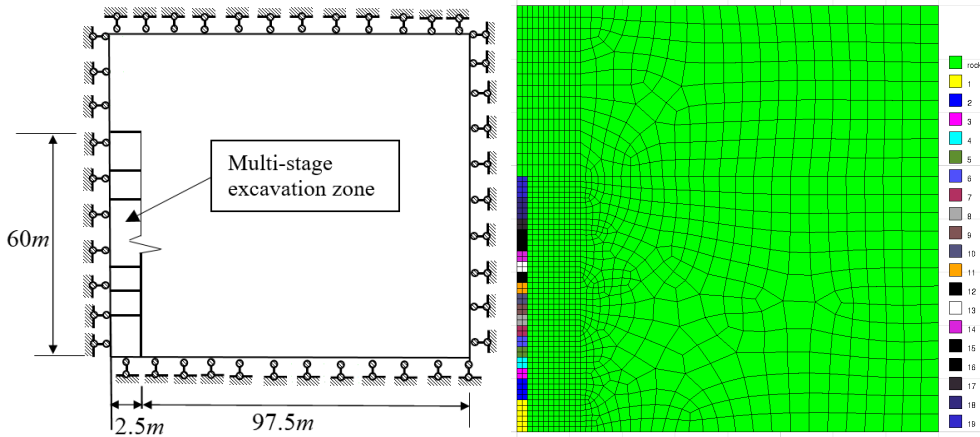Table 1. Strain-softening rock mass parameters

Figure 2. (a) The constraint, calculation domain and boundary conditions in numerical model;
(b) Mesh and geometry of the GID model.

Fig. 2 shows the comparison of LDPs between CODE_BRIGHT and the results in [8], for B2 and D2 Strain-Softening rock masses. A good match between the CODE_BRIGHT, FLAC3D [8] and analytical solutions [5] was apparent for different rock masses, which validates the proposed numerical method in CODE_BRIGHT.
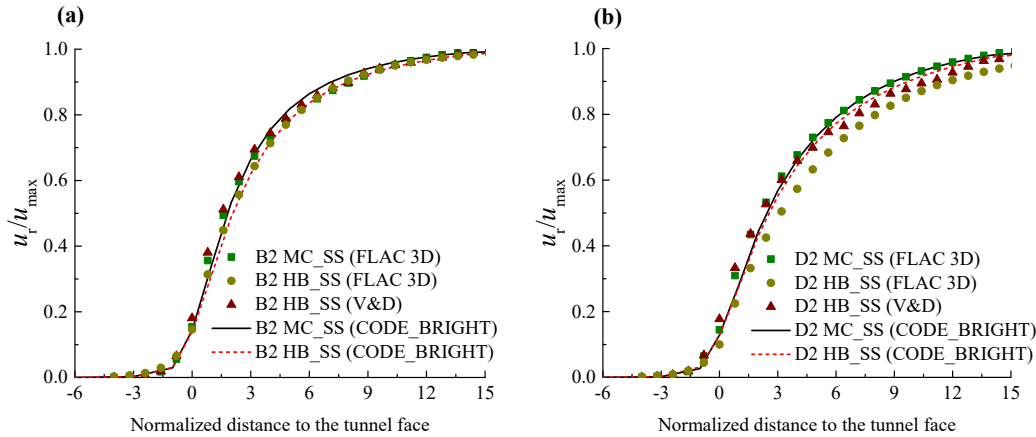

Figure 3. Comparative normalized LDPs for (a) B2, and (b) D2 rock masses, according to CODE_BRIGHT, FLAC3D [8], and analytical solutions [5].

4. RESULTS

In this sub-section, all analysis are based on B2 strain-softening rock masses. Fig. 4(a) shows the incremental displacements after excavation. Fig. 4(b) shows the derivative plastic strain (EDP), which can be used to define the plastic zone. It can be noted that the tunnel is more stability, where closer to the tunnel face.

Time-dependent parameter of rock masses, η_{visco}, is a crucial parameter in tunnel design. Five different viscosity are considered in this section, *i.e.* $\eta_{visco} = 10^{-2}$, 10^{-4}, 10^{-6}, 10^{-8}, 10^{-10}. The LDPs are plotted in Figure 5 for different viscosity and different failure criterions. The results show that smaller viscosity leads to smaller final *x*-displacements. The maximum differences of final *x*-displacements for Mohr-Coulomb and Hoek-Brown failure criterions at the five specific viscosity, account for around 70%, 60% of the corresponding largest values, respectively.
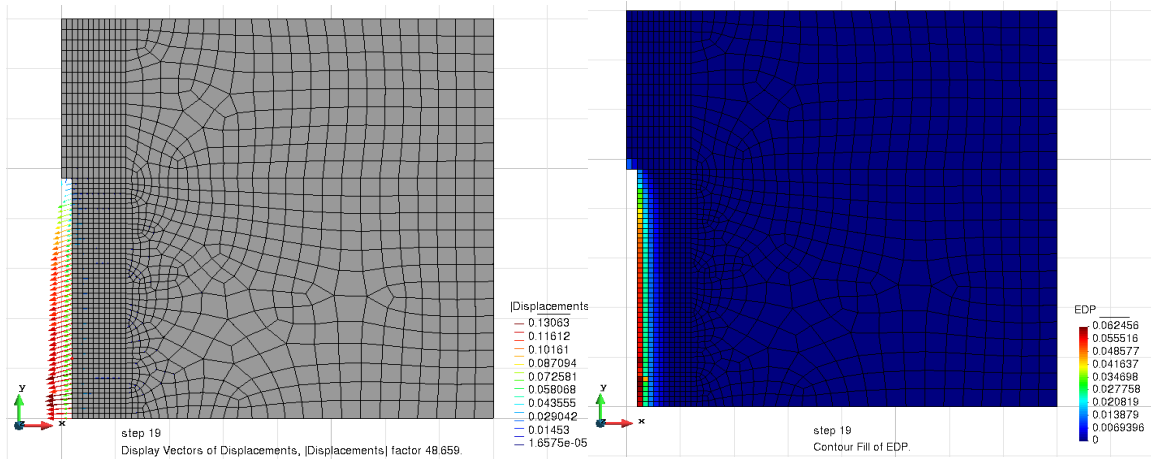
4

Figure 4. (a) The constraint, calculation domain and boundary conditions in numerical model;
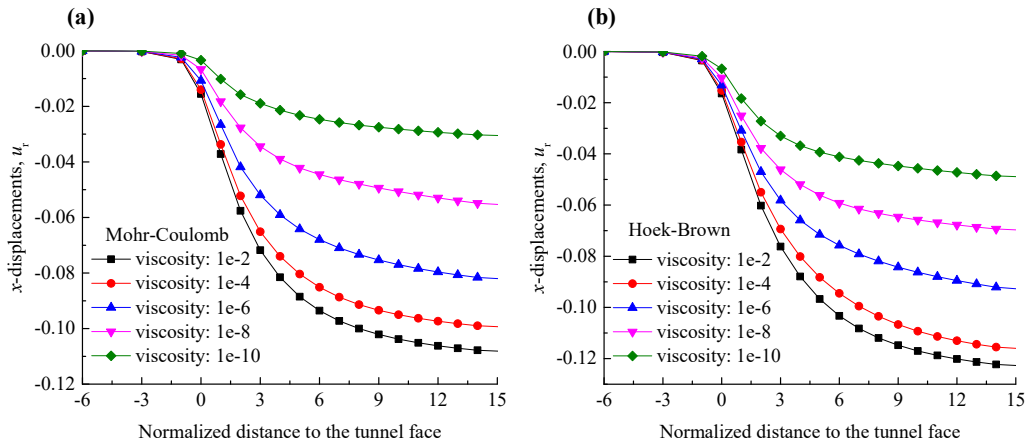(b) Mesh and geometry of the GID model.

Figure 5. LDPs for different viscosity, according to (a) Strain-Softening Mohr-Coulomb, and
(b) Strain-Softening Hoek-Brown failure criterions.

5. CONCLUSIONS

A viscoplastic damage model is implemented in CODE_BRIGHT, and the strain-softening Mohr-Coulomb and Hoek-Brown failure criterions were taken into account. As a validation step, a good agreement between CODE_BRIGHT, FLAC 3D and analytical solutions was obtained eventually. Parametric investigation was then carried out, and the viscosity make a significant effect on the behaviour of tunnels. The proposed numerical model provide a general method for obtaining LDPs in tunnel design.

REFERENCES

[1] Panet, M., 1995. Le calcul des tunnels par la méthode convergence-confinement, Presses ENPC.
[2] Unlu, T. , Gercek, H., 2003. Effect of Poisson's ratio on the normalized radial displacements occurring around the face of a circular tunnel. Tunnelling and Underground Space Technology, 18, (5), 547-553.

[3] Carranza-Torres, C. , Fairhurst, C., 1999. The elasto-plastic response of underground excavations in rock masses that satisfy the Hoek–Brown failure criterion. International Journal of Rock Mechanics and Mining Sciences, 36, (6), 777-809.

[4] Carranza-Torres, C. , Fairhurst, C., 2000. Application of the convergence-confinement method of tunnel design to rock masses that satisfy the Hoek-Brown failure criterion. Tunnelling and Underground Space Technology, 15, (2), 187-213.

[5] Vlachopoulos, N. , Diederichs, M., 2009. Improved longitudinal displacement profiles for convergence confinement analysis of deep tunnels. Rock mechanics and rock engineering, 42, (2), 131-146.

[6] Sharan, S., 2005. Exact and approximate solutions for displacements around circular openings in elastic–brittle–plastic Hoek–Brown rock. International Journal of Rock Mechanics and Mining Sciences, 42, (4), 542-549.

[7] Hoek, E. , Brown, E. T., 1997. Practical estimates of rock mass strength. International journal of rock mechanics and mining sciences, 34, (8), 1165-1186.

[8] Alejano, L. R. ,Rodríguez-Dono, A. , Veiga, M., 2012. Plastic radii and longitudinal deformation profiles of tunnels excavated in strain-softening rock masses. Tunnelling and Underground Space Technology, 30, 169-182.

[9] Alejano, L. ,Rodriguez-Dono, A. ,Alonso, E. , Manín, G. F.-. 2009. Ground reaction curves for tunnels excavated in different quality rock masses showing several types of post-failure behaviour. Tunnelling and Underground Space Technology, 24, (6), 689-705.

[10] Wang, H. ,Li, Y. ,Ni, Q. ,Utili, S. ,Jiang, M. , Liu, F., 2013. Analytical solutions for the construction of deeply buried circular tunnels with two liners in rheological rock. Rock mechanics and rock engineering, 46, (6), 1481-1498.

[11] Paraskevopoulou, C. , Diederichs, M., 2018. Analysis of time-dependent deformation in tunnels using the Convergence-Confinement Method. Tunnelling and Underground Space Technology, 71, 62-80.

[12] Song, F. ,Wang, H. , Jiang, M., 2018. Analytical solutions for lined circular tunnels in viscoelastic rock considering various interface conditions. Applied Mathematical Modelling, 55, 109-130.

[13] Sulem, J. ,Panet, M. , Guenot, A., An analytical solution for time-dependent displacements in a circular tunnel. Proc., International journal of rock mechanics and mining sciences & geomechanics abstracts, Elsevier, 155-164.

[14] Song, F. ,Wang, H. , Jiang, M., 2018. Analytically-based simplified formulas for circular tunnels with two liners in viscoelastic rock under anisotropic initial stresses. Construction and Building Materials, 175, 746-767.

[15] Perzyna, P., 1966. Fundamental problems in viscoplasticity. Advances in applied mechanics, Elsevier, 243-377.

[16] Zienkiewicz, O. C. ,Taylor, R. L. ,Nithiarasu, P. , Zhu, J., 1977. The finite element method, McGraw-hill London.

[17] Olivella, S. , Gens, A., 2002. A constitutive model for crushed salt. International journal for numerical and analytical methods in geomechanics, 26, (7), 719-746.

[18] Alonso, E. ,Alejano, L. ,Varas, F. ,Fdez‐Manin, G. , Carranza‐Torres, C., 2003. Ground response curves for rock masses exhibiting strain‐softening behaviour. International journal for numerical and analytical methods in geomechanics, 27, (13), 1153-1185.

[19] Abbo, A. , Sloan, S., 1995. A smooth hyperbolic approximation to the Mohr-Coulomb yield criterion. Computers & structures, 54, (3), 427-441.

[20] Sloan, S. , Booker, J., 1986. Removal of singularities in Tresca and Mohr–Coulomb yield functions. Communications in Applied Numerical Methods, 2, (2), 173-179.

THM CALCULATIONS FOR FISST EXPERIMENT

Erdem Toprak[1], Sebastia Olivella[2] and Xavier Pintado[3]

[1] International Center for Numerical Methods in Engineering CIMNE
UPC Campus Norte, 08034 Barcelona, Spain
E-mail: erdem.toprak@upc.edu

[2] Department of Civil and Environmental Engineering
UPC Campus Norte, 08034 Barcelona, Spain
E-mail:sebastia.olivella@upc.edu

[3] B+TECH Oy, Laulukuja 4, 00420 Helsinki, Finland
E-mail:xavier.pintado@btech.fi

Key words: THM coupled analysis, Fisst experiment, Nuclear spent fuel disposal

Abstract. *Posiva Oy has a plan for developing a number of demonstration tests in ONKALO underground research facility in Olkiluoto. Finland. The Full-scale In Situ System Test (FISST) is an ongoing project. The test area is located approximately 420 m below the ground surface. The FISST will be instrumented in order to measure the evolution of temperature, hydration and the development of swelling pressure. This paper presents the outcomes of the numerical thermo-hydro-mechanical (THM) modelling of FISST.*

1 INTRODUCTION

This work is a continuation of the modelling task performed and reported in Toprak et al. (2018) and has also been carried out by CIMNE under the supervision of A-Insinöörit Civil Oy in order to study the thermo-hydro-mechanical (THM) behaviour of the EBS clay components during the full-scale test (FISST).

Figure 1 shows the model domain and fracture orientation. The access tunnels, the demonstration tunnels, the surrounding rock volumes and the fractures are shown in Figure 1. Detailed information about the test set-up and system components have been described by Hassan et al., (2018).
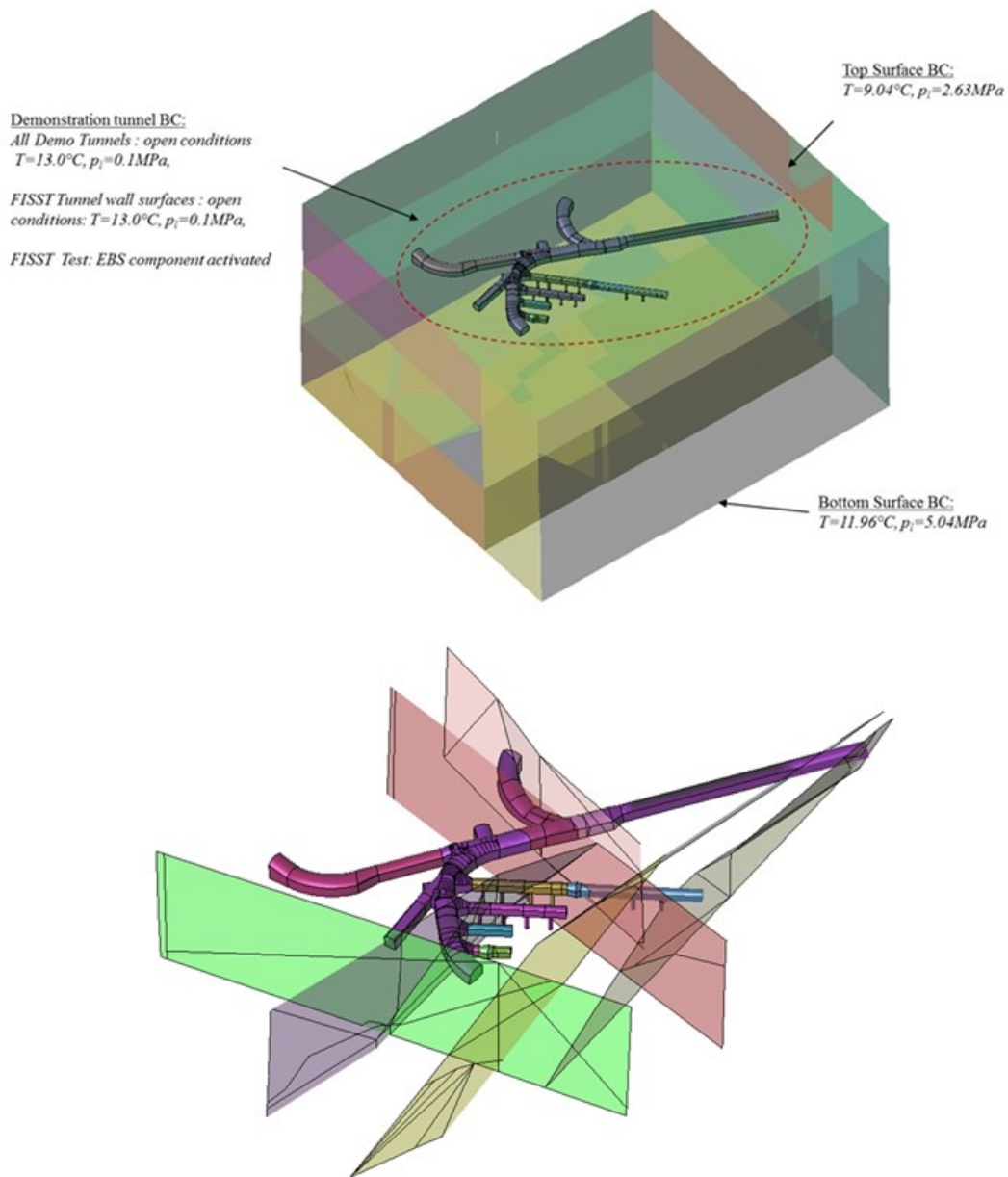
Figure 1. *The model domain of the ONKALO and six fractures in the model domain (Hassan et al., 2018).*

2   RESULTS FOR THM CALCULATIONS

THM calculations were performed under a simplified 3-D geometry (less rock volume and one quarter of the canister). TH boundary conditions for the smaller volume were obtained by the simulation of the full-scale test (Figure 2). This allows the THM calculation to represent one deposition hole and the tunnel section above it as immersed in the full geometry. Thus, the most relevant mechanical evolution can be effectively simulated with significantly reduced model complexity.

A linearization of mechanical properties has permitted to gain robustness of the numerical calculations. Elastic properties of materials are listed in Chapter 2. The rest of the TH parameters have been derived from Toprak et al. (2018).

The initial temperature of the system components and rock at the repository depth were around 13°C and 10.5°C respectively. At their initial state, all the Engineered Barrier System (EBS) components were in unsaturated conditions. However, the rock domain was considered in fully saturated state. The maximum temperature reaches 95 °C on the canister surface (Figure 2) as it is expected.

Table 1. Linear elastic parameters for materials.

Material parameters	K Bulk modulus	ν Poisson's ratio	E Young modulus	s Initial suction	α_s Swelling coeff. ($K_S/3$)	p' Swelling pressure
	(MPa)	(-)	(MPa)	(MPa)	(MPa^{-1})	(MPa)
Pillow pellets	29	0.3	35	83.7	$4{\cdot}10^{-4}$	2.3
Rod pellets	33	0.3	40	23	10^{-3}	2.2
Buffer blocks (MX-80)	89	0.35	80	35	10^{-3}	9.3
Backfill blocks (Friedland clay)	133	0.35	120	65	$3{\cdot}10^{-4}$	7.8
Granules	41	0.3	50	35	10^{-3}	4.3

Figure 3-A shows the evolution and distribution of degree of saturation in the representative points at the end of the simulation. The materials are initially in unsaturated conditions. It can be noted that the central backfill remains unsaturated. Most of the buffer volume reaches full saturation. However, buffer-backfill interface (granules) remains still in unsaturated conditions. The backfill roof (Friedland clay – rod pellets interface) seems fully saturated.

Figure 3-B shows the evolution and distribution of mean effective stress of system components. Buffer blocks have a larger swelling capacity and almost reach the full-saturation state. Therefore, swelling pressure develops faster and higher in buffer blocks. At the end of the simulation, mean effective stress reach 7.8 MPa in buffer blocks. Pillow pellets are also saturated faster because of their limited volume and location. Mean effective stress reaches 3.5 MPa in pillow pellets. Due to slower water intake and lower swelling capacity compare to buffer, mean effective stresses in backfill components have a range of maximum 2 MPa at the end of the simulation.
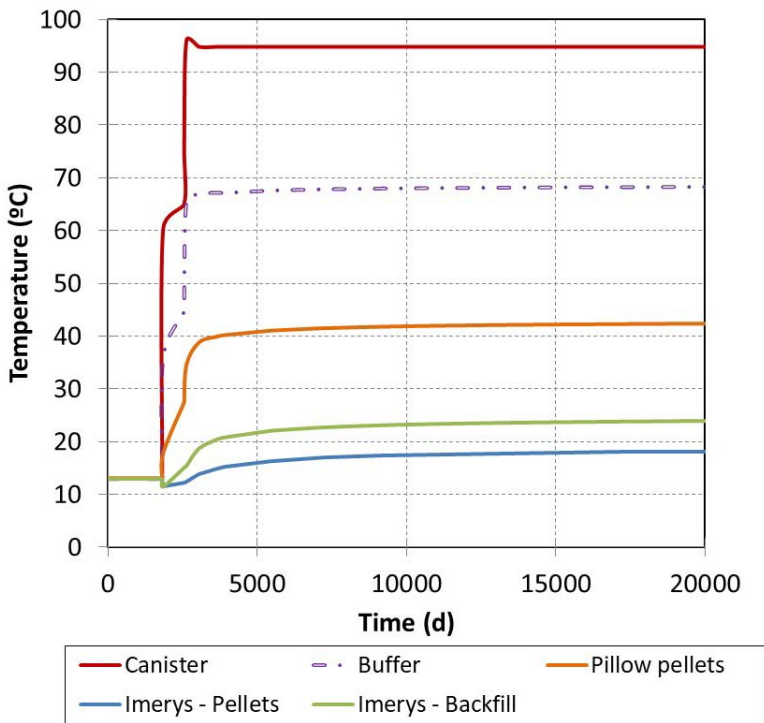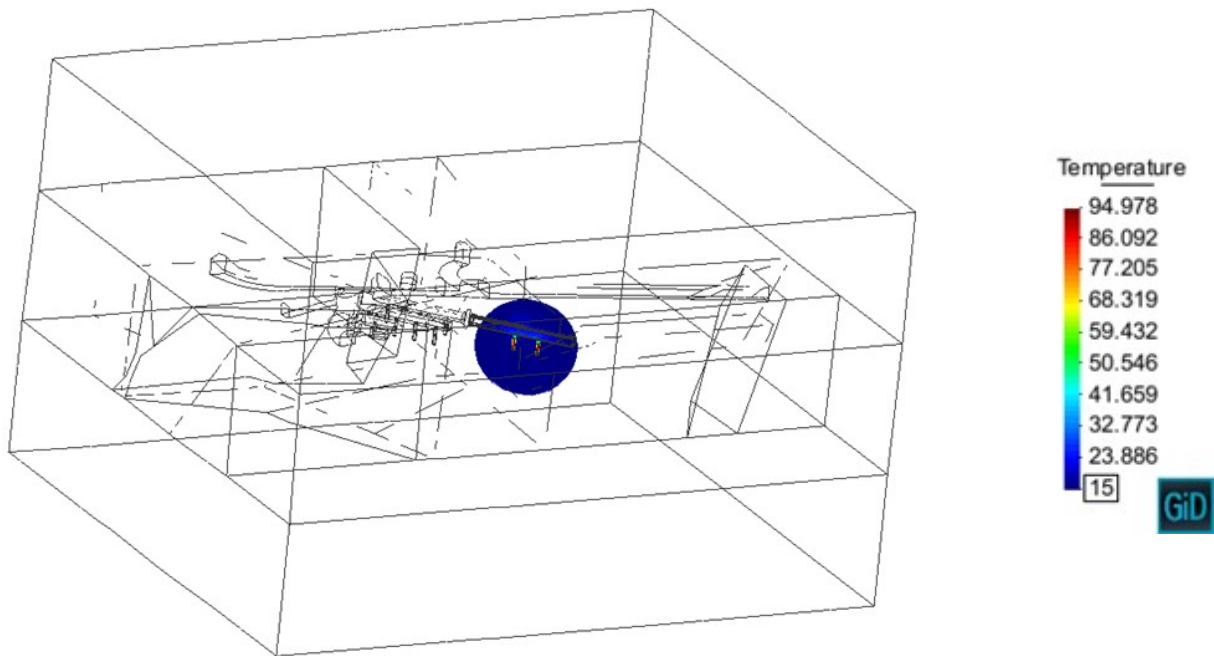
Figure 2. *Temperature distribution in model volume and evolution of temperature in representative points.*
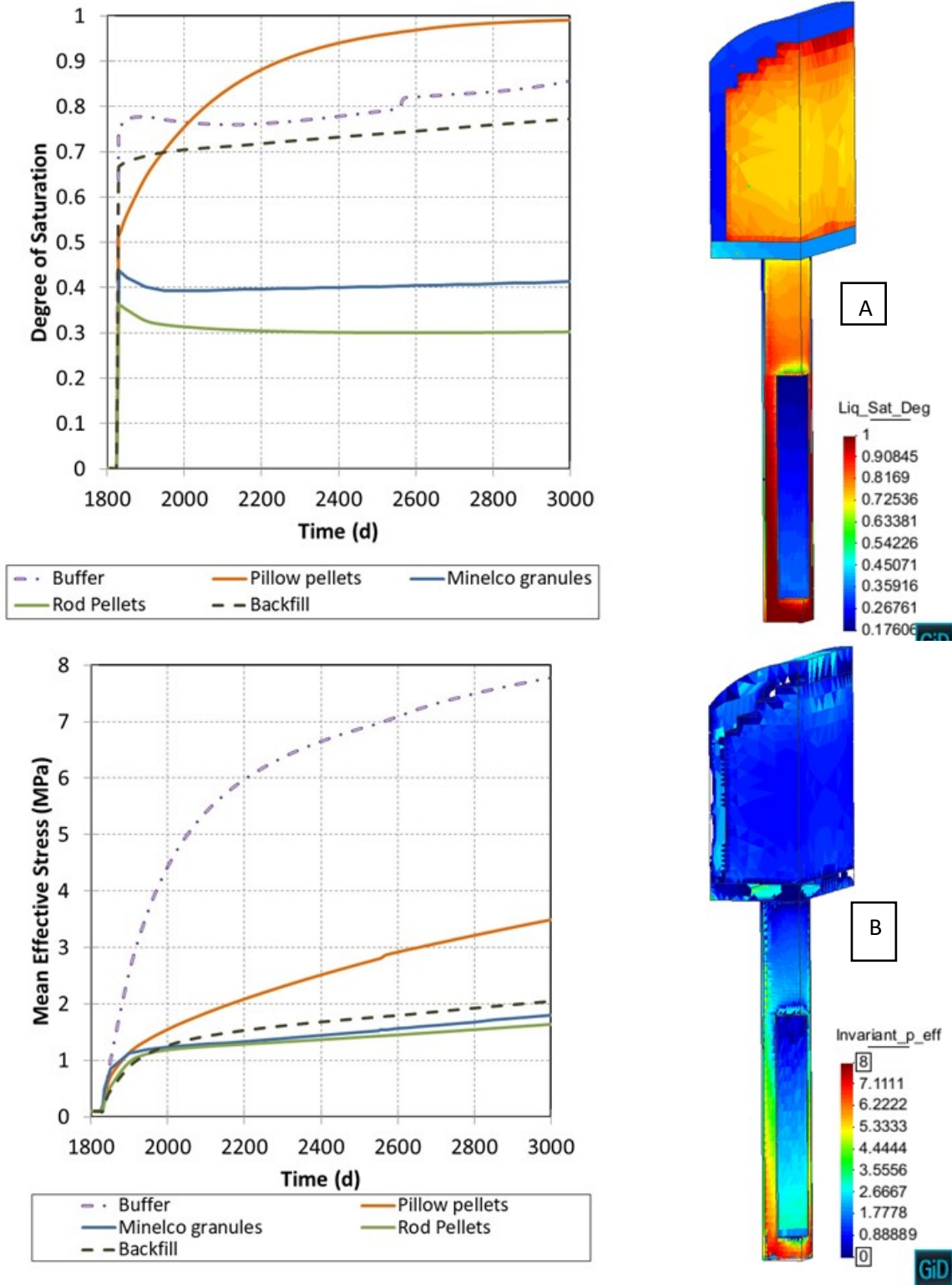
Figure 3. *Evolution of saturation degree (A) and mean effective stresses (B) on represantive points and their distrubution at the end of test (3000 days) respectively.*

3. CONCLUSIONS

In this study, TH calculations for FISST in a complete model domain have been investigated. The study of Hassan et al. (2018) has been considered as a reference report for the TH calculations. The complete model domain has been used to determine TH boundary conditions of simplified 3-D geometry. Once the TH boundary conditions were set by means of complete model domain calculations, a simplified geometry has been proposed for THM calculations. The materials in THM calculations have elastic parameters combining suction and thermal expansion effect. Retention curve parameters for pellets and granules have been updated according to recent data. A set of sensitivity analyses have been performed to fix the elastic parameters for the materials. Heating, saturation - desaturation process and also stress-displacement generation has been studied for simplified 3-D geometry.

There is still no data available from the test site. Therefore, a comparison of the model results over test data is not possible by means of this report. Checking model performance over test data is a future work. In this report, linear elastic parameters for materials have been calibrated. Performing elasto-plastic calculations in 3-D geometry is also a future task.

REFERENCES

Hassan, M., Pintado, X., & Laurila, T. (2018). Thermo-Hydro (TH) modelling of the FISST Experiment. Eurajoki, Finland, Posiva Oy. Technical Memorandum. Publication pending.

Toprak E. (2018). Long term response of multi-barrier schemes for underground radioactive waste disposal. PhD dissertation. Technical University of Catalonia. Barcelona, Spain

MODELLING HEAT TRANSPORT AT THE FRESH-SALTWATER INTERFACE IN COASTAL AQUIFERS

Laura del Val[*,‡]**, Maarten W. Saaltink**[*,‡]**, Albert Folch**[*,‡]**,Maria Pool**[†,‡]**, Jesús Carrera**[†,‡]

[*] Department of Civil and Environmental Engineering, Universitat Politècnica de Catalunya (UPC),
Jordi Girona 1-3, 08034 Barcelona, Spain
Email: lauradelvalalonso@gmail.com

[†]Institute of Environmental Assessment and Water Research (IDAEA), CSIC, Jordi Girona 18, 08034
Barcelona, Spain

[‡]Associated Unit: Hydrogeology Group (UPC-CSIC).

Abstract. *Fiber Optic Distributed Temperature Sensing (FO-DTS) is emerging as a data-rich technology for groundwater monitoring applications. Its potentials and limitations are object of many publications in recent years. In this case, this technology is tested to monitor the fresh-salt water interface of a Mediterranean coastal aquifer. Several months of continues temperature data were recorded. The data set reflects thermal changes associated to strong seawater intrusion events. A coupled heat and solute transport model of the fresh-salt water interface is built with Code_Bright. The model is used to confirm the conceptual model defined from the interpretation of the FO-DTS data and test the usability of this technology for coastal aquifers monitoring*

1   INTRODUCTION

As pressure on coastal fresh groundwater resources increases, interest in coastal aquifers monitoring rises. The weakest point of coastal aquifers occurs at the fresh-salt water interface induced by seawater intrusion (SWI), highly sensible to any change in the heads of the fresh and salt water bodies. Therefore, the position, width and dynamics of the interface is one of the main features of a costal aquifer to be monitored and understood. However, the interface is highly dynamic, responding to increases in sea level, sea surges, sea tides, seasonal recharge or groundwater pumping. These processes act at extremely different time and spatial scales, which make them difficult to be captured with ordinary monitoring techniques.

Traditionally, changes in electric conductivity have been used to identify and monitor the interface in coastal aquifers. Alternatively, natural differences in temperature between fresh and the saline groundwater bodies are also known to provide useful information [i]. In relation to the use of temperature as a groundwater tracer, Fibre Optic Distributed Temperature Sensing (FO-DTS) is increasingly being used in the field of hydrogeology because of its high spatial (0.25 m) and temporal resolution (10 s) [ii]. We want to use this high resolution for monitoring the fresh-salt water interface in coastal aquifers. However, one of the biggest limitations of FO-DTS applied to environmental monitoring is the temperature resolution, strongly dependent on the calibration processes, length of the cable, or amount of junctions. This implies that only phenomena causing enough contrast in temperature can be recorded.
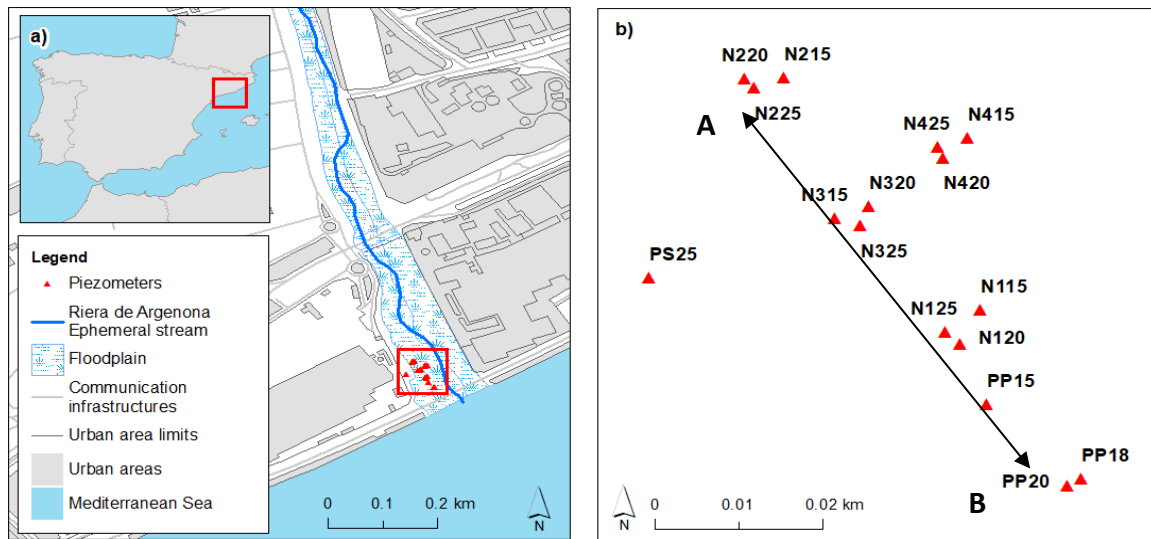
Figure 1: a) Location of the MEDISTRAES experimental site and b) distribution of piezometers in the field

Given the amount of uncertainty associated to the use of FO-DTS and temperature as a tracer for the fresh-sat water interface, a numerical model is built to confirm the conceptual model behind the FO-DTS field data. Code_Bright [iii] (Coupled Deformation of BRIne Gas and Heat Transport) is used to model the density driven fluxes at the fresh-salt water interface, as it accounts for heat and solute transport coupled with variable density.

2 FIELD EXPERIMENT

We test the FO-DTS technology in the MEDISTRAES (MEzcla y DISpersion en el TRAnsporte de Energia y Solutos) project experimental site (**Figure 1a and 1b**). Seventeen piezometers were equipped with fiber optic cable (Brugg Kabel AG, Switzerland). The cable was deployed with an Oryx+ (Sensornet, UK) distributed temperature sensor, with a spatial resolution of 1 m. The system was monitoring continuously for more than a year with a data acquisition frequency of 15 min. Additionally, data on groundwater levels, temperature and electric-conductivity was measured independently in each piezometer.

Distributed temperature data reflects some of the fresh salt-water interface dynamics, especially those related to sea surges, when an increase in sea level, due to low atmospheric pressure, leads to an advancing of the seawater intrusion inland. In those events the salt water intrusion and retreat is accompanied by a change in temperature of a couple of degrees (Figure 2)

3 NUMERICAL MODEL

Code_Bright is a 3D multiphase model able to solve coupled thermo-hydro-mechanical problems in porous media. In this case, we are interested in the coupling between solute transport and heat transport with variable density flow for fully saturated media. The problem is simplified in a 2D vertical cross-section (**from A to B in** Figure 1b) assuming groundwater gradient direction is perpendicular to the seashore and stratification is predominantly horizontal.
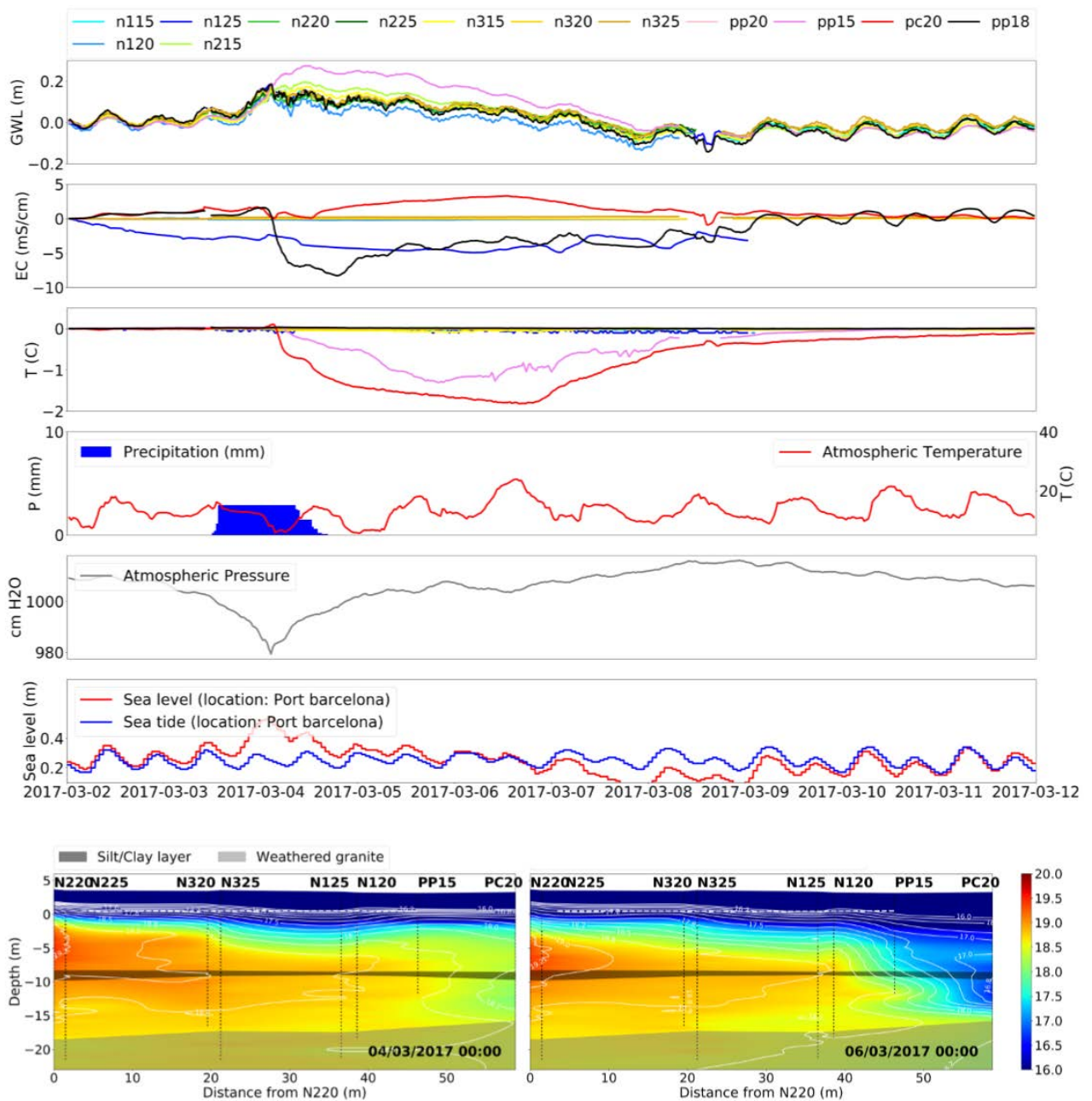
Figure 2 Time evolution of changes in Groundwater level (GWL), Electroconductivity (EC), and Temperature in each piezometer. Time evolution of Precipitation (P), atmospheric temperature (T), atmospheric pressure and sea level. 2D cross sectional interpolation of DTS data before and after rainfall event.

Boundary Conditions

The model extents around 250 m offshore, until the contact between the most confining silty layer with the bathymetry, and 300 m inland, where a piezometer is considered the upstream boundary condition (**Figure 3** Model conceptualization). The bottom is considered to be impermeable. An effective recharge function is imposed on the upper boundary.
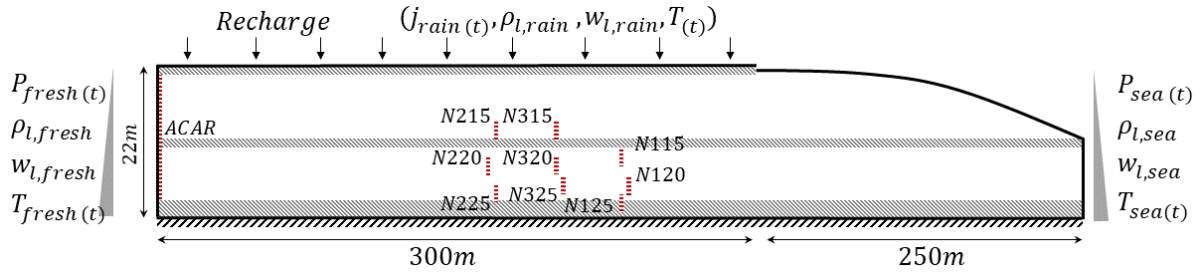
Figure 3 Model conceptualization

A key feature of coastal groundwater models is the way in which variable head boundary at the sea is considered. This boundary should fix a hydrostatic pressure to each node located below sea level (h), allowing nodes above the sea level to reach atmospheric pressure. This specific boundary condition has been implemented in Code_Bright as follows:

If the node is below the sea level($y_{node} \leq h$), we impose a hydrostatic pressure:

$$j_l = \gamma_l(P_l^0 - \rho_l^* \cdot \xi_l \cdot (y_{node} - h) - P_l) \qquad (1)$$

If the node is above sea level($y_{node} > h$), we impose a recharge with the possibility of seepage:

$$j_l = j_l^0 \quad If \ P_l < P_l^0 \Rightarrow \qquad (2)$$

$$j_l = j_l^0 + \gamma_l \cdot (P_l^0 - P_l) \ If \ P_l > P_l^0 \quad (3)$$

Where P_l [MPa] is the pressure at the node, P_l^0 is the reference pressure (atmospheric pressure) [MPa], j_l is the liquid flux at the node [kg s^{-1}], j_l^0 is a recharge flux specified by the user [kg s^{-1}], γ_l is a leakage coefficient or conductance, ρ_l^* is the density of the surface water [Kg m^{-3}], ξ_l is the gravitational acceleration (9.81·10^{-6} Mm·s^{-2}) and y_{node} is the elevation of the node [m].

This type of boundary conditions was used for both sea level and groundwater level upstream, where liquid pressure (P_l) and temperature (T [ºC]) were fixed through time functions, and concentration [Kg/Kg] was set to an average value. The recharge at the top is represented by imposed flux (j_l^0 [Kg s^{-1}]) and temperature [ºC] that varies in time. Concentration of the recharge water is kept constant.

Material properties

The horizontal discretization is composes of an alternation of silty and sandy layers, creating two main levels of semi-confined aquifers. The vertical discretization is bind at the top by a buffer layer with high storage coefficient, while the bottom layer represents the weathered granite. A low permeability layer situated above the impermeable granite represents the aquifer basement.

In groundwater flow problems where deformation and compressibility are not considered, hydraulic parameters are traditionally expressed through the hydraulic conductivity and the

storage coefficient. Code_Bright does not consider explicitly the storage coefficient as an input parameter.

The specific storage coefficient (S_s) can be expressed as function of the soil (α) and liquid compressibility (β):

$$S_s = (\alpha + \emptyset\beta)\rho g \quad (4)$$

Where ρ is the density of the liquid phase [Kg m^{-3}], $\emptyset$ is the porosity and g is the gravity [m s^{-2}].

We adapt the retention curve linear model (5) to account for the storage coefficient.

$$\frac{S_l - S_{rl}}{S_{ls} - S_{rl}} = 1 - \frac{(P_g - P_l - P_{CO})}{P_0} \quad (5)$$

Where, S_l is the liquid saturation, S_{rl} is the liquid residual saturation, which we consider to be cero, S_{ls} is the maximum saturation, P_g is the gas pressure [MPa] considered in this case to be 0.1 MPa, P_l is the liquid pressure [MPa], P_0 is a reference pressure [MPa] and P_{CO} is a residual saturation [MPa].

For the unsaturated top layer, parameters P$_0$ and P_{CO} in equation (5) are calculated based on the maximum and minimum groundwater levels (h) reached in the layer:

$$S_l = 1 + \frac{(\rho g h - P_{CO})}{P_0} \quad (6)$$

By combining equations (4) and (5), we calculate the P$_0$ the fully saturated layers, and with stablishing a maximum and minimum pressures and its corresponding saturation indexes we calculate P_{CO}:

$$P_0 = \frac{\emptyset}{\alpha} \quad ; \quad P_{CO} = P_g - P_{l\,max} \quad (7)$$

By setting the liquid relative permeability (kr) to 1, we ensure that the flux doesn't depend on the degree of saturation.

4 RESULTS

The model ran for a period of 30000 days until it reached steady state. The steady state results were used as initial conditions for the transient model. Time dependent boundary conditions were set for pressure and temperature for both upstream and sea boundary conditions. Time dependent effective recharge flux and temperature were imposed for the upper boundary. The transient period corresponds to data collected over more than two years (800 days).

Changes in pressure in 10 monitored piezometers compares well with preliminary results of the model (Figure 4). These results indicated that, at least with respect to the groundwater flux, the model reflects changes in groundwater levels due to changes in boundary conditions. The only exceptions (n215 and n315) are related to a possible semi-confinement of the upper aquifer layer, which is not considered at this stage. Further work needs to be done to calibrate the regional gradient of the model.
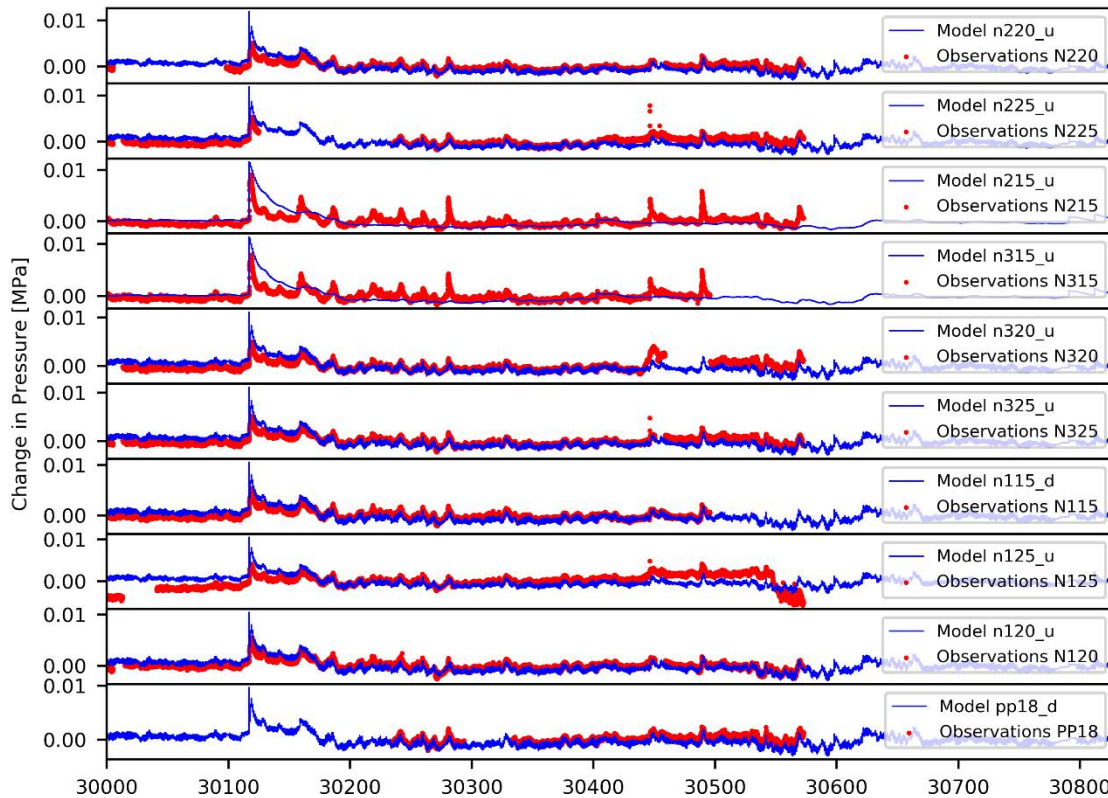
Figure 4 Change in pressure [MPa] in 10 piezometers comparing observed data versus modeled data

Results of solutes and temperature evolution at the not shown as further work is currently been done to calibrate them with respect to real data.

5 CONCLUSIONS

- FO-DTS is a promising technology for monitoring coastal aquifers response to intrusion events like storm surges.
- Code_Bright is a useful tool to model for density-depend problems in coastal aquifers.
- Current version of the model is able to model changes in groundwater levels due to changes in the boundary conditions.
- On-going work is focusing on calibrating the hydraulic component of the model , and in adding solutes and heat transport.

REFERENCES
[i]   M. Taniguchi, "Evaluations of the saltwater-groundwater borehole temperature in a coastal region," *Geophys. Res. Lett.*, vol. 27, no. 5, pp. 713–716, 2000.
[ii]   S. W. Tyler *et al.*, "Environmental temperature sensing using Raman spectra DTS fiber-optic methods," *Water Resour. Res.*, vol. 45, pp. 1–11, 2009.
[iii]   S. Olivella, A. Gens, J. Carrera, and E. E. Alonso, "Numerical formulation for a simulator (CODE_BRIGHT) for the coupled analysis of saline media," *Eng. Comput. (Swansea, Wales)*, vol. 13, no. 7, pp. 87–112, 1996.

SHEAR DEFORMATION ANALYSIS OF CANISTER-CLAY AS A ENGINEERED BARRIER PRINCIPLE FOR SPENT FUEL ISOLATION

Peiman Khadivipanah [a], **Xavier Pintado** [b], **Sebastia Olivella** [a], **Jean Vaunat** [a]

[a] Department of Civil Engineering, Technical University of Catalonia, Barcelona, Spain

[b] AINS Group, Espoo, Finland

Abstract

There is a necessity to adequately represent the canister behaviour under thermo-mechanical coupling in the context of a THM calculation using porous media tools. Elasto-visco-plastic theory can be used to represent the behaviour of the canister. Although the canister is very stiff and strong and although it will be emplaced in a clay volume, shear deformations occurring on the engineered barrier may have an impact on the canister. On the other hand, a repository of spent nuclear fuel is analysed under extreme conditions as it is a long-life system and has to resist all types of environmental conditions, for instance including earthquakes and glaciations.

In the present work, Canister-clay shear tests using total stress and effective stress methods are modeled and calculated in CODE_BRIGHT. Sensitivity analysis on the types of meshes and important parameters of two methods was performed and finally, these two models are compared together.

Sensitivity analyses represent alternate models or data to those of the Base Case to develop a better understanding of the modelled system but remain within the scope of the base. Analyses of the sensitivity cases illustrate the effect of model and data uncertainties.

Keywords: Shear test, Copper canister, Hydro-mechanical analysis, CODE_BRIGHT

Shear test modelling using effective stress approach in 2 dimensional

Mock-up scale

In buffer design, where the saturation process and swelling pressure development are assessed, the canister is more a boundary condition than an element that should be analysed. The canister is a source of heat, an impervious volume and an almost rigid element without strains. This assumption can be considered exact in thermo-hydraulic analysis and almost accurate when the mechanical problem is considered but the stresses developed in canister are still far from the yield stress of its components (copper and cast iron). In buffer shearing due to an earthquake or a relative movement between the lips of a fracture crossing a deposition hole, there could be possible to reach yield stresses in canister, so this element should be considered as accurate as possible in order to have realistic movements on its surface that could influence on the stress state of the buffer.

In effective stress, the dimensions and boundary conditions of shear test are similar to the dimensions and boundary conditions in the shear test in total stress and flow in hydraulic boundary condition is zero in Figure 2. The initial stress is -8 MPa. The MX80 bentonite clay is fully saturated. The degree of saturation is directly related with water content and dry density. The porosity is related directly with the dry density. In all lines of boundaries (two dimensional), hydro-static water pressure is applied.
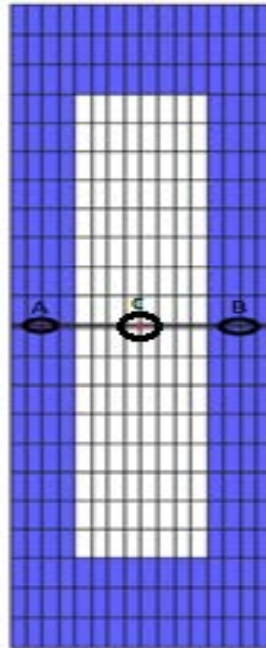

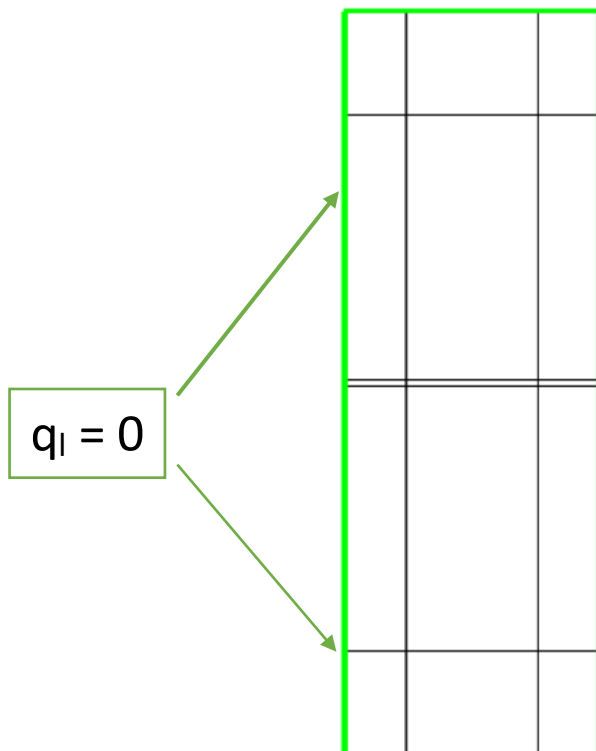**Fig. 1.** Canister-clay shear test using effective stress approach
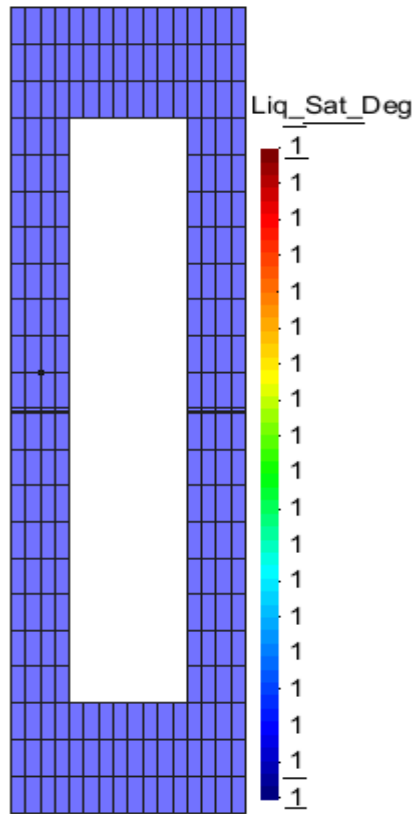

$q_l = 0$

Fig. .2. Flux boundary condition

Fig. 3. Contour fill of Degree of saturation at the end of test in laboratory scale.

In effective stress approach, BBM model [6] is used for the bentonite and it is shown in Table 1. The model is saturated and has drained condition.

Table 1. Input parameters of the bentonite in effective stress approach [6].

	ν		0.3	Poisson's Ratio
	k_{min}	MPa	10	Minimum bulk modulus
	K_{i0}		0.05	Initial elastic slope for specific volume-mean stress
	$\lambda(0)$		0.15	Slope of void ratio-mean stress curve at zero suction
BBM Model	r		0.8	Parameter defining the maximum soil stiffness
	β	$(MPa)^{-1}$	0.02	Parameter controlling the rate of increase of soil stiffness with suction
	p^c	MPa	0.1	Reference pressure
	p_0^*	MPa	10	Initial preconsolidation mean stress for saturated soil
	M		1.07	Critical state line parameter

For the canister, linear elasticity model and Bodner-Partom Viscoplasticity model [2] is used for effective stress approach. It is shown in Table 3.2.

Table 2. Input parameters of the copper in effective stress approach [4].

Linear elasticity	v		0.35	Poisson's Ratio
	E	MPa	133000	Young modulus
Bodner-Partom Viscoplasticity	D_0	s^{-1}	10^4	Limiting strain rate
	Z_0	MPa	31	Initial value of the internal state variable Z
	Z_1	MPa	237	Saturated value of the internal state variable Z
	m_0	$(MPa)^{-1}$	0.15	Initial value of hardening parameter
	m_1	$(MPa)^{-1}$	0.25	Saturated value of hardening parameter
	α	$(MPa)^{-1}$	0.50	A material constant

Fig 4. Initial Porosity

Constant 0.01

Constant 0.388

Fig 5. The liquid pressure (P_l) in initial unknown

_Constant 0 0 0

-35.4 0 0 0 0 0 0 0

0 0 0 0 0 0 0 0 0

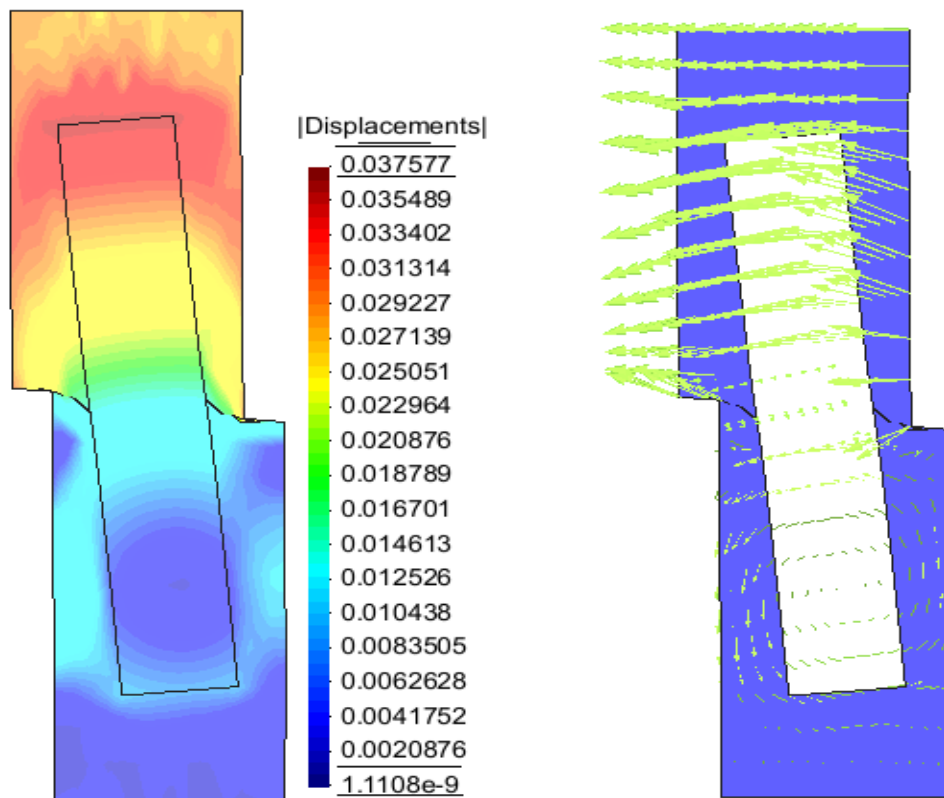_Constant 0 0 0 1 0

0 0 0 0 0 0 0 0 0 0

0 0 0 0 0

Fig 6. Deformation and Display vector of canister-clay in Hydro-Mechanical modelling

Fig. 7. Interface of Canister-clay with green colour.

The liquid pressure for copper is equal to -35.4 MPa and this is due to the fact that liquid pressure could not enter to the canister and liquid pressure for bentonite is equal to 1 MPa. On the other hand, liquid pressure of canister-clay interface is 1 MPa because the water is in out of the copper, and the copper is under the liquid pressure of the bentonite. The interface is shown in Figure 7.

The undrained shear strength for BBM model is calculated in following equation:

$$C_u = P' \cdot \frac{M}{2} \ (\frac{P_0^*}{2P'})^{\frac{\lambda-k}{\lambda}}$$

(3 − 1)

$$C_u = (7) * \frac{1.07}{2} * \left(\frac{10}{2*7} \right)^{\frac{0.15-0.05}{0.15}} = 3 \ MPa$$

$$P' = 8 - 1 = 7 \ MPa$$

Sensitivity analysis of mesh

Sensitivity analysis of mesh in three types of rough, medium and fine meshes for permeability of 5.59×10^{-20} m^2 was performed. The fine mesh has 672 elements and 731 nodes, the medium mesh has 384 elements and 425 nodes and the rough mesh has 224 elements and 225 nodes.
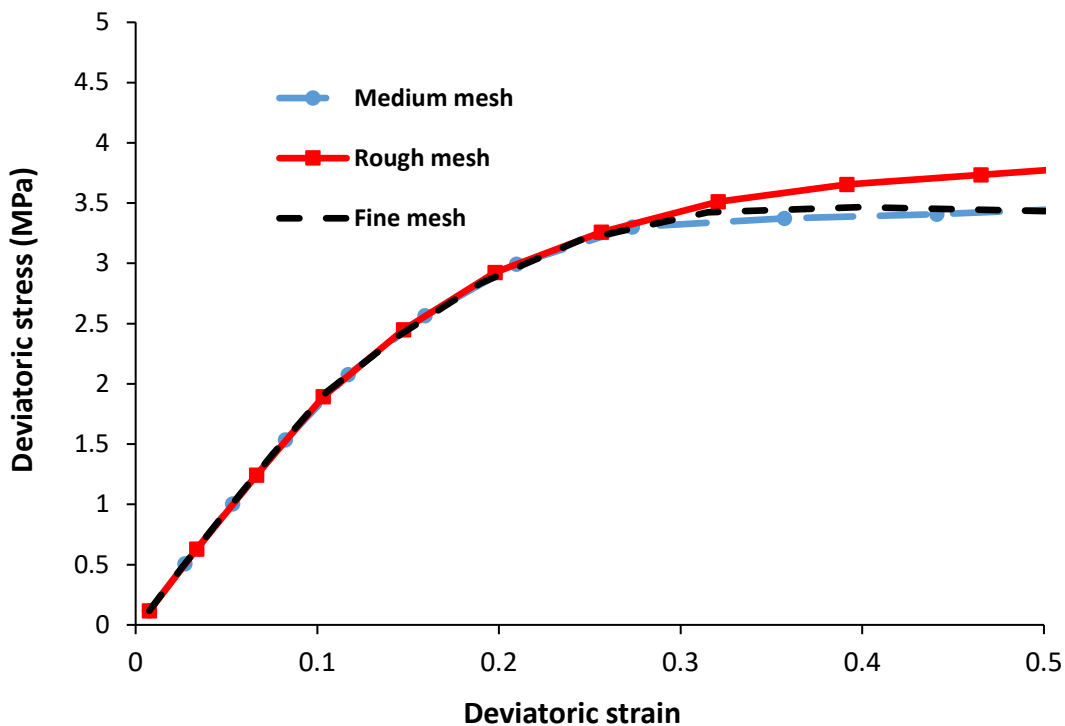

Fig. 8. Comparison between rough, medium and fine meshes for bentonite in effective stress approach (Point A).
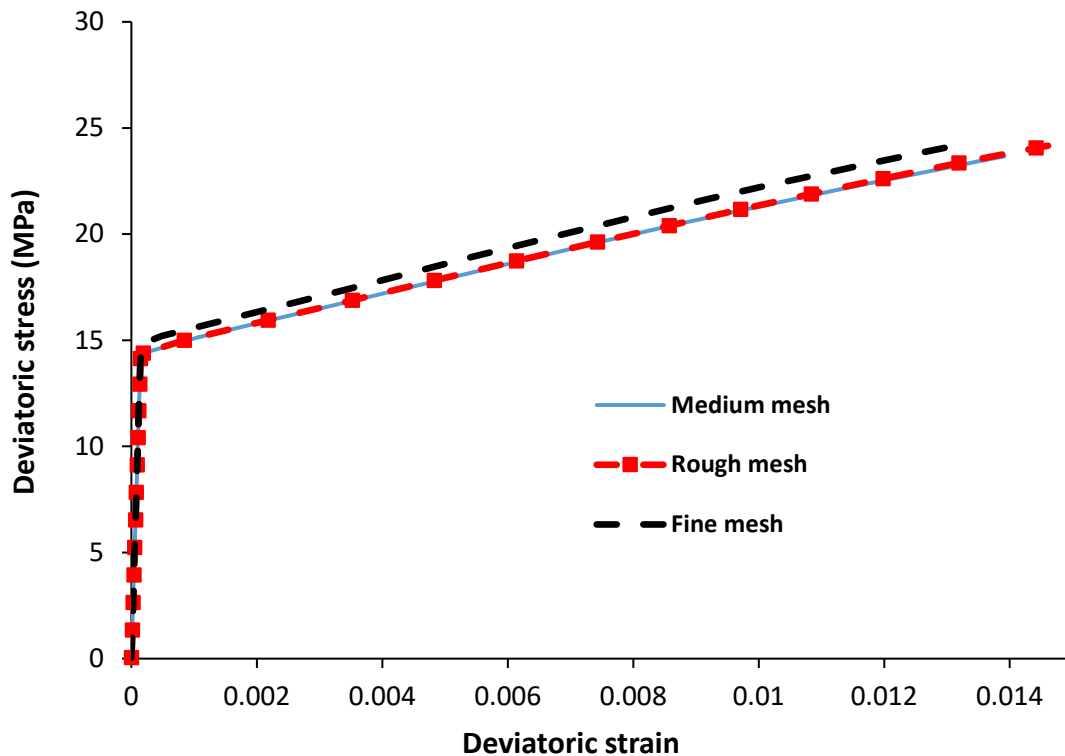
Fig. 9. Comparison between rough, medium and fine meshes for copper in effective stress approach

(Point B).

The point A is chosen from Figure 1 and according to the Figure 8, the deviatoric stress in rough mesh is bigger than the deviatoric stress in medium and fine mesh for bentonite. Finally, the point C is selected in Figure 1 for copper and then it is shown in Figure 9 in which deviatoric stress in rough and medium meshes is the same but the deviatoric stress in fine mesh is bigger than the other meshes.

References

[1] Terzaghi, K. 1925.Erdbaumechanik(in German), Franz Deuticke, Vienna.

[2] CODE_BRIGHT USER'S MANUAL 2018. UPC Geotechnical Group.

[3] Börgesson, L. (1986). Model Shear Tests of Canisters with Smectite Clay Envelopes in Deposition Holes. SKB Technical Report 86-26.

[4] Drucker, DC and Prager, W. (1952) "Soil mechanics and plastic analysis or limit design", Quart. Applied Math. Vol. 10, No. 2, pp 157-165.

[5] Bodner. S.R, Merzer. A. (1978). "Viscoplastic constitutive Equations for Copper with strain rate History and temperature Effects", Faculty of Mechanical Engineering, Technion - Israel Institute of Technology, Haifa, Israel.

[6] Alonso EE, Gens A and Josa A (1990) A constitutive model for partially saturated soils. Géotechnique 40(3): 405-430. 1990. pp. 405-430.

[7] Börgesson L, Dueck A, Johannesson L-E. (2010). Material model for shear of the buffer. Evaluation of laboratory test results. SKB TR-10-31, Svensk Kärnbränslehantering AB.

[8] Rajendran. A. M, Grove. D. J. (1987). "Bodner-Partom viscoplastic model in Stealth finite difference code", University of Dayton Research institute 300 College Park Dayton, OH 45469.

[9] Heikki Raiko, VTT, Håkan Rydén, Magnus Johansson. (2010). Design analysis report for the canister, Svensk Kärnbränslehantering AB.

[10] Olivella. S, Gens, A., Carrera, J. EE Alonso. (1996). "Numerical formulation for a simulator (CODE_BRIGHT) for the coupled analysis of saline media", Polytechnic University of Catalonia (University in Barcelona, Spain).

[11] Sierakowski. R. L. (1997)." Strain rate behavior of metals and composites", Civil and Environmental Engineering and Geodetic Science the Ohio State University, Columbus, Ohio USA.

[12] Jan Hernelind. (2014). Modelling of a canister with broken insert subjected to earthquake induced shear and subsequent glacial load, 5T Engineering AB.

[13] Skipor. A.F, Harren. S.V. (1998). Thermal cycling of temperature and strain rate dependent solder joints. Mechanics of Time-Dependent Material, 2: 59-83.

[14] Olivella. S., Gens. A. and Vaunat. J, Garitte. B. (2009). Application of multiphysical geomechanics in underground nuclear waste storage. Eur. J. Env. Civil Engng 13, No. 7-8, 937-962.

[15] Klosowski. P, Woznica. K.(2004). Numerical treatment of elasto viscoplastic shells in the range of moderate and large rotations. Computational Mechanics, 34: 194-212.

[16] Klosowski. P, Zagubien. A, Woznica K.(2004). Investigation on rheological properties of technical fabric Panama. Archives of Applied Mechanics, 73(9-10): 661-681.

[17] Perzyna. P.(1996). Fundamental problems in viscoplasticity. Advances in Mechanics, 9:243-377.

[18] Johnson. G.R, Cook. W.H.(1983). A constitutive model and data for metals subjected to large strains, high strain rates and high temperatures. 7th International Symposium on Ballistics, The Hague, pp. 541-547.

[19] Zerilli. F.J, Armstrong R.W.(1997). Dislocation-mechanics-based constitutive relations for material dynamics calculations. Journal of Applied Physics, 61(5): 1816-1825.

[20] Khan. A.S, Huang. S.(1992). Experimental and theoretical study of mechanical behaviour of 1100 aluminum in the strain rate range 10^{-5}-10^{4} s^{-1}. International Journal of plasticity, 8: 397-424.

[21] Jiang. L, Wang. H, Liaw. P.K, Brooks. C.R, Klarstrom. D.L.(2004). Temperature evolution during low-cycle fatigue of ULTIMET alloy: experimental and modeling. Mechanics of materials, 36: 73-84.

[22] Skipor. A.F, Harren. S.V.(1998). Thermal cycling of temperature and strain rate dependent solder joints. Mechanics of Time-Dependent Material, 2: 59-83.

[23] Rubin. M.B.(1989). A time integration procedure for plastic deformation in elastic-viscoplastic metals. Zeitschrift fur Angewandte Mathematics und Physik (ZAMP), 40(6): 846-871.

[24] Sung. J.C, Achenbach J.D.(1990). Heating at a propagating crack tip in a viscoplastic material. International Journal of Fracture, 44(4): 301-309.

[25] Foringer. M.A, Robertson D.D, Mall. S.(1997). A micromechanics-based approach to fatigue life modeling of titanium-matrix composites. Composites Part B, 28B: 507-521.

[26] Arya. V.K.(1996). Efficient and accurate explicit integration algorithm with application to viscoplastic models. International Journal for Numerical Methods in Engineering, 39(2): 261-279.

[27] Freed. A.D, Virrilli M.J.(1988). A viscoplastic theory applied to copper. Proceeding of the MECAMAT, Besançon, Vol. I, pp. 27-39.

BENCHMARKING FOR VALIDATION AND VERIFICATION OF THM SIMULATORS WITH SPECIAL REGARD TO FLUID DYNAMIC PROCESSES IN REPOSITORY SYSTEMS (BENVASIM)

Larissa Friedenberg[b], Oliver Czaikowski[b], Jörg Feierabend[g], Bastian J. Graupner[f], Jürgen Hansmann[f], Stephan Hotzel[c], Mengsu Hu[d], Ingo Kock[c], Manuel Lorenzo Sentís[f], Karl-Heinz Lux[g], Jobst Maßmann[a], Antonio P. Rinaldi[d, e], Michael Rutenberg[g], Jonny Rutqvist[d]

[a] Federal Institute for Geosciences and Natural Resources (BGR), Sub-Department Geotechnical Safety Analyses, Stilleweg 2, 30655 Hannover, Germany

[b] Gesellschaft für Anlagen- und Reaktorsicherheit (GRS) gGmbH, Repository Research Departement Theodor-Heuss-Straße 4, 38122 Braunschweig, Germany,
E-mail: Larissa.Friedenberg@grs.de

[c] Gesellschaft für Anlagen- und Reaktorsicherheit (GRS) gGmbH, Decomissing and Waste Management Division, Schwertnergasse 1, 50667 Köln, Germany

[d] Lawrence Berkeley National Laboratory (LBNL), Department Hydrology, 1 Cyclotron Road, Berkeley, CA 94720, USA

[e] Swiss Federal Institute of Technology in Zurich (ETH), Rämistrasse 101, 8092 Zurich, Switzerland

[f] Swiss Federal Nuclear Safety Inspectorate (ENSI), Department Disposal and Analyses, Industriestraße 19, 5200 Brugg, Switzerland

[g] Clausthal University of Technology (TUC), Chair for Waste Disposal Technologies and Geomechanics, Erzstraße 20, 38678 Clausthal-Zellerfeld, Germany

Key words: benchmarking, phase flow, THM-coupling

Abstract. *The project BenVaSim was initiated as a benchmarking for different simulators which have been already used in the field of final repository research. The objective is to gain independent numerical simulation tools due to investigate fundamental thermal-hydraulic-mechanical coupled processes related to a repository for high-level waste and gaining a deepened process understanding. Therefore, the basic processes are investigated with increasing complexity in a one-dimensional model with simple geometry and a generic material.*

1 INTRODUCTION

The project BenVaSim was started in 2017 for the verification and validation of several numerical simulators which are in use for dealing with issues related to final repository research. The main objective of the project is to gain independent numerical simulation tools which are verified and meaningful related to geotechnical aspects, especially for thermal-hydraulic-mechanical (THM) coupled processes of the host rock and engineered barrier systems (EBS) in a repository. This represents quality assurance which should result in improved forecast reliability leading to a strengthening confidence in prognostic statements. In Germany for example, where the project has been initiated, the knowledge resulting from this project could support the new site selection procedure for a repository for high-level waste. Further, the project partners will get personal advancement of new skills and a deepened expertise with their used simulators, as well as with the basic THM processes [v]. There are six partners participating with several simulation codes in the benchmarking which are shown in Table 1. The project was initiated and is coordinated by the Clausthal University of Technology.

Organization	Simulator
Federal Institute for Geosciences and Natural Resources (BGR), Sub-Department Geotechnical Safety Analyses, Hannover, Germany	OpenGeoSys[iii]
Gesellschaft für Anlagen- und Reaktorsicherheit gGmbH, Repository Research Department (GRS BS), Braunschweig, Germany	CODE_BRIGHT[vii]
Gesellschaft für Anlagen- und Reaktorsicherheit gGmbH, Decomissing and Waste Management Division (GRS K), Köln, Germany	TOUGH-FLAC-Coupling[ii]
Lawrence Berkeley National Laboratory (LBNL), Department Hydrology, Berkeley, USA	TOUGH-FLAC[vi]
Swiss Federal Nuclear Safety Inspectorate (ENSI), Department Disposal and Analyses, Brugg, Swiss	TOUGH-FLAC[iv] COMSOL Multiphysics[i] OpenGeoSys[iii]
Clausthal University of Technology (TUC), Chair for Waste Disposal Technologies and Geomechanics, Clausthal-Zellerfeld, Germany	FLAC-TOUGH-Kopplungssimulator[v]

Table 1: Overview of project partners and applied simulators

Regarding the structure of this paper, the numerical model will be introduced first and then the simulation results from GRS BS will be shown in chapter two. Second, a comparison with the project partner's results will be done followed by a discussion. At the end, a conclusion and an outlook will be given.

2 NUMERICAL SIMULATION

For a fundamental investigation and an extended process understanding, the modelling work is done stepwise with increasing complexity. First, it should be concentrated on the basic processes and comparing their implementation in the different simulation codes. Therefore, a horizontal one-dimensional model with a simple geometry and a generic material

is chosen (Figure 1). By using a one-dimensional model possible differences in the results can be outlined and feasible reasons can be figured out because of the elementariness. This leads to a more precise estimation of simulation and process quality [v].
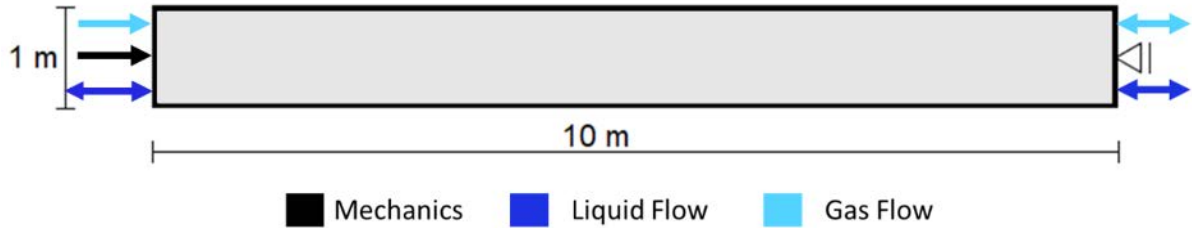

Figure 1. Model geometry

In the first step, only one-phase flow is considered by keeping the gas phase at a fixed reference pressure. Also phase interactions are neglected for comparing the numerical results with analytical ones. CODE_BRIGHT follows a poromechanical approach requiring phase interactions due to the specification of a retention curve. The simulation work is done using a very flat linear retention curve, achieving good results. However, because of this adjustment the emphasis in this paper is on the next step of simulation work considering two-phase flow coupled with mechanics. Therefore, Figure 2 shows the model including initial and boundary conditions where the values of liquid pressure correspond to the prescribed degree of saturation ($S_{l,0}$ = 0.63, $S_{l,right}$ = 0.9, $S_{l,left}$ = 0.5). For describing the mechanical behaviour, a linear elastic approach was chosen and for hydraulic processes a retention curve following van Genuchten.

Table 2: Material parameters

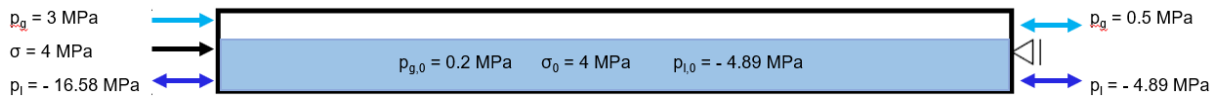| E	650 MPa
Φ	0.33
K	$2.5*10^{-21}$ m^2

Figure 2. Initial and boundary conditions

Simulation results from GRS BS using CODE_BRIGHT are shown in Figures 3 to 6, including: gas pressure evolution with time, profiles of gas pressure, liquid saturation degree and displacements. In the analysis of time evolutions five points are considered and marked due to the distance to the left model border. The evaluation of profiles is done at six different points of time.

Considering the gas pressure evolution with time, the achievement of steady state after approximately 1,000 years is shown. The steady state in liquid saturation degree adjusts quite later (~ 60,000 years) leading to the conclusion that gas flow processes are much faster than liquid flow processes in this model. Referring to mechanics, a compaction of the model occurs with a maximal displacement of 2.8 cm on the left border of the model.
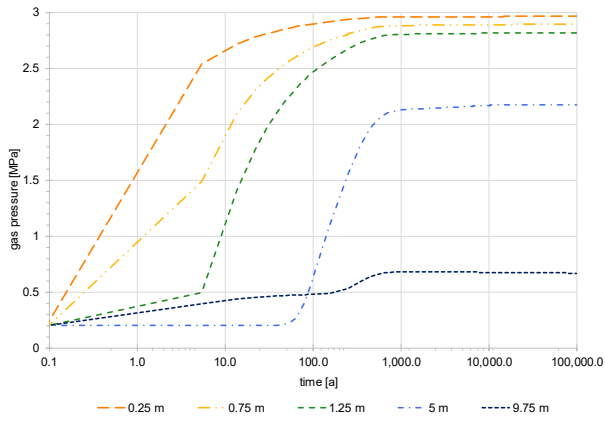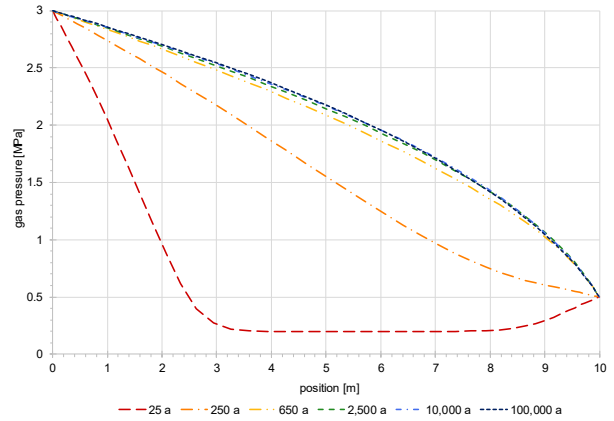
3

Figure 3. Gas pressure evolution in selected points

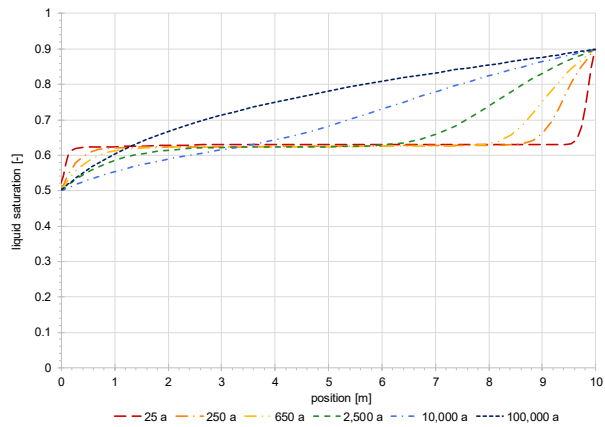

Figure 4. Profile of gas pressure

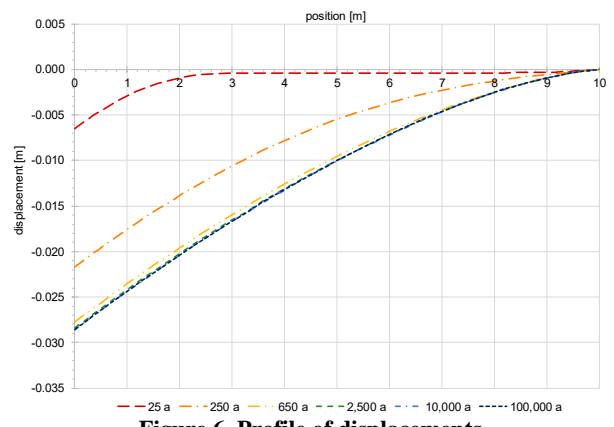Figure 5. Profile of liquid saturation degree

Figure 6. Profile of displacements

3   DISCUSSION

In this chapter, the numerical results presented above are compared with the results of the project partners, shown in Figures 7 to 10. Only differences in the modelling with reference to GRS BS with CODE_BRIGHT are dealt with.

Considering the diagram of displacements (Figure 10), there are distinctions to be seen. The displacements of GRS BS are smaller than the displacements of the other partners. In maximum displacement there is a difference of 2.6 cm. This phenomenon is assumed to the different definitions of effective stresses. In the model specifications the effective stresses related to Bishops definition are given which includes average pore pressures (Equation 1). In CODE_BRIGHT the effective stresses consider the maximum value of the pore pressures (Equation 2).

$$\sigma_{eff} = \sigma_{tot} - \left(\sum_{\varphi} S_{\varphi} p_{\varphi} \right) \tag{1}$$

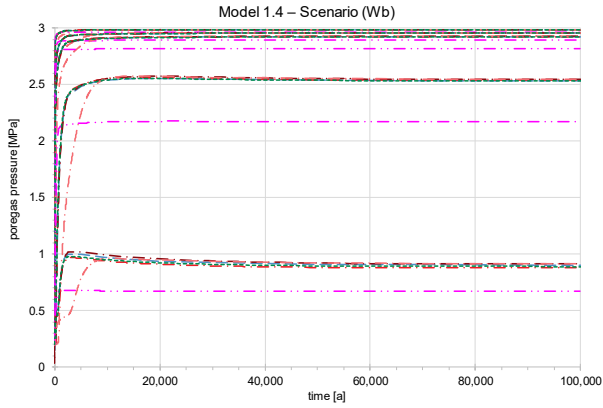$$\sigma_{eff} = \sigma_{tot} - \max(p_g; p_l) \tag{2}$$

4

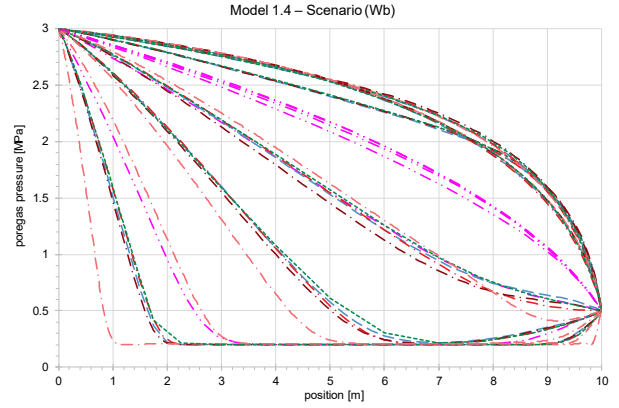Figure 7. Comparison: gas pressure evolution

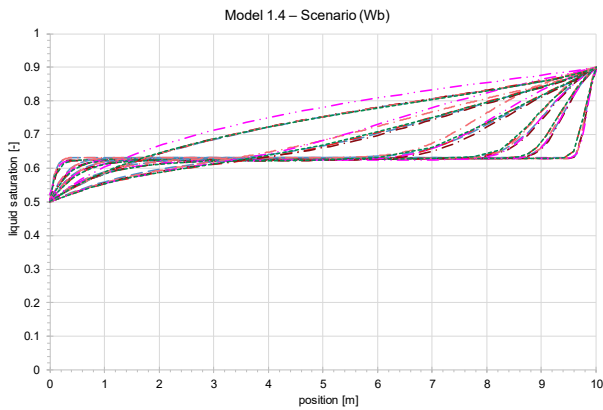Figure 8. Comparison: profiles of gas pressure

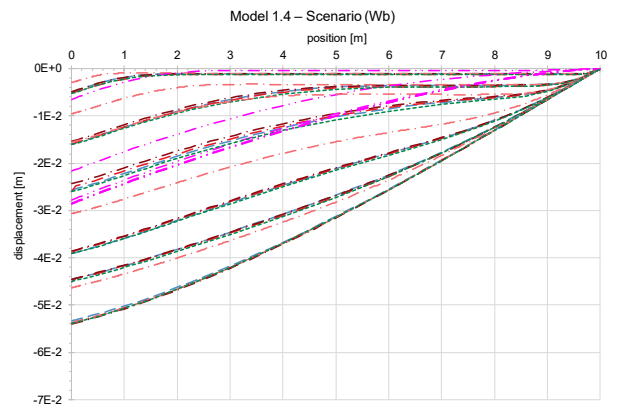Figure 9. Comparison: profiles of liquid saturation degree

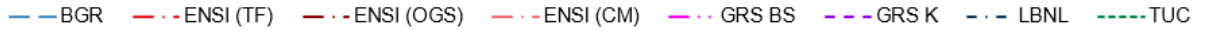Figure 10. Comparison: profiles of displacements

Figure 11. Legend for figures 7 - 10

Considering the diagrams of gas pressure (Figure 7, Figure 8) some differences could be seen. The gas pressures in the first- and second-time step of the profile, calculated by GRS BS, is higher than the comparable curves, thus, resulting of a faster gas flow. However, the steady-state gas pressure of GRS BS is much smaller than the others.

These phenomena are assumed to be related to diverse definitions of gas phase relative permeability. In the model specifications the gas phase relative permeability follows the Mualem/van Genuchten approach (Equation 3), whereas, GRS BS uses a default law in CODE_BRIGHT (Equation 4). Due to this difference in definitions, there are big deviations in the values of gas phase relative permeability leading to a faster gas flow on the side of GRS BS.

$$K_{rel;g} = (1 - S_{l;eff})^{\frac{1}{2}} (1 - S_{l;eff}^{1/\lambda})^{2\lambda} \tag{3}$$

$$K_{rg} = 1 - k_{rl} \tag{4}$$

$$K_{rel;l} = S_{l;eff}^{1/2} \left(1 - \left(1 - S_{l;eff}^{1/\lambda}\right)^{\lambda}\right)^2 \tag{5}$$

5

Figure 12 presents the functions of liquid phase and gas phase relative permeabilities related to the definitions in the specifications and CODE_BRIGHT. For the diagram the saturation is given as effective saturation (Table 3). Regarding the liquid phase relative permeability, the van Genuchten approach (Equation 5) is implemented in both, so the curves are superposable. The differences in gas phase relative permeability mentioned above are marked exemplary for the initial and boundary conditions of liquid saturation degree. It could be seen that the curves of gas phase relative permeability are totally different from each other. The relative permeability is always higher in CODE_BRIGHT favouring the gas flow. In Table 3 the values of the diagram are summarized, and the differences are calculated.
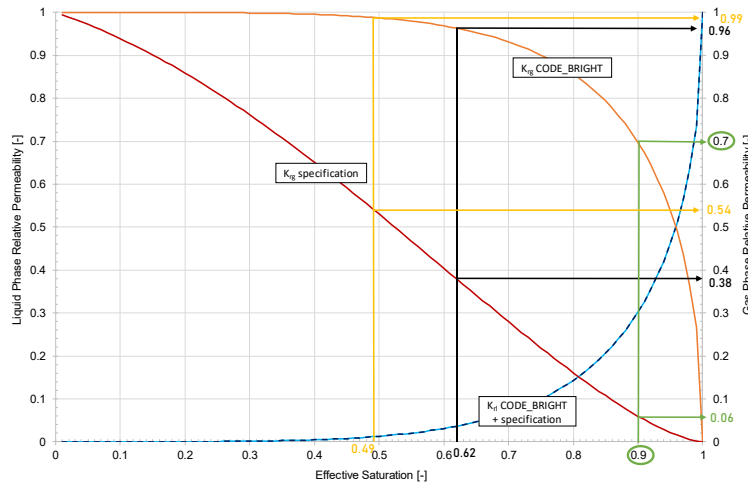

Figure 12. Comparison of the functions of relative permeabilities prescribed by specifications and used in CODE_BRIGHT. Dark blue line = specified liquid phase relative permeability, dotted blue line = liquid phase relative permeability in CODE_BRIGHT, orange line = gas phase relative permeability in CODE_BRIGHT, red line = specified gas phase relative permeability

Table 3: Differences in gas phase relative permeabilities

S_l	$S_{l;eff}$	$K_{rel;g}$ CB	specified $K_{rel,g}$	Difference
0.5	0.489	0.99	0.54	0.45
0.63	0.622	0.96	0.38	0.58
0.9	0.898	0.7	0.06	0.64

4 CONCLUSION AND OUTLOOK

The benchmarking work leads to a deeper investigation and resulting understanding of the basic processes. In the first simulations steps, good results are obtained, however, some differences between the simulation codes and their constitutive laws are found. A discussion about the validity of the approaches used should not and cannot be conducted within this framework, as this concerns fundamental and individual aspects. For the principle of comparability, the additional definitions for gas phase relative permeability and effective stress shall be implemented, if possible. This would lead to an expansion of the spectrum of CODE_BRIGHT.

As a next step in the project, thermal aspects will be added resulting in the end in a full THM-coupled one-dimensional model, building up the basic processes in a repository.

5 ACKNOWLEDGEMENTS

REFERENCES

[i]   COMSOL Inc., COMSOL Multiphysics 4.5, User's Guide, 2012

[ii] Hotzel, S., Gasausbreitung in unverritztes Steinsalz – Hydro-mechanisch gekoppelte Modellrechnungen mit dem Simulationstool TFC, Report GRS-339, BMUB project 3610R03230, Cologne, Germany, 2014

[iii] Kolditz, O., Bauer, S., Bilke, L., Böttcher, N., Delfs, J.-O., Fischer, T., Görke, U.-J., Kalbacher, T., Kosakowski, G., McDermott, C.I., Park, C.-h., Radu, F., Rink, K., Shao, Hua, Shao, Haibing, Sun, F., Sun Y., Singh, A.K., Taron, J., Walther, M., Wang, W., Watanabe, N., Wu, Y., Xie, M., Xu, W., Zehner, B., OpenGeoSys: an open-source initiative for numerical simulation of thermo-hydro-mechanical/chemical (THM/C) processes in porous media, Environ. Earth Sci., 67(2), 589–599, 2012

[iv] Rinaldi, A.P., Rutqvist, J., Blanco-Martín, L., Hu, M., Sentis, M.L., 2018, Coupling TOUGH3 with FLAC3D for parallel computing of fluid flow and geomechanics, Proceedings of the TOUGH Symposium 2018

[v]   Rutenberg, M., Feierabend, J., Lux, K.-H., Maßmann, J., Lorenzo Sentís, M.L., Graupner, B.J., Hansmann, J., Czaikowski, O., Wieczorek, K., Friedenberg, L., Hotzel, S., Kock, I., Rutqvist, J., Hu, M., Rinaldi, A.P., 2018, BenVaSim – A Benchmarking of Simulators for Modelling TH[2]M Processes in the Context of Radioactive Waste Disposal. Proceedings of TOUGH Symposium 2018

[vi] Rutqvist, J., 2011, Status of the TOUGH-FLAC simulator and recent applications related to coupled fluid flow and crustal deformations, Computers & Geosciences 37, 739 – 750

[vii] Universitat Polytechnica de Catalunya, CODE_BRIGHT User's Guide, Version 7.4, Barcelona, June 2017

MODELING A LONG-TERM CO₂ INJECTION EXPERIMENT AT THE UNDERGROUND ROCK LABORATORY OF MONT TERRI

Victor Vilarrasa[*], Dorothee Rebscher[†], Roman Y. Makhnenko[††]

and Christophe Nussbaum[†††]

[*] Institute of Environmental Assessment and Water Research (IDAEA)
Spanish National Research Council (CSIC)
Jordi Girona 18-26, 08034 Barcelona, Spain
Associated Unit: Hydrogeology Group UPC-CSIC
e-mail: victor.vilarrasa@idaea.csic.es, web page: h2ogeo.upc.edu/en/12-directorio-personal-ghs/539-victor-vilarrasa-4

[†] Department of Underground Space for Storage and Economic Use
Bundesanstalt für Geowissenschaften und Rohstoffe (BGR)
Stilleweg 2, 30655 Hannover, Germany
e-mail: dorothee.rebscher@bgr.de, web page:
https://www.bgr.bund.de/EN/Home/homepage_node_en.html

[††] Department of Civil and Environmental Engineering (CEE)
Illinois University at Urbana-Champaign
2221 Newmark Civil Engineering Bldg, 61801 Urbana, Illinois, USA
e-mail: romanmax@illinois.edu, web page: https://rockmechanics.cee.illinois.edu

[†††] Swiss Geological Survey, Federal Office of Topography, swisstopo
Route de la Gare 63, CH -2882 St-Ursanne, Switzerland
e-mail: christophe.nussbaum@swisstopo.ch, web page: https://www.mont-terri.ch/en/homepage/meta/contact.html

Key words: HM Coupled Analysis, Fluid injection, Geologic Carbon Storage, Geo-energies, Caprock Integrity, Opalinus Clay

Abstract. *Geologic carbon storage is considered as a key technology to reach zero emissions by 2050 in order to meet the objective of the Paris Agreement of limiting temperature increase below 2 ºC. Yet, a number of concerns exist about the long-term caprock integrity to permanently storing CO₂ in deep geological formations. To gain knowledge on the sealing properties of clay-rich geomaterials that serve as caprock, field experiments in underground research laboratories are required. Here, we present preliminary results of the modeling of a long-term CO₂ injection experiment into Opalinus Clay (shale) at Mont Terri, Switzerland. Simulation results show that the high entry pressure hinders CO₂ penetration in free phase into the shale, but CO₂ does get into Opalinus Clay dissolved into the resident pore water. The presence of fractures in the caprock provide preferential paths for pressure propagation and for CO₂ migration provided that the CO₂ entry pressure is low enough to permit CO₂ entering into it. The modeling of the experiment is ongoing in order to define the design of the experiment.*

1 INTRODUCTION

Predictions show that in order to meet the ambitious objective of the Paris Agreement of limiting the temperature increase below 2 ºC, we should reach zero emissions by 2050. To achieve carbon neutrality, several actions will be required, such as shifting to carbon-free fuels, fostering renewable energies and storing carbon dioxide (CO_2) in deep geological formations[i]. Geologic carbon storage has the potential to significantly reduce CO_2 emissions to the atmosphere, contributing to climate change mitigation. According to the International Energy Agency (IEA), the amount of stored CO_2 should progressively increase until reaching some 8 Gt/yr by 2050[i].

In order to permanently store large amounts of CO_2 deep underground, we should ensure that the sealing capacity of the low-permeability formations placed on top of the storage formations, known as caprock, can prevent upwards CO_2 leakage in the long-term. Caprock integrity may be compromised by[ii] 1) fracture opening as a result of pressure buildup, 2) cooling-induced thermal stresses, 3) geochemical reactions induced by the acidic nature of CO_2 when it dissolves into water, 4) shear slip of pre-existing fractures that may induce microseismicity or cause aseismic slip, 5) fault reactivation and consequent permeability enhancement, and 6) porosity waves enhancing permeability. Experience with existing CO_2 injection sites has shown that caprocks seem to be effective seals[iii]. Even though the overall sealing capacity is unlikely to be compromised[iv,v], a close look into the lower portion of the caprock, i.e., the one in contact with the storage formation, reveals that caprock integrity may be affected by CO_2 injection[vi-viii], which may lead to CO_2 penetration into it.

To gain knowledge on the processes that may affect the sealing caprock capacity, field experiments under controlled experimental conditions in underground research laboratories are essential. We are designing a long-term CO_2 injection experiment in Opalinus Clay at the Underground Rock Laboratory in Mont Terri[ix], Switzerland. Opalinus Clay is a shale that possesses properties of suitable caprocks. We present here simulation results of the preliminary modeling stage of the experiment.

2 METHODOLOGY

We model a vertical cross section of the long-term CO_2 injection experiment. We use a 2D plane strain model of 40 m by 20m, in which a 20-m long injection borehole is placed in the center of the model. The borehole is modeled by assigning a high porosity and permeability. The relatively reduced dimensions of the model are justified by the low-permeability of Opalinus Clay (Table 1). Note that Opalinus Clay has anisotropic permeability, with higher permeability along the bedding planes than perpendicular to them. The bedding planes are inclined at Mont Terri, with an average dip angle of 45º.

Table 1. Hydro-mechanical properties of Opalinus Clay measured in the laboratory[x,xi]

Property	Effective mean stress, P' (MPa)	Permeability, k_{xx} (m²)	Permeability, k_{yy} (m²)	Relative water permeability, k_{rw} (-)	Relative CO_2 permeability, k_{rc} (-)	Entry pressure, p_0 (MPa)	van Genuchten shape parameter m (-)	Residual water saturation, S_{rc} (-)	Porosity, φ (-)	Young's modulus, E (GPa)	Undrained Poisson ratio, v (-)
Opalinus Clay	2.5	$2.4 \cdot 10^{-20}$	$8 \cdot 10^{-21}$	S_w^6	S_c^6	10.0	0.3	0.3	0.12	1.8	0.4

The initial conditions are hydrostatic fluid pressure, temperature of 20 ºC, and a normal faulting stress regime. At the depth of the underground rock laboratory (300 m), the fluid pressure is of 2 MPa, and the stress state is such that the vertical stress equals 6.5 MPa, the in-plane horizontal stress equals 4.5 MPa and the out-of-plane horizontal stress equals 2.5 MPa. The hydraulic boundary conditions are constant pressure on the top boundary equal to 2 MPa and a CO_2 injection pressure on the borehole of 3 MPa for 1 year. The mechanical conditions are constant overburden equal to the lithostatic stress on the top boundary and no displacement perpendicular to the other boundaries. We solve this two-phase flow coupled problem in deformable porous media using CODE_BRIGHT[xii,xiii], with the modifications made by Vilarrasa et al.[xiv] to model CO_2 injection.

3   RESULTS

CO_2 injection causes a pressure increase of 1 MPa with respect to the initial pore pressure. However, the CO_2 entry pressure has been measured in the laboratory to be of 10 MPa (recall Table 1). Thus, no CO_2 penetrates into the Opalinus Clay as a free phase. Nonetheless, the pressure increase imposed in the injection wellbore induces a water pressure buildup around the borehole (Figure 1). Pressure diffusion advances preferentially through the bedding planes because of their higher permeability. As a result, the pressure front has an inclined shape following the dip of the bedding planes, which is of 45º. The pressure perturbation front is limited to some 4 m away from the borehole. However, deformation-induced pressure changes are observed further away. For example, note that the pressure is not hydrostatic at the top of Figure 1, presenting lower pressure in the central part above the borehole, than on the sides of the borehole. This is due to the pressure-induced expansion of the shale around the borehole causing bending of the rock that extends above the borehole and compacts on its sides. Thus, the pore volume increases above the borehole, leading to a slight pressure drop.
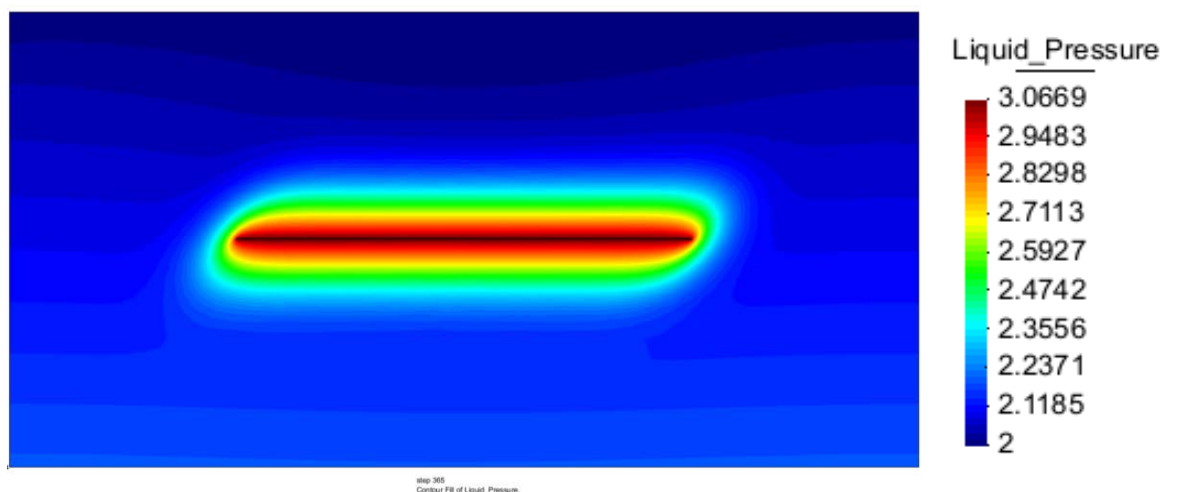

Figure 1. Liquid pressure (in MPa) distribution after 1 year of CO_2 injection at 3 MPa

Despite CO_2 being unable to enter into Opalinus Clay because of the high entry pressure, CO_2 progressively dissolves into the formation pore water and advances by diffusion (Figure 2). After 1 year of injection, CO_2 barely advances 1 m into the caprock. This penetration length is important because the pH of water with dissolved CO_2 is reduced, which

generates dissolution and precipitation of minerals that may alter the caprock properties[xv].
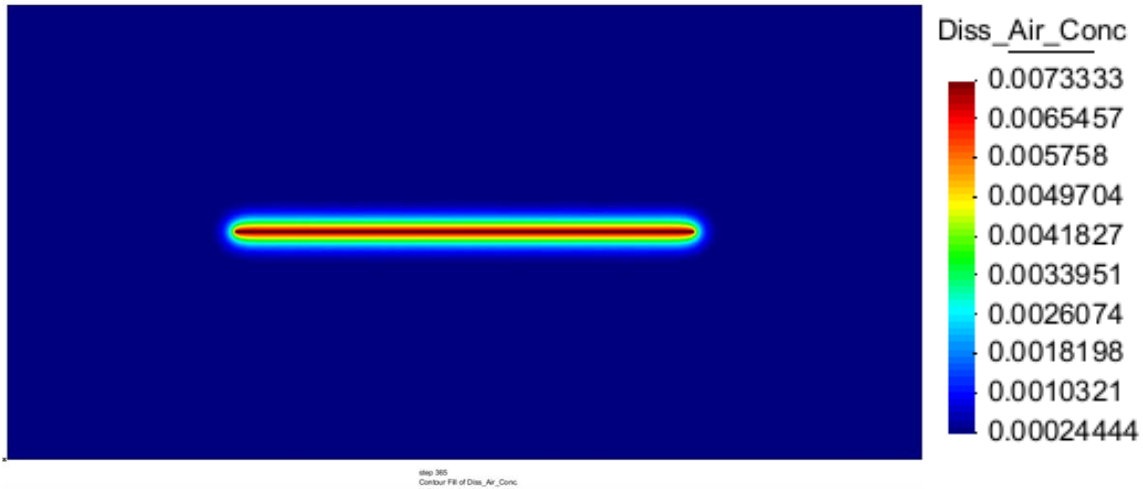

Figure 2. CO_2 dissolution (in %) distribution after 1 year of CO_2 injection at 3 MPa

Pressure changes modify the effective stresses and as a result, the caprock deforms (Figure 3). The pressure changes in this experiment will be relatively small because the initial minimum effective stress is of just 0.5 MPa and the intention is not to induce hydraulic fractures. The total stresses increase as a result of pore pressure increase, so the effective stress decrease is smaller than the pressure increase. Nevertheless, simulation results show that the minimum principal effective stress becomes tensile, being –0.05 MPa after 1 year of CO_2 injection. Even though this value is smaller than the tensile strength of Opalinus Clay and new fractures would not be created, pre-existing fractures or bedding planes might be opened. Since the objective of the experiment is not to open or to reactivate pre-existing fractures that may induce aseismic slip or induced microseismicity (actually, other experiments at Mont Terri aim at reactivating faults[xvi]), the injection pressure will need to be decreased.
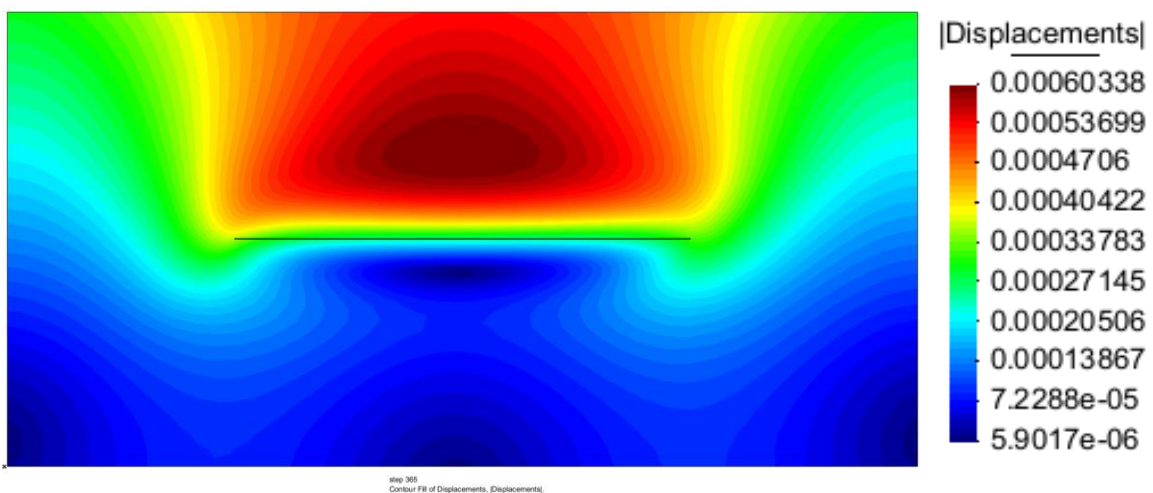

Figure 3. Displacement (in meters) distribution after 1 year of CO_2 injection at 3 MPa

4 CONCLUSIONS

We have modeled CO_2 injection experiment into Opalinus Clay (shaly facies) at the underground rock laboratory of Mont Terri using CODE_BRIGHT. Even though CO_2 does not penetrate into the shale because of the high CO_2 entry pressure of Opalinus Clay, CO_2 dissolves into the formation pore water, which will induce geochemical reactions around the injection borehole. The anisotropy of Opalinus Clay, which is controlled by the bedding planes, leads to a pressure perturbation front that follows the dip angle of the bedding planes. Deformation-induced pressure changes are also observed further away than the pressure diffusion front. The initially considered injection pressure of 3 MPa leads to tensile stresses in the out-of-plane direction and thus, it will need to be lowered to avoid fracture reactivation and/or formation and subsequent induced microseismicity.

REFERENCES

[i] IEA, 2010. Energy technology perspectives. Scenarios & strategies to 2050. Executive summary, International Energy Agency.

[ii] Vilarrasa, V., Makhnenko, R. Y., Rutqvist, J., 2019. Field and laboratory studies of geomechanical response to the injection of CO_2. In *Science of Carbon Storage in Deep Saline Formations* (pp. 159-178). Elsevier.

[iii] Verdon, J. P., Kendall, J. M., Stork, A. L., Chadwick, R. A., White, D. J., Bissell, R. C., 2013. Comparison of geomechanical deformation induced by megatonne-scale CO_2 storage at Sleipner, Weyburn, and In Salah. *Proceedings of the National Academy of Sciences*, 110(30), E2762-E2771.

[iv] Busch, A., Alles, S., Gensterblum, Y., Prinz, D., Dewhurst, D. N., Raven, M. D., ... Krooss, B. M., 2008. Carbon dioxide storage potential of shales. *International Journal of Greenhouse Gas Control*, 2(3), 297-308.

[v] Rutqvist, J., Vasco, D., W. Myer, L., 2010. Coupled reservoir-geomechanical analysis of CO_2 injection and ground deformations at In Salah, Algeria. *International Journal of Greenhouse Gas Control*, 4(2), 225-230.

[vi] Gor, G. Y., Elliot, T. R., Prévost, J. H., 2013. Effects of thermal stresses on caprock integrity during CO_2 storage. *International Journal of Greenhouse Gas Control*, 12, 300-309.

[vii] Goodarzi, S., Settari, A., Keith, D., 2012. Geomechanical modeling for CO_2 storage in Nisku aquifer in Wabamun Lake area in Canada. *International Journal of Greenhouse Gas Control*, 10, 113-122.

[viii] Vilarrasa, V., Rutqvist, J., Rinaldi, A. P., 2015. Thermal and capillary effects on the caprock mechanical stability at In Salah, Algeria. *Greenhouse Gases: Science and Technology*, 5(4), 449-461.

[ix] Bossart, P., Bernier, F., Birkholzer, J., Bruggeman, C., Connolly, P., Dewonck, S., ... Mayor, J. C., 2018. Mont Terri rock laboratory, 20 years of research: introduction, site

characteristics and overview of experiments. *In Mont Terri Rock Laboratory, 20 Years* (pp. 3-22). Birkhäuser, Cham.

[x] Vilarrasa, V., Makhnenko, R., Gheibi, S., 2016. Geomechanical analysis of the influence of CO_2 injection location on fault stability. *Journal of Rock Mechanics and Geotechnical Engineering*, 8(6), 805-818.

[xi] Makhnenko, R. Y., Vilarrasa, V., Mylnikov, D., Laloui, L., 2017. Hydromechanical aspects of CO_2 breakthrough into clay-rich caprock. *Energy Procedia*, 114, 3219-3228.

[xii] Olivella, S., Carrera, J., Gens, A., Alonso, E. E., 1994. Non-isothermal Multiphase Flow of Brine and Gas through Saline media. *Transport in Porous Media*, 15, 271-293.

[xiii] Olivella, S., Gens, A., Carrera, J., Alonso, E. E., 1996. Numerical Formulation for a Simulator (CODE_BRIGHT) for the Coupled Analysis of Saline Media. *Engineering Computations*, 13(7), 87-112.

[xiv] Vilarrasa, V., Silva, O., Carrera, J., Olivella, S., 2013. Liquid CO_2 injection for geological storage in deep saline aquifers. *International Journal of Greenhouse Gas Control*, 14, 84-96.

[xv] Song, J., Zhang, D., 2012. Comprehensive review of caprock-sealing mechanisms for geologic carbon sequestration. *Environmental Science & Technology*, 47(1), 9-22.

[xvi] Guglielmi, Y., Birkholzer, J., Rutqvist, J., Jeanne, P., Nussbaum, C., 2017. Can fault leakage occur before or without reactivation? Results from an in situ fault reactivation experiment at Mont Terri. *Energy Procedia*, 114, 3167-3174.

DEVELOPMENTS IN CODE_BRIGHT TO SIMULATE THE THM PHENOMENA IN METHANE HYDRATE BEARING SEDIMENTS

M. De La Fuente[*, †], J. Vaunat[×], H. Marín-Moreno[†]

[*] National Oceanography Centre, University of Southampton, European Way, Southampton, SO14 3ZH, United Kingdom.
e-mail: mdlf1g15@soton.ac.uk,
[×] Department of Geotechnical Engineering and Geosciences. Technical University of Catalonia (UPC) Campus Norte UPC, 08034 Barcelona, Spain.
e-mail: jean.vaunat@upc.edu
[†] National Oceanography Centre, University of Southampton Waterfront Campus, European Way, Southampton SO14 3ZH, United Kingdom.
e-mail: hector.marin.moreno@noc.ac.uk

Abstract. *The occurrence of methane hydrates (MH) within pores alters significantly the hydraulic and mechanical properties of the sediment and govern its Thermo-Hydro-Mechanical (THM) behaviour. The numerical modelling of Methane Hydrate Bearing-Sediments (MHBS) require robust and efficient mathematical models capable of capturing the highly interdependent physical processes that characterize their response upon mechanical loading and thermal stimulation in a coupled manner. These processes include sediment deformation, fluid and heat transport and fluid/solid phase transformations. Here, we develop a new fully coupled THM formulation to simulate the behaviour of MHBS, particularly focusing on hydrate dissociation scenarios. Our formulation extends Code_Bright's governing equations of energy and mass conservation to incorporate the hydrate phase. The equations have been rewritten considering a volumetric distinction between potential porosity (i.e., space between mineral grains) and available porosity of the sediment (i.e., space available after hydrate and ice formation). The distinction between both of these porosities allows the model to isolate the effects of mechanical deformation and hydrate and ice phase change on the hydraulic and mechanical properties of the sediment. It is also key at implementing the novel constitutive model Hydrate-CASM, which attributes stress-strain changes observed in MHBS to variations in the void ratio, swelling line slope and isotropic yield stress of the sediment caused by pore invasion during hydrate formation. The thermo-hydraulic capabilities of our formulation are validated against the results from a series of state-of-the-art simulators involved in the NETL-USGS first international gas hydrate code comparison study. Finally, the mechanical coupling is investigated by modelling the experimental data from a synthetic MHBS specimen subjected to hydrate dissociation via depressurization under triaxial shear.*

MODELLING GAS FLOW EXPERIMENTS IN MX80 BENTONITE: ANALYSIS OF PREFERENTIAL GAS PATHS

I.P. Damians[*]**, S. Olivella**[*]**, and A. Gens**[*]

[*] Department of Civil and Environmental Engineering
Universitat Politècnica de Catalunya – BarcelonaTech (UPC)
Campus Nord UPC, 08034 Barcelona, Spain
Email: ivan.puig@upc.edu

Key words: Hydro-Mechanical 3D model, Gas flow, Mx80 bentonite

Abstract. *A gas injection test, performed on compact bentonite, was carried out at the British Geological Survey. The test is composed by two stages (i.e. hydration followed by gas injection testing). After gas breakthrough and a period of gas flow through the sample, the injection pump was stopped whilst the stresses and porewater pressures were continuously monitored. A Hydro-Mechanical 3D numerical model has been developed to simulate the gas injection test and to achieve similar gas pressure, gas outflow, and stress evolution responses.*

1 INTRODUCTION: MX80-D TEST

A gas injection test performed on compacted Mx80 bentonite was carried out at the British Geological Survey. This experiment, designated as Mx80-D, represents the first test dataset for a series of tests analyzed by DECOVALEX Task A [1]. These tests are useful to increase the understanding of gas flow potential trough this low permeability materials.

Figure 1a presents the testing cell apparatus with some outer instrumentation details. Figure 1b presents the model of the bentonite sample (dimensions: 12 cm-length × 6 cm-diameter) including injection and backpressure porous stone filters, the model mesh discretization by layers definition, and the external volumes related to the linked radial array sensors.

The Mx80-D test is composed by two main stages: hydration stage followed by helium gas injection. The injected gas pressure was fixed to 1 MPa from 7.3 to 39.3 days and 3 MPa from 39.4 to 46 days according to test duration. After that, gas flow rate was continuously increased at the injection from 0 to 8.0×10^{-7} kg/s/m^2 (from 46 to 67 days) and then maintained constant (i.e., flow rate value of 8.0×10^{-7} kg/s/m^2) until a breakthrough point occurred (i.e., at 71.5 days). After breakthrough and a period of gas flow through the sample, the injection pump was stopped whilst the stresses and porewater pressures were continuously monitored at several sample control point locations up to the end of the test at day 121.

2 MATERIAL PROPERTIES, NUMERICAL MODEL, BOUNDARY CONDITIONS

The problem was modelled accordingly with gas flow rate previously detailed. Table 1 presents the material properties and some details of the constitutive equations of the embedded fracture model assumed. Figure 2 presents the random porosity strategy assumed at each model sample layer, and Figure 3 presents the intrinsic permeability trends obtained as a function of the strains development according to the random permeability weighting distribution assumed (see Table 1 – Note-a) returning an initial equivalent global permeability of 3.3×10^{-21} m^2 (which was a problem input). Elastic modulus of 307 MPa and Poisson's ratio of 0.4 were considered.
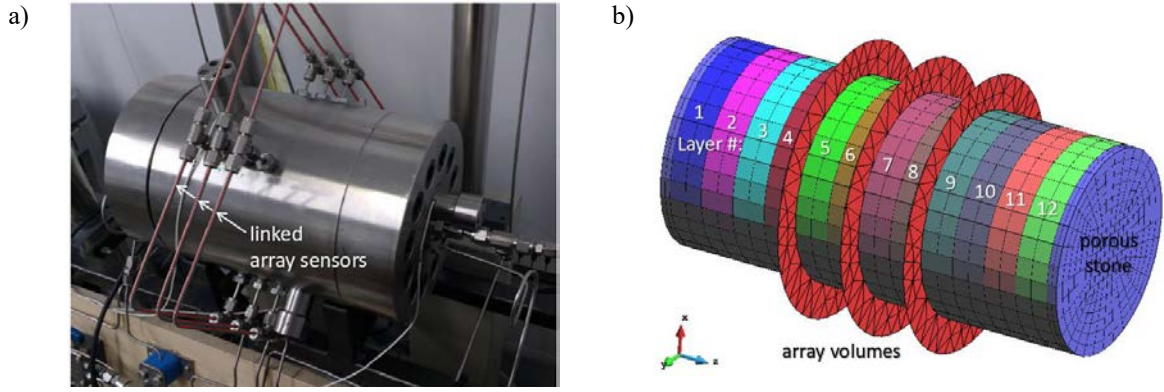
Figure 1: Mx80-D test: pressure vessel and arrays (a) and inner Mx80 sample model mesh detail (b).

Table 1: Material model parameters for the Mx80 bentonite:

Initial porosity	Intrinsic permeability [a]	Water retention curve [b]		Relative permeability [c]	Embedded fractures definition parameters [a-d]			
		P_0	λ		a	b_0	b_{max}	ε_0
	1.0×10^{-19}	10.8		$n_l = 3$,	5.0×10^{-4}	9.5×10^{-9}	7.5×10^{-7}	0.01
0.44	1.0×10^{-20}	22.5	0.45	$n_{g,matrix} = 2$,	5.0×10^{-5}	5.0×10^{-9}	3.5×10^{-7}	0.03
	1.0×10^{-21}	48.6		$n_{g,fractures} = 1$	5.0×10^{-6}	1.5×10^{-9}	1.5×10^{-7}	0.05
-	m^2	MPa	-	n-power				

Notes: [a] Initial matrix random intrinsic permeability according to 1/6-weighting distribution for 1×10^{-19} m² and 1×19^{-20} m², and 2/3-weighting distribution for 1×10^{-21} m² (see Figure 2). The global intrinsic permeability is defined as a function of material matrix and internal fracture permeabilities: $k_{ii} = k_{matrix} + k_{fractures}$ (see Note-d below);

[b] Water retention curve according to Van Genuchten model (λ: shape function);

[c] Liquid and gas relative permeability defined by the effective saturation: $k_r = (S)^n$, where S is the degree of saturation;

[d] Definition parameters of the embedded fractures related to the associated width of the fractures (a), fracture apertures (b_0 and b_{max}), and strain development (ε and ε_0).
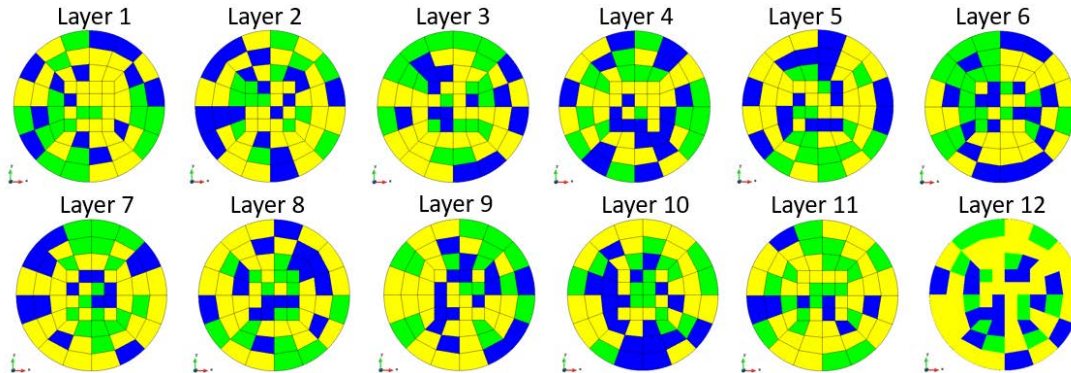

Figure 2: Layer-by-layer random permeability distribution (with different weighting) for the not-connected case: Green: $k_0 = 1 \times 10^{-19}$ m² (1/6 weighting), blue: $k_0 = 1 \times 19^{-20}$ m² (1/6 weighting), and yellow: $k_0 = 1 \times 10^{-21}$ m² (2/3 weighting). Note: Layer 11th was the one selected for the connected permeability case, randomly rotated and distributed along sample's axial axis)
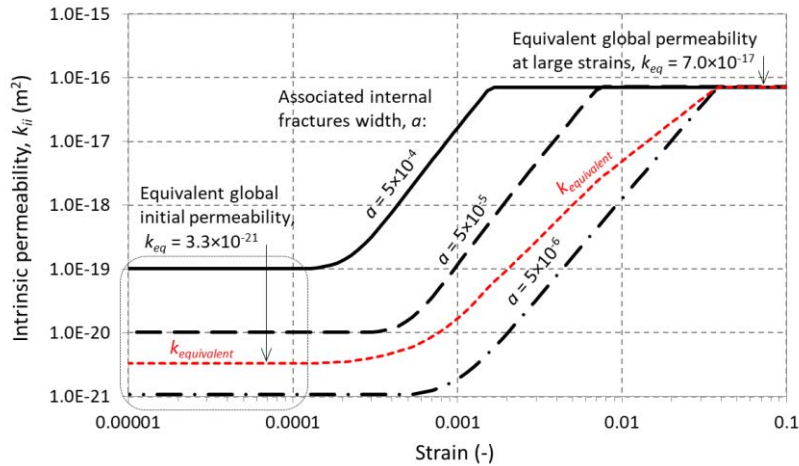
Figure 3. Intrinsic permeability evolution related/equivalent global permeability representation (generated by weighted geometric mean).

Two alternative preferential path strategies of permeability distribution were performed:

a) Not-connected permeability case: Random distribution of three different permeabilities through all model layers (2/3 weighting to the lowest permeability zone and 1/6 weighting to the middle and higher permeability zones; see Figure 2).

b) Connected permeability case: Random distribution of the three different permeabilities specified in a selected/representative layer (Layer 11th as per Figure 2), which was then randomly rotated to both directions to define the other sample layers, generating a sort of connectivity along the axial axis of the sample.

3   RESULTS

Figure 4 presents the injection gas pressure and backpressure outflow evolution results for both not-connected and connected permeability cases. Despite better agreement was obtained for the not-connected permeability case if the dissipation trend of the gas pressure is analysed, much better agreement was obtained in terms of the gas pressure peak-value and outflow magnitude for the connected permeability case. Figure 5 shows the advective gas flux ($m^3/m^2/s$) vectors for both cases of connectivity during injection at day 65 (just before the breakthrough) and at day 95 (during gas dissipation). The same scale (vectors size factor) is maintained to ease the comparison. As expected, different location of the larger flow-vector magnitudes take place before and after the breakthrough. Also, as it can be noticed, the vectors appeared more addressed in the connected permeability case than in the not connected case due to the less connectivity between elements. In addition to the injection gas pressure, also radial porewater at three different locations was obtained. As it can be observed in Figure 6, reasonably well agreement was achieved for the connectivity cases analysed. Also here, the peak and first dissipation trending shape was better approximated by the connected case (Fig.6b) whereas the long-term dissipation trending shape was probably better fitted by the not-connected case (Fig.6a). Figure 7 presents the evolution of both axial and radial stresses evolution during the test. As it can be seen, both connectivity cases returned reasonably well agreement with the measured data, with a good approximation of the ranging values due to the gas breakthrough jump despite the smoother increasing trend obtained by both the model calculations.
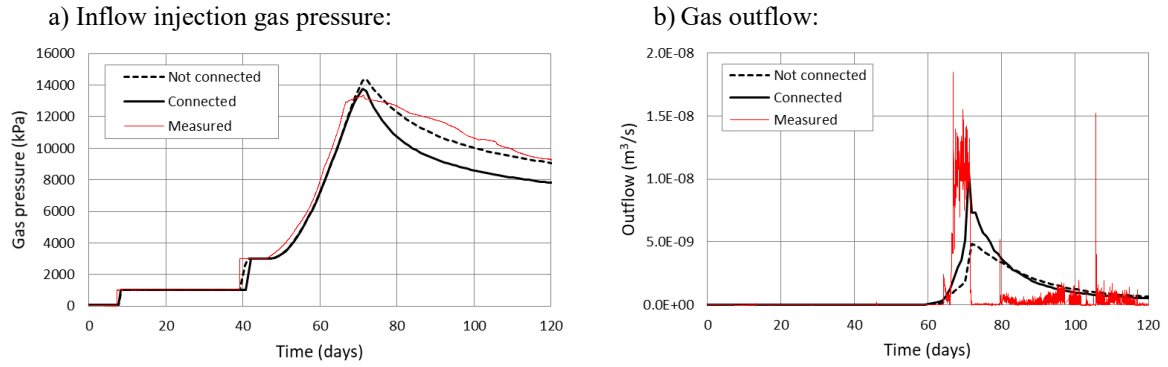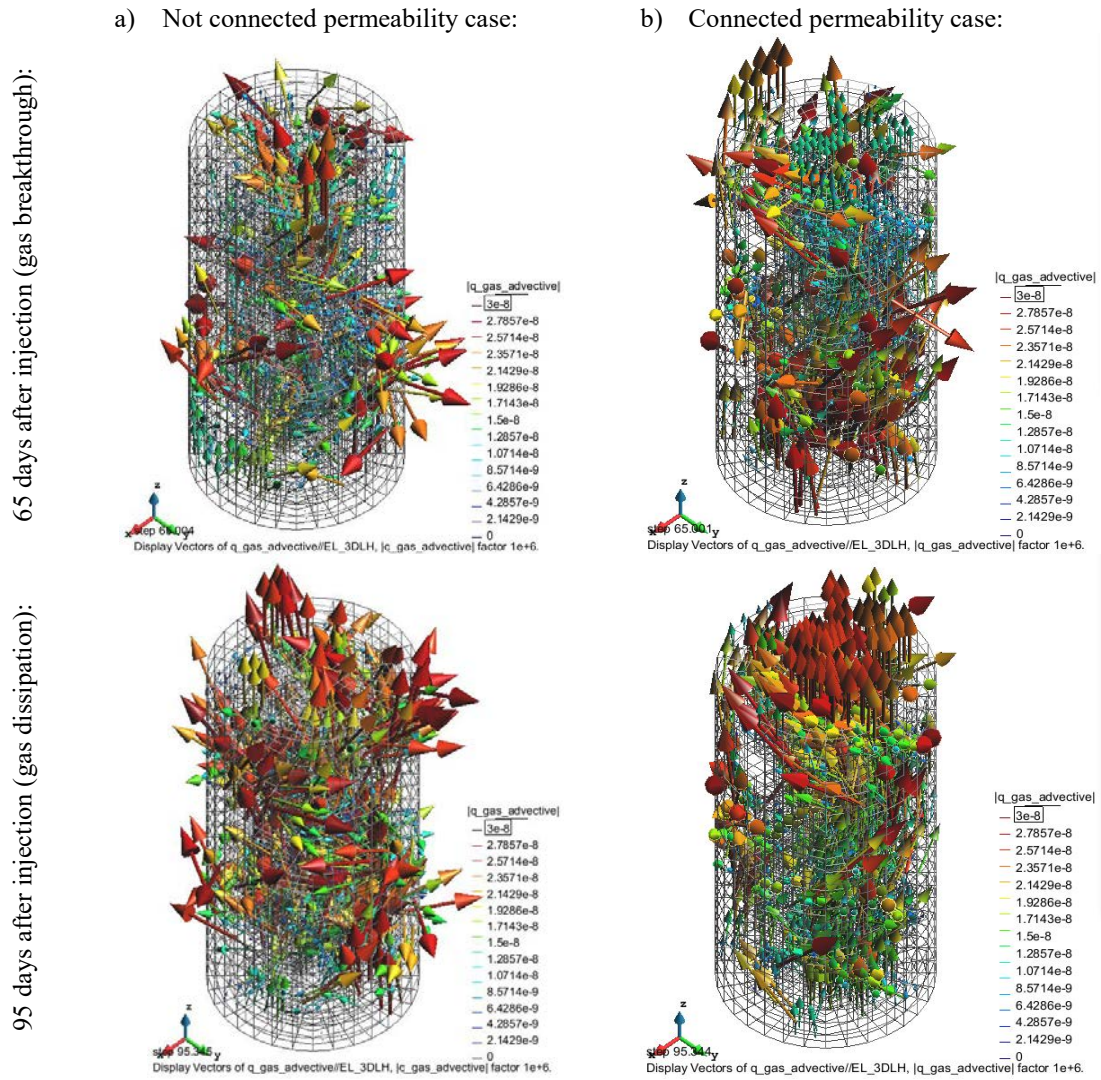
a) Inflow injection gas pressure:

b) Gas outflow:

Figure 4: Injection gas pressure (a) and gas outflow (b) evolution.

a) Not connected permeability case:

b) Connected permeability case:

Figure 5: Advective gas flux at day 65 (a: gas breakthrough) and at day 95 (b: gas dissipation).

a) Not connected: b) Connected:

Figure 6: Gas pressure evolution at arrays: not connected (a) and connected (b) permeability cases.

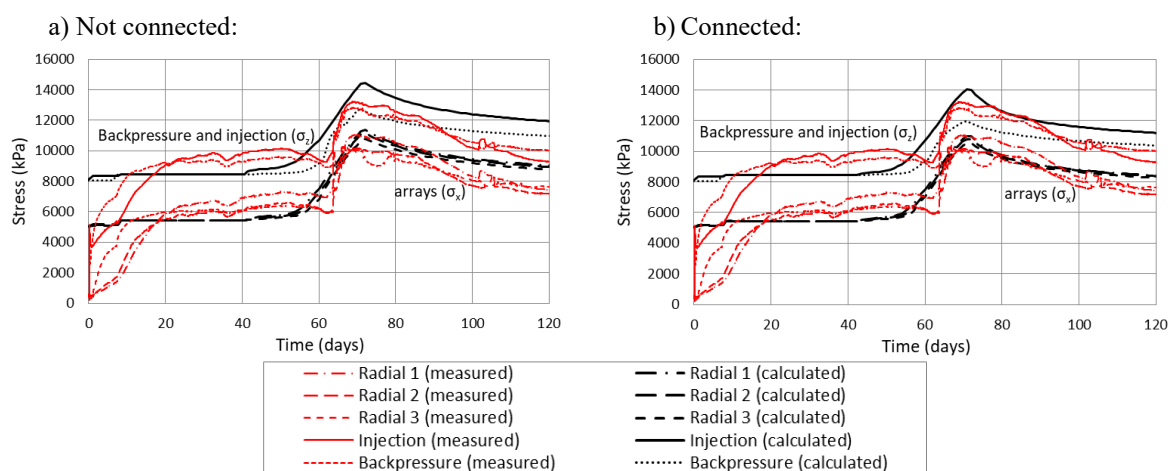

a) Not connected: b) Connected:

Figure 7: Axial and radial stress evolution: not connected (a) and connected (b) permeability cases.

4   CONCLUSIONS

- It has been possible to incorporate the mechanical effect on the previous just hydraulic 3D model, in addition to the soil permeability based on embedded discontinuities (which in turn depends on deformation).
- The proposed methodology for the preferential paths analyses provides results reasonably satisfactory for both connectivity cases assumed.

ACKNOWLEDGEMENTS

REFERENCES

[1] Harrington, J, R Cuss, C Graham, S, British Geological Survey, Radioactive Waste Management Limited, ENGINEER (modElliNg Gas INjection ExpERiments), DECOVALEX 2019, Specifications for Task A.

TEMPERATURE INDUCED WATER FLUX AROUND OPENING IN COX FORMATION: THE CASE OF EPT EXPERIMENT

C.J. Villarraga[*], J. Vaunat[*], M. Lundy [†], and M. Vu [††]

[*] Department of Civil and Environmental Engineering
Technical University of Catalonia (UPC)
Campus Nord UPC, 08034 Barcelona, Spain
E-mail : claudia.juliana.villarraga@estudiant.upc.edu, jean.vaunat@upc.edu
[†] Andra, Centre de Meuse/Haute-Marne, RD 960, 55290 Bure, France
[††] Andra, R&D department, 1 rue Jean Monnet, 92290 Châtenay-Malabry

Key words: Nuclear waste disposal, Argillaceous rocks, THM **Key words:** Radioactive waste disposal, GiD interface, THM coupled analysis, Callovo-Oxfordian rock

Abstract.

When HAVL waste are placed in underground disposal cells, they induce an increment in temperature in the surrounding geological media, which could affect flux and chemistry of pore water. In order to study more in detail these perturbations, an in-situ experiment is being carried out in the MHM underground research laboratory. This paper presents a numerical model that has been developed to support the experiment and analyse the temperature induced water fluxes.

1. INTRODUCTION

The Meuse/Haute-Marne underground research laboratory (MHM-URL) has been constructed in the Callovo-Oxfordian (COX) with the objective to analyse the viability of storing high-level and intermediate-level long-lived nuclear waste in this type of formation. As such, Different in-situ experiments have been implemented in the URL in order to evaluate the THM characteristics and response of the COX formation to different conditions involving the final radioactive waste disposal.

When the radioactive waste is emplaced into the disposal cells, the heat emitted will generate a transitory increase of temperature in the surrounding geological media, possibly reaching the 90ºC. Temperature could have an influence on the water-rock interactions that govern the pore water chemistry, and the pore water composition may play an important role regarding the processes involved in the durability of the disposal materials. Thus, the EPT experiment was designed in order to characterize the effect of a temperature increase on the geochemical composition of COX pore water. The experiment also allows the monitoring of the evolution of temperature, pore pressure and seepage water flux that could be modified under the effect of hydro-mechanical disturbances generated by a temperature increase.

This paper presents a numerical modelling focused on the THM coupled response observed during the execution of the EPT experiment.

2. EPT EXPERIMENT DESCRIPTION

The EPT experiment has been installed in the NED gallery of the Meuse/Haute-Marne underground research laboratory, in order to evaluate the effect of thermal load on the chemistry and water flux of the pore water in the COX rock. It consists in 7 vertical ascending boreholes drilled from the roof of the gallery (see Figure 1), divided into:

- One 15-m long central borehole (EPT1201): seepage water is collected for chemical analysis in a 5-m long interval open to the rock. A pore water pressure sensor is located in a second interval located 2 m below.
- Four heating boreholes (EPT1202 to EPT1205) located approximately 0.5 m around the central borehole to simulate the thermal load imposed by the radioactive waste.
- Two instrumentation boreholes (EPT1206 and EPT1207) installed to evaluate the evolution of the far field in terms of temperature and liquid pressure. Borehole EPT1206 contains 12 temperature sensors installed between 2 and 18 m and borehole EPT1207 contains 3 sensors of temperature and pore water pressure located at 7, 11 and 14 m from the gallery roof.
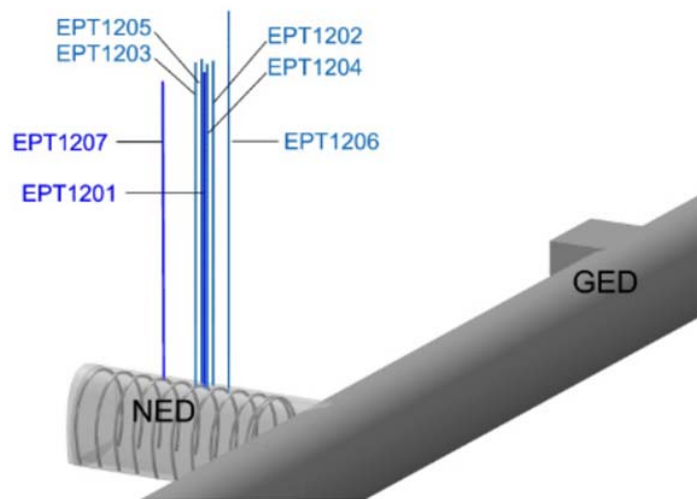

Figure 1 Location of the seven vertical boreholes for EPT experiment.

Central borehole EPT1201 and the four heating boreholes are equipped with temperature sensors at four different depths between 10 and 15 m.

Thermal load has been imposed by circulating heated water in the last 6 meter of each heating boreholes (EPT1202 to EPT1205). Temperature controlled heater modules with water tanks are located in the drift. One liquid pressure sensor has been installed in each borehole at 10 m from the top of the gallery to survey the water pressure evolution induced by temperature[1].

3. NUMERICAL MODELLING

The numerical modelling task focuses on the study of the Thermo-Hydro-Mechanical response of the host rock during the experiment as well as on the interpretation of temperature, pore pressure and water flux measurements. Water chemistry is not studied.

3.1 Numerical modelling characteristics and properties

The numerical modelling has been carried out using the finite element code CODE_BRIGHT[2]. It is based on a three-dimensional geometry in order to tackle the effect of heating boreholes vertical deviation on experiment measurements. Geometry and mesh considered are presented in Figure 2. Mesh has been refined in the zone between the central and the heating boreholes and the central interval. It contains 20835 elements and 22136 nodes.

Heating boreholes are represented as lines, while the central borehole is simulated as a recess in the geometry.
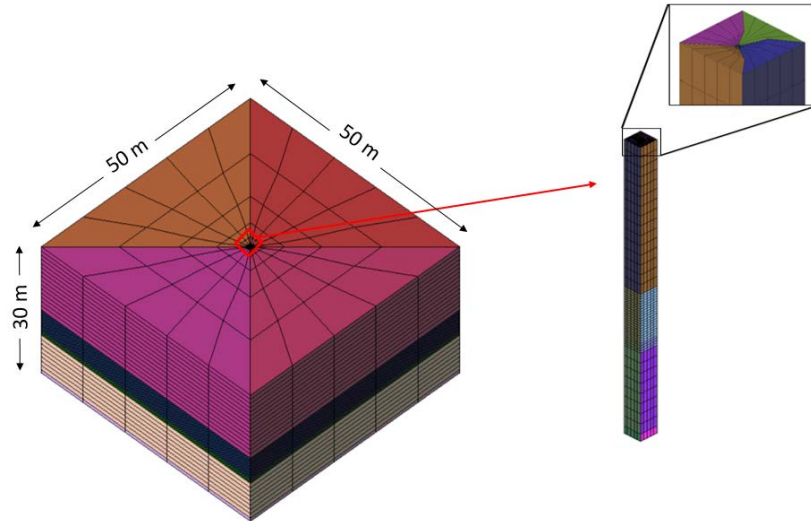

Figure 2 Geometry and mesh considered

Four principal stages were considered:
- Equilibrium phase: short period aiming at equilibrating the initial conditions before the excavation of the gallery.
- Phase of gallery excavation: in this stage, a drainage condition is imposed at the bottom of the geometry. The duration of this phase has been back-analyzed in order to obtained a liquid pressure profile similar to the one observed in borehole EPT1207 (far-field) before the beginning of the experiment.
- Generation of central borehole phase: in this stage the excavation and pressurization of central borehole are considered.
- Heating phase: a sequence of 14 heating intervals has been imposed in the four heating boreholes in order to reproduce the experiment. During this phase, the temperature is imposed directly at the nodes that represent the heating boreholes allowing prescribing the measured temperatures at that points.

Properties used for the numerical modelling are presented in Table 1. Values used come from the back-analysis of a former in-situ experiment (TED[3] test).

Table 1 COX Properties

Properties	Symbol	Value	Unity
Porosity	n	0.13	–
Young modulus in the stratification plane	$E_{//}$	6000	MPa
Poisson's ration in the stratification plane	$n_{//}$	0.25	–
Young modulus orthogonal to the stratification plane	$E_\perp$	3500	MPa
Poisson's ration orthogonal to the stratification plane	$n_\perp$	0.35	–
Shear modulus orthogonal to the stratification plane	$G_\perp$	3500	MPa
Biot coefficient	b	0.6	–
Linear thermal expansion	a_T	$1.4\ 10^{-5}$	K^{-1}
Intrinsic permeability in the stratification plane	$K_{i//}$	2.10^{-20}	m^2
Intrinsic permeability orthogonal to the stratification plane	$K_{i\perp}$	1.10^{-20}	m^2
Thermal conductivity in the stratification plane	$l_{//}$	1.96	$W.K^{-1}.m^{-1}$
Thermal conductivity orthogonal to the stratification plane	$l_\perp$	1.26	$W.K^{-1}.m^{-1}$
Solid phase specific heat	C_s	800	$J.K^{-1}$
Solid phase density	r_s	2700	$kg.m^{-3}$

3.2 Numerical modelling results

Modelling results are presented in Figure 3 for heating borehole EPT1202. Temperature follows obviously the measurements since measured values have been prescribed along the line corresponding to the borehole. Temperature induced liquid pressure follows closely the evolution of field measurements, which indicates a good capture of, on the one hand, rock-water differential thermal expansion and, on the other hand, rock permeability.

In the central borehole (EPT1201), numerical simulation reproduces adequately the trend of temperature evolution observed during the experiment. However, computed values are between 2ºC to 5ºC degrees higher than measurements, as can be observed in Figure 4. In terms of liquid pressure, the numerical model is able to reproduce the general evolution observed during the experiment, nevertheless, the peaks observed at the beginning of each heating phases cannot be reproduced by the model. This indicates that the model computes a too high dissipation of thermally induced pore pressure. This can be due to the fact that model predicts a too high stiffness or permeability close to the central borehole.
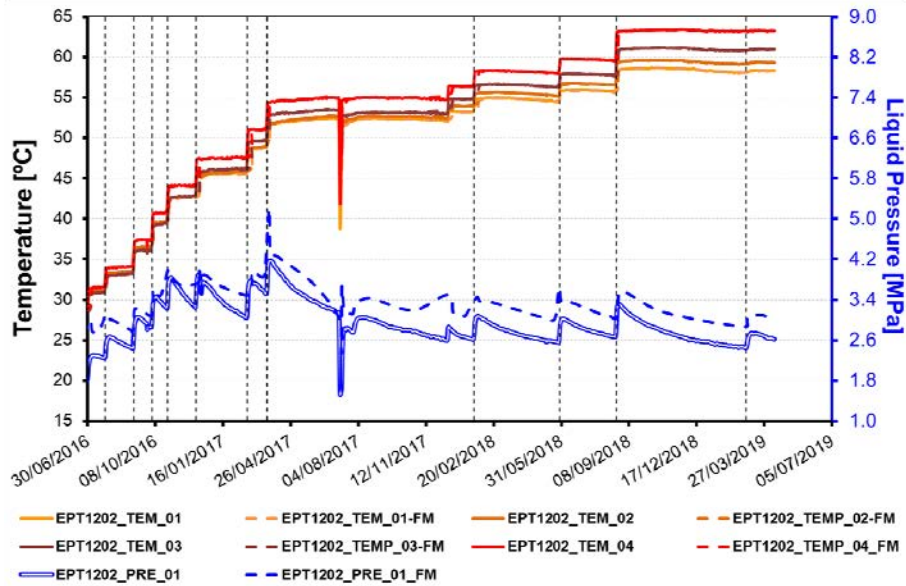
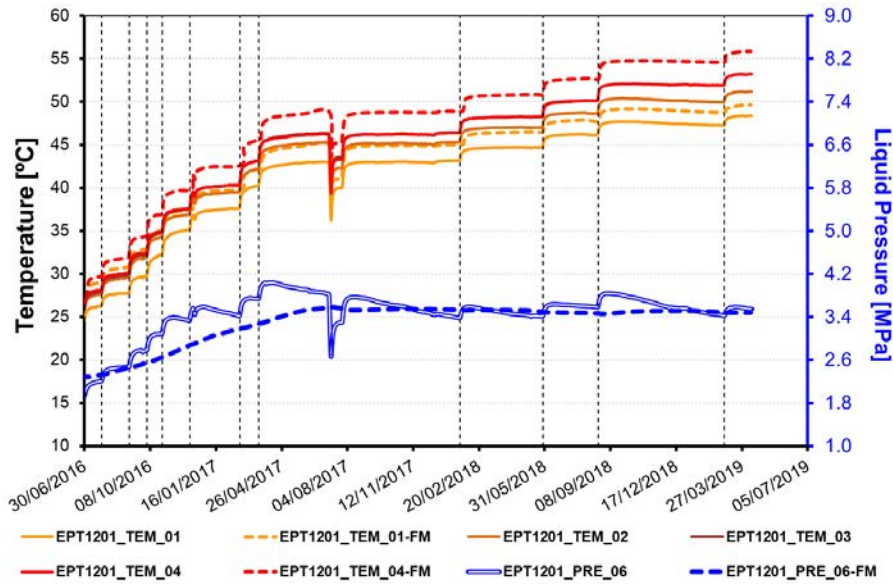**Figure 3 Simulation results for heating borehole EPT1202**

Figure 4 Simulation results for central borehole EPT1201

4. CONCLUSIONS

The EPT experiment has been realized to evaluate the CTHM response of the COX rock. It has been supported by three-dimensional numerical THM simulations in order to interpret the

temperature and pore pressure field.

Measurements and computational results consistently evidence that water flux and liquid pressure are affected by the thermal load imposed in the heating boreholes, demonstrating the THM coupled behaviour of the rock.

The numerical model proposed is able to reproduce adequately the evolution of temperature and liquid pressure observed with the increment of temperature in the heating boreholes.

REFERENCES

1.   Lundy M, Garitte B, Lettry Y, Vinsot A. Experimental Design for in situ Characterization of the Callovo-Oxfordian Pore Water Composition at 85°C. Procedia Earth Planet Sci. 2013;7(0):533-536. doi:10.1016/j.proeps.2013.03.091
2.   Olivella S, Gens A, Carrera J, Alonso EE. Numerical formulation for a simulator (CODE_BRIGHT) for the coupled analysis of saline media. Eng Comput. 1996;13(7):87-112. doi:10.1108/02644409610151575
3.   Gens, A., Garitte, B., Rostovanyi M & Vaunat, J. THM Modelling of the TED Experiment. Final Report.; 2013 UPC-CIMNE, Barcelone, Spain, 89 p.

THERMO-HYDROMECHANICAL RESPONSE AROUND LARGE EXCAVATIONS IN THE CALLOVO-OXFORDIAN

Matias Alonso[*], Jean Vaunat[*] and Minh-Ngoc VU[†]

[*] Department of Civil and Environmental Engineering
Technical University of Catalonia (UPC)
Campus Nord UPC, 08034 Barcelona, Spain
E-mail: matias.alonso@upc.edu

[††] French National Radioactive Waste Management Agency (Andra),
1 rue Jean Monnet, 92290 Châtenay-Malabry, France

Key words: Nuclear waste disposal, Argillaceous rocks, THM coupled analysis

Abstract. *Modelling work have been carried out to study the coupled thermo-hydro-mechanical response around a gallery with the compressive lining. Model includes a large geometry (1000 m high), a constitutive law developed for model the viscoelastoplastic response of Callovo-Oxfordian host rock, and a bilinear model to represent the effect of a compressible lining on the damaged zone developing around the excavation and on the stress increase within the concrete lining. Results allow to highlight the behavior of the gallery in terms of mechanical damaged and disturbed zone, hydraulic and thermal perturbed zones and efforts in the lining.*

1 INTRODUCTION

Argillaceous rocks and stiff clay formations have great potential as possible geological host medium for radioactive waste[i]. These materials have low permeability, significant retention capacity for radionuclide and no economic value in most cases.

In the present paper, the work carried out related to the repository reserved for intermediate-level activity and long life nuclear waste (MAVL for the acronym in French) in the framework of the Cigéo project leaded by Andra (National Agency for the Nuclear Waste Management in France) is presented.

In the Figure 1, a scheme of the Cigéo project is presented. It is located in northeast France, at the fringe of the Meuse and Haute-Marne departments

The Callovo-Oxfordian formation (the layer delighted in the scheme of Figure 1) is a sedimentary argillaceous rock. It is around 150 meters thick and lies between about 400 m and 600 m in depth and overlain and underlain by poorly permeable carbonate formations.

The MAVL repository section consists on several parallel galleries of long length and of about 10 m diameter.They are separated by 50 m from each other.
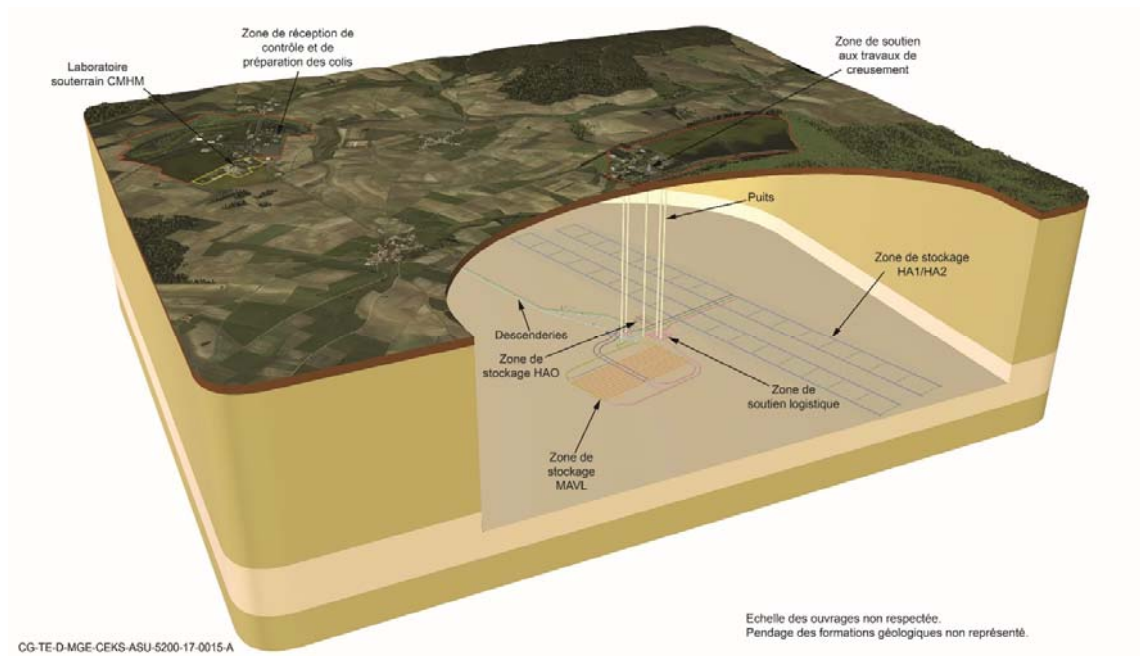
Figure 1: Scheme of the CIGEO project and the MAVL repository section

The support of the MAVL cell consist in a compressive lining with two layers: 20 cm compressible materialand 50 cm precast concrete . The general idea of the compressible material is to delay in time the increase of stresses in concrete during the exploitation phase of the repository.

The motivation of the work is to evaluate the effect of the galleries excavation and the effect of thermal loading generated by exothermic nuclear waste on the host rock. These has been done considering complex phenomena like the excavation induced fractured zone in the rock, the change of the properties as a function of the damage evolution and the creep.

2 MODEL DESCRIPTION

From preliminary tests it was concluded that model that represents a considerable depth of stratum was necessary in this case to simulate the phenomena related to heat flow and the corresponding water pressure increments. Because that, a model representing 1000 m deep of geological formation was considered.

Heat flow is modeled through Fourier's law. Due to the stratification of the rock different values for the thermal conductivity parallel and perpendicular to the stratification plane were considered.

Water flow was modeled through Darcy's law. Due to the high air entry values, no retention curve is considered, so the rock is always saturated and the relative permeability is always equal to one. Intrinsic permeability varies regarding Kozeny's model and the impact of damage on the permeability was included in the elastoplastic-model.

Elastoplastic behaviour was only considered for the Callovo-Oxfordian layer, while the other geological formation were considered as linear elastic. The elastoplastic model considered includes some important aspects of the argillite behavior[ii]. With it, it is possible to simulate the hardening behaviour prior peak and the softening behaviour after peak, as one can see in a triaxial tests shown in Figure 3.

Two affected zones were defined regarding the hardening and softening behaviour of the rock. In the right-hand side of Figure 3 a scheme of what is expected in an excavation parallel to the major principal stress in a rock with some degree of strength anisotropy is presented[iii]. The excavated disturbed zone (EdZ) corresponds to the area where the rock is in hardening regime. The excavated damaged zone (EDZ) corresponds to the area inside the first one where a softening regime is occurring.

The increase of permeability is limited to the EDZ. This aspect is incorporated in the model by including a dependency of the intrinsic permeability on the plastic multiplier as indicated in the exponential function of Figure 3, where K_o is the intrinsic permeability for the intact rock, η is a constant that controls the rate of change, λ is the cumulative value of the plastic multiplier and λ_{soft} is the plastic multiplier threshold from which increase of permeability is activated, corresponding to the cumulative value of the plastic multiplier at the peak response.

It is known that the strength of these rocks depends on the loading direction respect to the stratification plane. The cross-anisotropy in strength is considered in this model through a non-uniform scaling of the stress tensor[iv].

An additional time-dependent mechanism was considered to simulate viscoplastic strains, characterized by a modified form of Lemaitre's law. It was assumed that viscoplastic deformations are mainly caused by deviatoric stresses and are activated when the deviatoric stress exceed a certain threshold values.
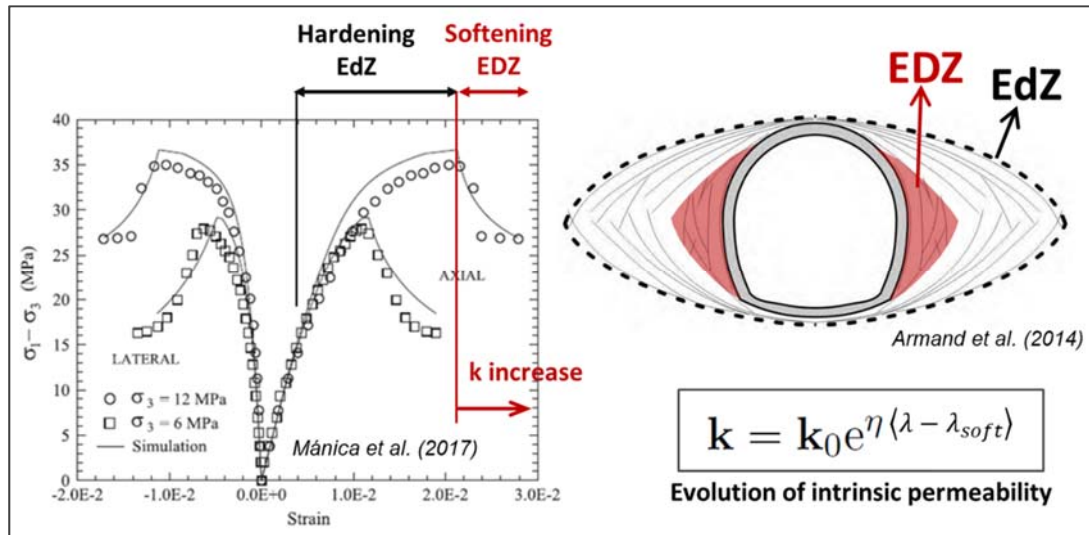

Figure 2: Features of the elastoplastic model considered

The concrete is considered linear elastic and the compressible material is defined through the response shown in Figure 4. Stiffness appears to be much lower than the ones of the neighboring materials (concrete and host rock).
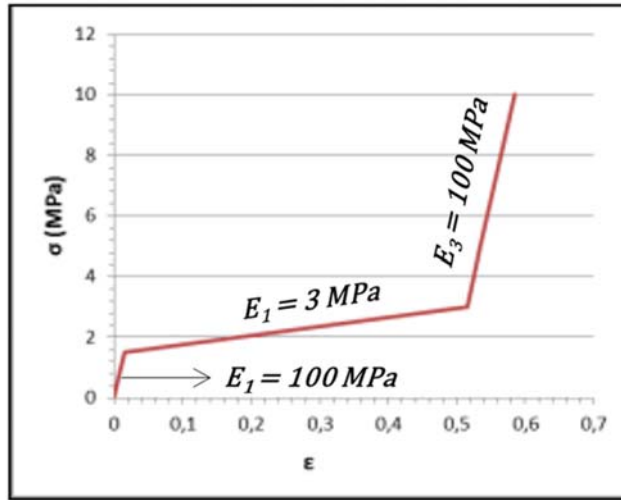
Figure 3: Compressible material response

Four modelling phases, described in Table 1, were considered. The first phase corresponds to the excavation. During this phase, confinement ratio is reduced from 1 to 0.04 and water pressure from the initial value to 0 MPa at excavation wall.

The second phase corresponds to the support construction phase, where the elements representing the support are generated. The third phase is named the "Waiting phase" and corresponds to the time between the end of construction of the gallery and the time of deposition of the nuclear waste four years later. The last phase is the "Operational phase" and corresponds to the heat flow application due to the presence of the exothermic nuclear waste.

Phase N°	Initial Time	Final Time	Description
1	0 [days]	0.5 [days]	Excavation: confinement ratio (C.R.) from 1 to 0.04 and water pressure from initial to 0 MPa
2	0.5 [days]	1 [days]	Support construction: equilibrium with compressible material and concrete
3	1 [days]	4 [years]	Waiting phase
4	4 [years]	500 [years]	Operational phase: heat flow application

Table 1: Example of the construction of one table

The temperature in the surface was considered constant and equal to 8.7 ºC. Then, with the geothermal gradient, the initial temperature at any depth can be determined. For the tunnel depth for example, the initial temperature is of around 22.5 ºC.

Regarding initial water pressures, the observations show an overpressure of the order of 0.5 MPa with respect to the hydrostatic distribution in the Callovo-Oxfordian layer. For this reason, the initial water pressure is linear as a function of depth except in the Callovo-Oxfordian layer where this small overpressure was considered.

The minor horizontal stress was considered equal to the vertical stress. The major horizontal stress, parallel to the tunnel axis, was also considered equal to the vertical stress for the upper

layers and equal to 1.3 times the vertical stress for the Callovo-Oxfordian layer.

3 RESULTS

Plot of contour fill for values of temperature, water pressure, plastic multiplier and deviatoric stress are presented in Figures 5-8 respectively.

A quick increase of temperature is observed around the tunnel at first and then a slow dissipation towards the adjacent layers (Figure 5). The largest variations of temperature are confined in the Callovo-Oxfordian formation but the effects in the neighboring layers are also really significant.

Due to the excavation a large suctioned area is generated (the black zone close to the tunnel in Figure 6) and the water pressure in the middle between two adjacent tunnels increases considerably. With heat flow application the water pressure increases and the suctioned zone starts to decrease slowly in size. The water overpressure generated is then dissipated towards the adjacent layers and also by the drainage effect of the galleries.

The perturbed zone extends up to 10 or 15 meters from the tunnel wall. It does not change significantly at time of heat flow application and during the further phase of pore pressure dissipation (Figure 7). The black region close the tunnel corresponds to the damaged zone, where a softening regime is occurring in the rock. It is in this reduced area where the permeability increases considerably, around two orders of magnitude.

The evolution of deviatoric stresses provides insights about the development of creep strains (Figure 8). The black region corresponds to the area where creep strains are not developing. Immediately after excavation a small area close to the tunnel where relative large creep strain are developing is generated. The deviatoric stress is almost immediately reduced close the tunnel when the support begins to interact with the rock. With heat flow application, the deviatoric stress increases slightly in a considerable large area. Then, as time proceeds, the deviatoric stress reduces considerably but the region where creep strains are occurring is still important at 500 years.
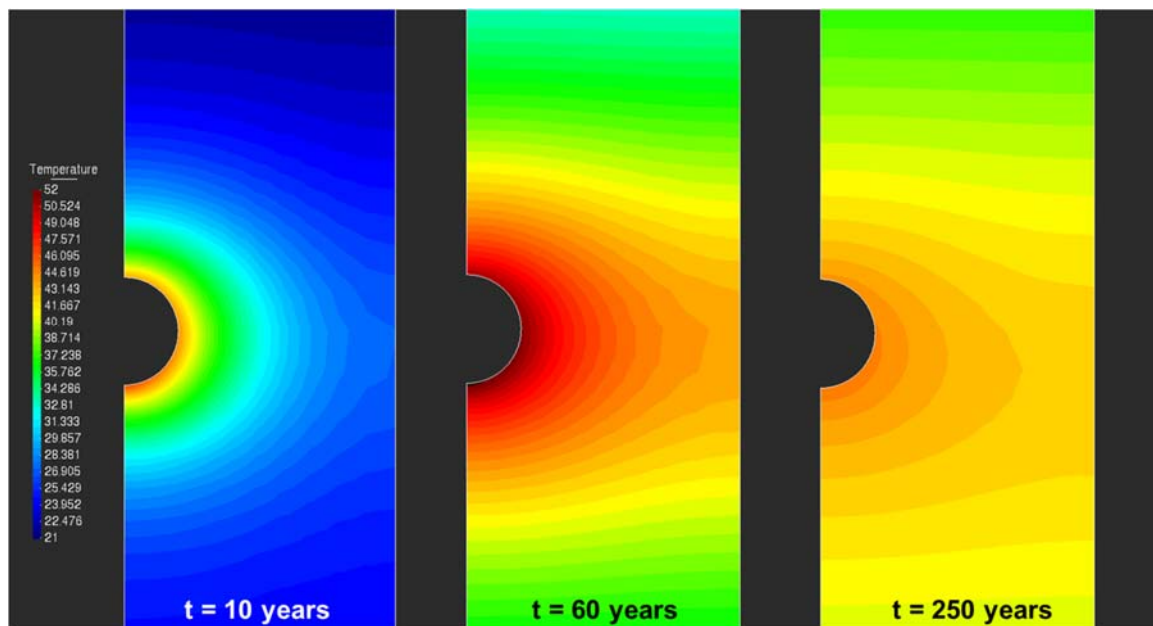

5

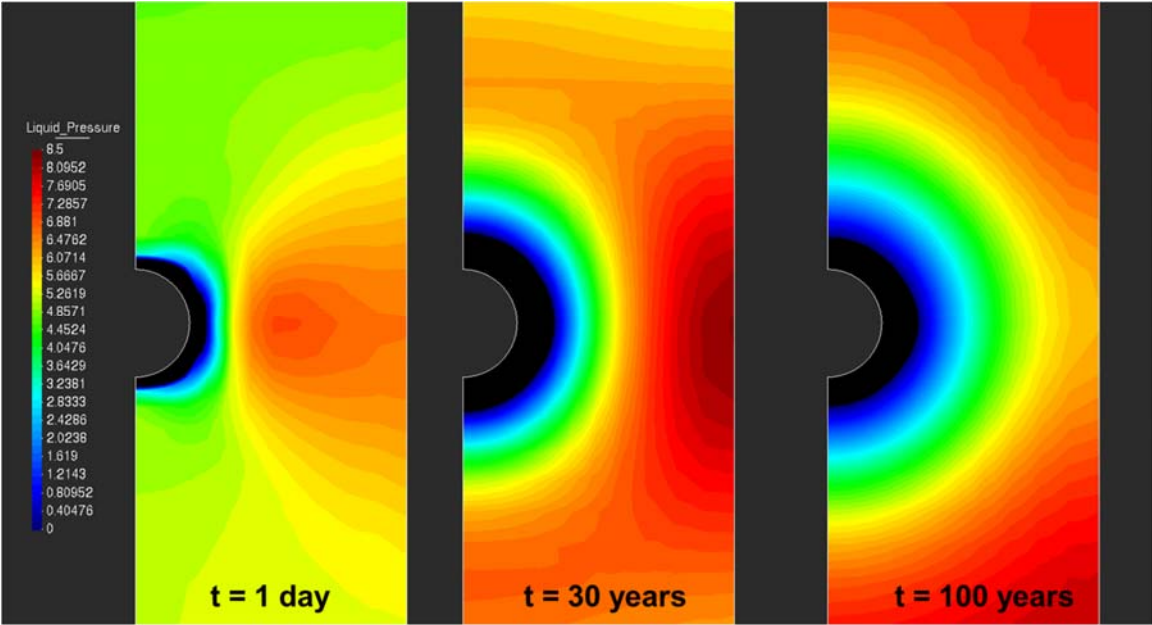Figure 4: Contour fill of temperature values

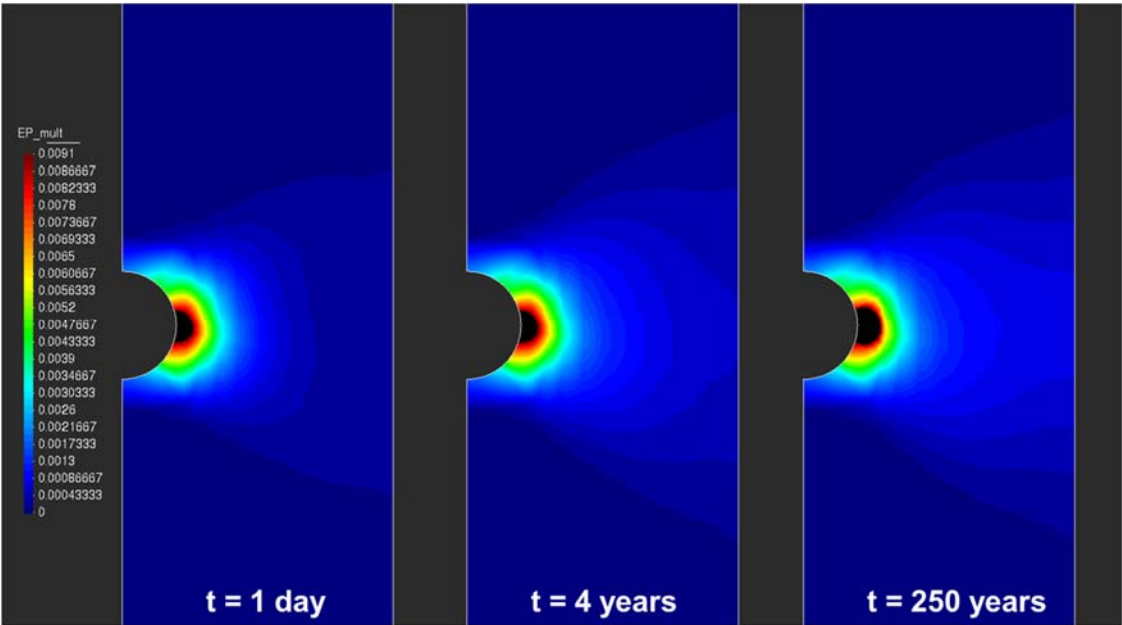
Figure 5: Contour fill of water pressure values
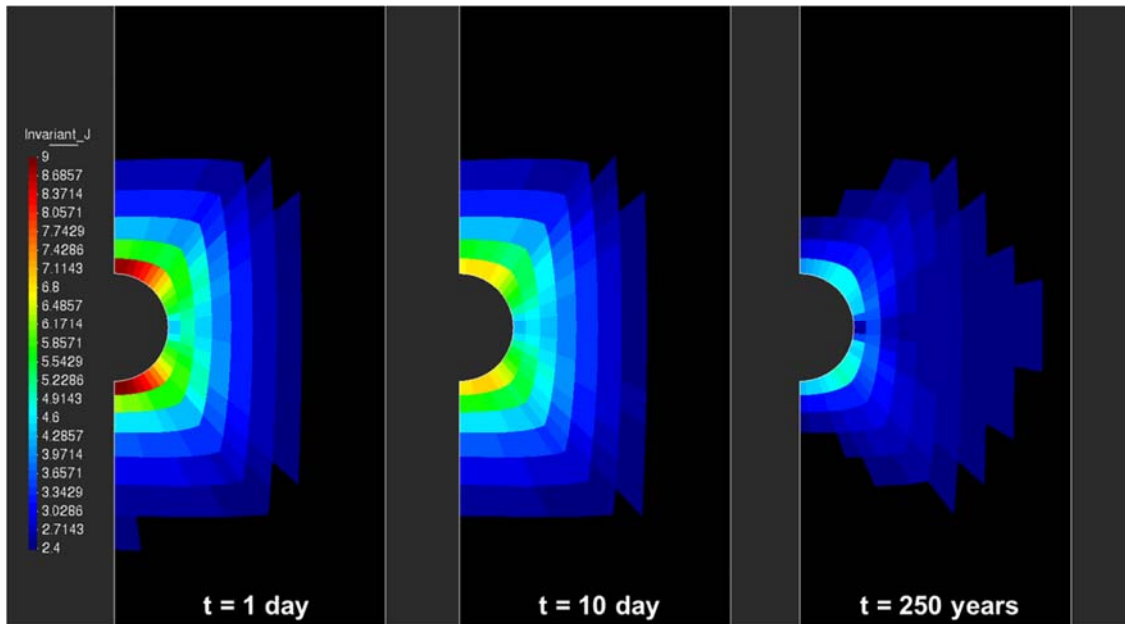

Figure 6: Contour fill of plastic multiplier values

Figure 7: Contour fill of deviatoric stresses values

11 CONCLUSIONS

A preliminary modelling of a gallery containing MAVL nuclear waste has been carried out. Results evidence:

- The largest variations of temperature and water overpressures are confined in the Callovo-Oxfordian formation but the effects in the neighboring formations are considerable.
- A large area with negative values of water pressure (i.e. suction) is formed around the excavation which extends up to 3 m from the wall of the tunnel. It decreases slowly with heat flow application.
- During excavation a large perturbed zone is formed around the tunnel which extend up to 10 m from the wall of the tunnel.
- A reduced damaged zone is formed close to the lateral wall of the tunnel and it extend up to 2 m. In this zone the permeability increases around two order of magnitude.
- Creep strains continues to be relative important even when a long time has passed.

These results allow to set an initial context for the storage of MAVL and open the way for more detailed computations, where, particularly, local effects due to rock softening in the damaged zone will be studied.

REFERENCES

[i]   Gens A. The role of geotechnical engineering for nuclear energy utilisation. In: Vanicek I et al., editors. Proc 13th European conference on soil mechanics and geotechnical engineering, vol. 3. Prague: CGtS; 2004. p. 25–67

[ii] Mánica MA, Gens A, Vaunat J, Ruiz DF (2017). A time-dependent anisotropic model for argillaceous rocks. Application to an underground excavation in Callovo-Oxfordian claystone. Computers and Geotechnics 85, 341-350.

[iii] Armand, G., Leveau, F., Nussbaum, C., de La Vaissiere, R., Noiret, A., Jaeggi, D., Landrein, P. & Righini, C. (2014). Geometry and properties of the excavation-induced fractures at the Meuse/ Haute-Marne URL drifts. Rock. Mech. Rock. Engng 47, No. 1, 21–41.

[iv] Mánica MA, Gens A, Vaunat J, Ruiz DF (2016). A cross-anisotropic formulation for elasto-plastic models. Géotechnique Letters 6, 1–7.